Université de Montréal

Deep radio observations of a high-redshift galaxy cluster

par

Ariane Trudeau

Département de physique
Faculté des arts et des sciences

Mémoire présenté à la Faculté des études supérieures
en vue de l'obtention du grade de
Maître ès sciences (M.Sc.)
en physique

7 août 2018

SOMMAIRE

Dans le centre d'un amas de galaxies, on trouve une galaxie elliptique géante, qui domine les autres en termes de taille et de masse. Cette galaxie est appelée la *galaxie la plus brillante de l'amas* (BCG). Grâce à sa position privilégiée proche du centre du puits de potentiel de l'amas, la BCG héberge souvent un trou noir supermassif qui accrète activement. En relâchant une énorme quantité d'énergie, ce *noyau galactique actif* (AGN) empêche le milieu intra-amas de refroidir et de se déposer sur la BCG. Cette rétroaction de l'AGN tend à arrêter la formation d'étoiles dans la BCG.

Cependant, la façon dont la rétroaction de l'AGN opère dans les BCGs primitives n'est pas bien comprise. De plus, des études récentes semblent indiquer que les BCGs à haut décalage vers le rouge ont une quantité significative de formation d'étoiles in situ. L'une de ces BCGs à sursaut de formation stellaire est dans l'amas de galaxies SpARCS104922.6+564032.5 (raccourci en SpARCS1049). Elle forme des étoiles à un rythme de 950 ± 100 $M_\odot$ an^{-1} et a une morphologie qui rappelle les fusions de galaxies riches en gaz. Dans ce mémoire, je présenterai des observations radio multi-longueurs d'ondes de SpARCS1049 obtenues avec le Very Large Array (VLA), en mettant l'accent sur sa BCG.

J'ai trouvé trois sources radios non résolues, incluant la BCG. La morphologie compacte de l'émission radio de la BCG, tout comme son bon alignement avec le centre optique de la galaxie, suggère que l'émission radio provient de l'AGN et non de la formation d'étoiles. Cependant, la distribution spectrale de l'énergie en radio (Spectral energy distribution ; SED) de cette source est trop mal contrainte pour déterminer définitivement ses origines.

En supposant que toute l'émission radio vient de l'AGN, j'ai trouvé que le niveau d'activité radio est comparable à l'activité moyenne des BCGs à plus bas décalage vers le rouge. C'est inattendu, car une étude précédente a trouvé un immense réservoir de gaz moléculaire froid de $1.1 \pm 0.1 \times 10^{11}$ $M_\odot$ au centre de SpARCS1049, suggérant que quelque chose empêche partiellement le gaz de tomber dans le trou noir.

J'ai calculé la nouvelle SED (de l'optique jusqu'au radio) avec mes nouvelles mesures de flux en radio. J'ai trouvé que l'essentiel de la formation d'étoiles a probablement lieu non loin de la BCG mais pas en elle. Comme la formation d'étoiles ne semble pas avoir été détectée en radio, j'ai calculé une limite supérieure sur celle-ci et je l'ai utilisée en combinaison avec le

flux infrarouge lointain (estimé par la SED), pour explorer l'étendue de la formation d'étoiles. J'ai découvert que la formation d'étoiles est probablement très diffuse.

Finalement, j'ai exploré trois scénarios de formation pouvant expliquer la morphologie inhabituelle de la BCG et la présence d'un réservoir de gas moléculaire substantiel, en utilisant les données radio (et les non-détections) pour les contraindre : 1) une fusion majeure de galaxies riches en gaz, 2) dépouillement du gaz de quelques petites galaxies ou 3) déplacement d'un flot de gaz refroidi. Le scénario de fusion majeure de galaxies riches en gaz est peu probable, mais davantage de données sont nécessaires pour favoriser un des deux scénarios restants.

Mots-clés : amas de galaxies - continuum radio des galaxies - évolution des galaxies - galaxies actives - interaction de galaxies - sursaut de formation stellaire dans les galaxies

SUMMARY

In the centre of a cluster of galaxies lies a giant elliptical galaxy, dominating the others in terms of size and mass. This galaxy is called the Brightest Cluster Galaxy (BCG). Due to its privileged position near the gravitational potential well of the cluster, the BCG often hosts an actively accreting supermassive black hole. By releasing a tremendous amount of energy, this Active Galactic Nucleus (AGN) prevents the intracluster medium from cooling and condensing onto the BCG. This AGN *feedback* tends to quench star formation in BCGs.

However, the way AGN feedback operates in primitive BCGs is not well understood. Moreover, recent studies seem to indicate that high redshift BCGs have a significant amount of in-situ star formation. One of those stabursting BCGs is in the cluster SpARCS104922.6+564032.5 (shortened into SpARCS1049). It forms stars at a rate of 950 ± 100 $M_\odot$ yr^{-1} and has a morphology reminiscent of a major gas-rich merger. In this dissertation, I will present multiwavelength radio observations of SpARCS1049 obtained with the Very Large Array (VLA), focussing on its BCG.

I found three unresolved radio sources in SpARCS1049, including the BCG. The compact morphology of the radio emission from the BCG, as well as its good alignment with the galaxy optical centre, suggests that the radio emission originates from the AGN and not from star formation. However, the radio spectral energy distribution (SED) of this source is too poorly constrained to definitely determine its origin.

Assuming all the radio emission of the BCG comes from its AGN, I found that the level of radio activity is comparable to the average activity of lower redshift BCGs. This was unexpected because a previous study found an immense cold molecular gas reservoir of $1.1 \pm 0.1 \times 10^{11}$ $M_\odot$ in the centre of SpARCS1049, suggesting that something partially prevents the infalling of the gas into the black hole.

I computed a new SED (from optical to radio) with my new radio flux measurements. I found that the bulk of the star formation probably takes place in the vicinity of the BCG but not inside. Since the star formation does not seem to be detected at radio wavelengths, we computed an upper limit on it and used this limit in combination with far infrared fluxes estimated from the SED to explore the extent of the star formation. I discovered that the star formation is probably very diffuse.

Finally, I explored three formation scenarios that could explain the unusual infrared morphology of the BCG and the presence of a substancial molecular gas reservoir, using radio data (and non-detections) to constrain them: 1) a major gas-rich merger, 2) gas stripping from several small galaxies or 3) a displaced cooling flow. I found that the major gas-rich merger scenario is unlikely, but more data are needed to favour one of the two remaining scenarios.

Keywords: active galaxies - galaxy clusters - galaxy evolution - galaxy interaction - radio continuum in galaxies - starburst in galaxies

CONTENTS

LIST OF TABLES

LIST OF FIGURES

LIST OF ACRONYMS AND ABBREVIATIONS

AGN	*Active Galatic Nuclei* i.e. a supermassive black hole actively accreting
BCG	*Brightest Cluster Galaxy* the dominant galaxy of a cluster in size and mass
BGG	*Brightest Group Galaxy* idem for galaxy groups
CASA	*Common Astronomy Software Application*, the software for data reduction
CFHT	*Canada France Hawaii Telescope*
CTIO	*Cerro Tololo Inter-American Observatory*
FIR	*Far Infrared*
FR I	*Fanaroff-Riley type I*
FR II	*Fanaroff-Riley type II*
FUV	*Far Ultraviolet*
HST	*Hubble Space Telescope*
ICM	*Intracluster Medium*
IR	*Infrared*
IRAC	*InfraRed Array Camera*, onboard Spitzer
IRS	*InfraRed Spectrograph*, also onboard Spitzer
JVLA	*Karl G. Jansky Very Large Array*
JWST	*James Webb Space Telescope*

MIPS	*Multiband Imaging Photometer*, onboard Spitzer
ngVLA	*Next Generation Very Large Array*
NRAO	*National Radio Astronomy Observatories*
PI	*Principal Investigator*
RFI	*Radio Frequency Interference*
SED	*Spectral Energy Distribution*
SFR	*Star Formation Rate*
SKA	*Square Kilometer Array*
SDSS	*Sloan Digital Sky Survey*
SpARCS	*Spitzer Adaptation of the Red-sequence Cluster Survey*
SpARCS1049	*SpARCS104922.6+564032.5*
sSFR	*Specific Star Formation Rate*
SWIRE	*Spitzer Wide InfraRed Extragalactic Legacy Survey*
UKIDSS	*United-Kingdom Infrared Deep Sky Survey*
UKIRT	*United-Kingdom Infrared Telescope*
UV	*Ultraviolet*
VLA	*Very Large Array*
WFC3	*Wide Field Camera 3*, onboard Hubble Space Telescope

DÉDICACE

À mon père, qui a répondu patiemment à toutes mes questions sur l'astronomie et la physique quand j'étais petite. Maintenant, c'est lui qui m'en pose.

REMERCIEMENTS

Je tiens tout d'abord à remercier mes parents. Si vous n'aviez pas été là durant mon baccalauréat pour vous occuper de l'épicerie, de la pharmacie, du transport et occasionnellement de la bouffe, je ne sais pas comment j'aurais fait. Je remercie tout particulièrement mon père de m'avoir initié aux sciences dès l'âge de 4 ans. Je me souviens aussi des encyclopédies pour enfants que tu m'as achetées quand j'avais 6 ou 7 ans et que j'ai lu et relu durant une bonne partie de mon primaire. Je remercie aussi ma mère et mon frère d'avoir supporté les nombreuses discussions père-fille auxquelles ils ne comprenaient pas grand-chose. Merci aussi à ma grand-mère (alias mamie), dont la maison est devenue mon bureau principal en été.

Je remercie l'Institut de Recherche sur les Exoplanètes et tout particulièrement Pierre Bastien de m'avoir donné la chance d'expérimenter et de prendre goût à la recherche l'espace d'un été. Je remercie aussi Julie Hlavacek-Larrondo de m'avoir fait découvrir l'univers extrêmement énergétique et extrêmement intéressant des trous noirs supermassifs dans les amas de galaxies. Merci à Tracy Webb de m'avoir guidé à travers les méandres mal connus de la singulière évolution des BCGs et dans le choix d'une université pour mon doctorat. Merci aussi au département de physique de l'Université de Montréal, au McGill Space Institute et au Centre de Recherche en Astrophysique du Québec. Sans vos bourses, ma maîtrise aurait été sérieusement compromise.

Merci à Marie-Lou de m'avoir montré les rudiments de la réduction de données radio, quelques trucs de spécialiste et aussi de m'avoir indiqué comment poser des questions au NRAO helpdesk, ressource essentielle quand les choses se corsent. J'espère t'avoir aidé à mon tour. Merci à Myriam qui a contribué elle aussi à mon apprentissage, à Mar et à Annabelle pour leur gentillesse et à tous les autres membres de X-tra que j'ai côtoyés de près ou de loin. Merci aux deux Marie-Eve et à Frédérique de m'avoir écouté quand j'en avais besoin ou simplement quand j'avais envie de jaser. Bonne chance dans tous vos projets.

Chapter 1

INTRODUCTION

1.1. Clusters of galaxies

On large scales, the Universe exhibits filaments made of dark matter, gas and galaxies. At the intersections of these filaments stand clusters of galaxies (e.g. Plionis et al., 2008). Galaxy clusters are the largest gravitationally bound structures in the Universe. They are made of dark matter ($\gtrsim 85\%$), hot diffuse gas called the IntraCluster Medium (ICM; $\sim 10\%$) and stars organized in galaxies ($< 5\%$) (e.g. Plionis et al., 2008). Clusters of galaxies have typical masses of $10^{14} - 10^{15}$ $M_\odot$ and contain $10^2 - 10^3$ galaxies (e.g. Oswalt and Keel, 2013). These structures are very rare in comparison to lower mass systems like galaxy groups.

Big elliptical galaxies are common in the central parts of clusters. The dominant one, the Brightest Cluster Galaxy (BCG), usually stands near the centre of the gravitational potential well of the cluster. The BCG is often a cD galaxy, a type of galaxy characterized by a large diffuse envelope that can extend to hundreds of kpc (e.g. Von Der Linden et al., 2007; Oemler, 1976). The privileged position of the BCG in the galaxy cluster plays a dominant role in its evolution and gives it distinct properties. One of these is a greater probability of Active Galactic Nuclei (AGN) activity (e.g. Best et al., 2007).

AGN often produce jetted outflows that are generally observable at radio wavelengths, due to synchrotron emission. However, other structures in the cluster emit synchrotron radiation: for example diffuse extended structures called haloes or mini-haloes (e.g. Gendron-Marsolais et al., 2017; Hlavacek-Larrondo et al., 2013). As well, synchrotron radiation originating from cosmic-ray electrons can be produced by star formation.

The central AGN also plays a dominant role in the ICM dynamics, preventing the gas from cooling: with a temperature ranging between $10^7 - 10^8$ K, the ICM thermally emits in X-rays. Clusters often show an X-ray bright, dense core: these are called cool core clusters.

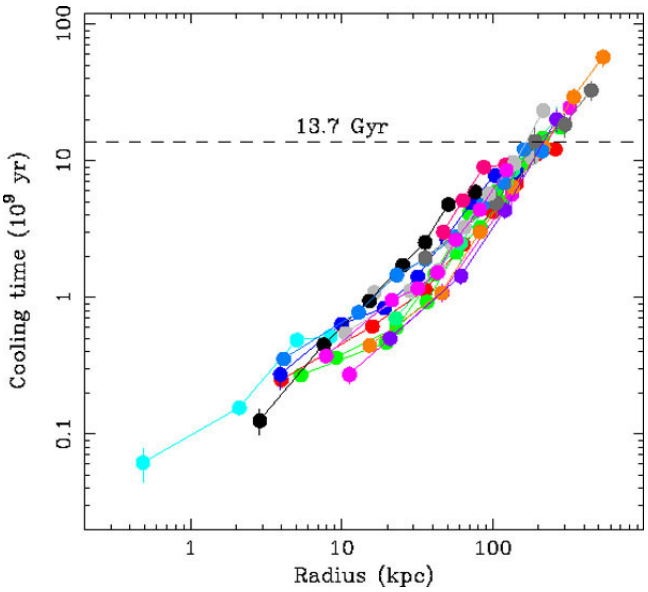

Figure 1.1 This plot shows the cooling time as a function of the radius for several cool core clusters. According to this plot, the gas within a radius of $\sim$ 150 kpc should have had the time to cool, since clusters have existed for Gyrs. From Voigt and Fabian (2004).

1.2. Cool core and non cool core clusters

Clusters are usually divided into two categories: cool core and non cool core clusters (e.g. Hudson et al., 2010). This classification was mainly made to distinguish between clusters with central cooling times much shorter than the Hubble time ($\sim 10^8$ yr, according to e.g. Voigt and Fabian, 2004, see Figure 1.1) and the other clusters whose cooling times are comparable to or greater than the Hubble time (e.g. Hudson et al., 2010). The cooling time can be estimated by the ratio of the gas enthalpy per unit volume to the energy lost per unit time per unit volume (ϵ) given by :

$$t_{cool} = \frac{5}{2}\frac{nk_BT}{\epsilon} \tag{1.1}$$

where n is the particle density, k_B the Boltzmann constant and T the temperature. Based on the observed cooling times, the cooling flow model assumed that the cold gas was compressed by the overlying hotter gas, generating an inflow of gas (e.g. Hudson et al., 2010). Such an inflow should trigger high levels of star formation, but detected rates were orders of magnitude lower than expected (e.g. McNamara and O'Connell, 1989). Today, heating by AGN feedback is seen as the most probable mechanism for preventing large inflows of cool gas in cluster cores (e.g. Hudson et al., 2010; McDonald et al., 2013b; Chen et al., 2007), especially through cavity growth and shock fronts (e.g. Markevitch and Vikhlinin, 2007, see sections 1.4.1 and 1.4.2).

As a result of the cooling flow model failure, cooling flow clusters were renamed cool core clusters (e.g. Hudson et al., 2010). No clear definition of this expression exists (e.g.

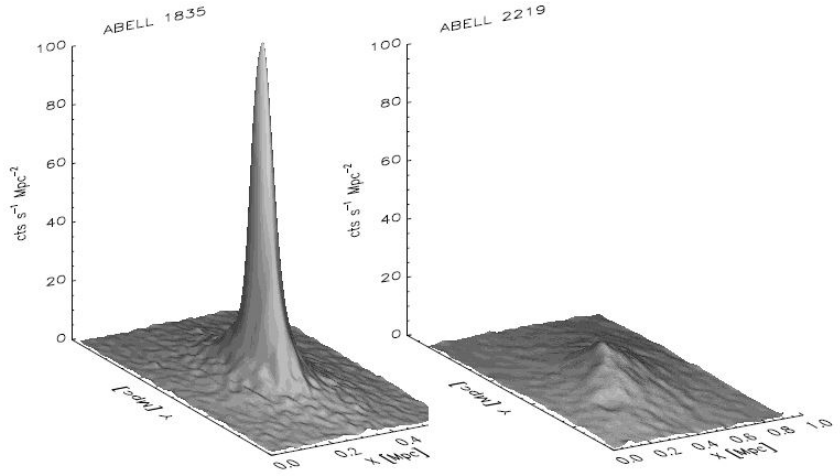

Figure 1.2 A comparison of the surface brightness distribution of Abell 1835 (left) and Abell 2219, which are respectively a cool core cluster located at $z = 0.2532$ and a non cool core cluster at $z = 0.228$. From Hlavacek-Larrondo (2012).

Hudson et al., 2010), but several common features of cool core clusters can be listed. For example, they have strongly peaked surface brightness distributions in X-ray (e.g. Hudson et al., 2010; Santos et al., 2008) as shown in Figure 1.2. As a measure of the *peakness* of the surface brightness, Santos et al. (2008) defined the surface brightness concentration parameter as follows:

$$c_{SB} = \frac{SB(R < 40 \text{ kpc})}{SB(R < 400 \text{ kpc})} \tag{1.2}$$

where $SB(R < 40$ kpc) is the surface brightness inside a radius of 40 kpc around the cluster's centre and $SB(R < 400$ kpc) is the same measurement for a radius of 400 kpc (e.g. Santos et al., 2008). As written above, the cooling time (e.g. Santos et al., 2008; Hudson et al., 2010) evaluated at or near the cluster centre, is a widely used criterion to distinguish between cool core and non cool core clusters. Some of the other characteristics of cool core clusters are low central entropies (e.g. Santos et al., 2010; Hudson et al., 2010), temperature drops in the centre (e.g. Hudson et al., 2010) and cuspinesses above 0.75, defined as

$$\alpha = \frac{d\log(n_e)}{d\log(R)} \text{ at } R = 0.04 r_{500} \tag{1.3}$$

where n_e is the electron density number, R is the distance to the cluster centre, and r_{500} is the radius where the mean gas density is 500 times larger than the critical density of the Universe. All these characteristics can be measured by using X-ray observations. However, although many cool core clusters have a central AGN (e.g. Burns, 1990, found that 71% of the central galaxies in his sample are radio-loud) some non cool core clusters, like Abell

2104, also harbour central AGNs (e.g. Santos et al., 2008). Thus, the presence of an AGN in the BCG is not a good indication of the cluster category.

Several authors divided clusters into three categories: strong cool core clusters, which follow the characteristics listed above, non cool core clusters and an in-between class called weak (e.g. Hudson et al., 2010) or moderate (e.g. Chen et al., 2007) cool core clusters. These clusters have higher central entropies than the strong cool core clusters, short to moderate central cooling times and a temperature drop shallower or even a flat temperature profile at the centre (e.g. Hudson et al., 2010).

1.3. AGN

An AGN is an actively accreting supermassive black hole at the centre of a galaxy. There are generally two accretion modes, the radiative (or quasar) mode and the mechanical mode. AGN mechanical feedback is characterized by jetted outflows and by the presence of a variety of structures in the ICM (or intergalactic medium, in the case of group and isolated galaxies), like X-ray cavities and shock fronts.

1.3.1. Physics of jets

One of the first models of jets was developed by Blandford and Rees (1974). They described the jets as pipes with variable cross-sections, subject to the Bernoulli equation. Choudhuri (1998) did a demonstration of this model based on the differentiation of the continuity equation (1.5) and on the Euler equation in one dimension (1.6):

$$\rho(x)u(x)A(x) = B \tag{1.4}$$

$$\frac{1}{\rho}\frac{d\rho}{dx} + \frac{1}{u}\frac{du}{dx} + \frac{1}{A}\frac{dA}{dx} = 0 \tag{1.5}$$

$$u\frac{du}{dx} = -\frac{1}{\rho}\frac{dp}{dx} \tag{1.6}$$

$$u\frac{du}{dx} = -\frac{c_s^2}{\rho}\frac{d\rho}{dx} \tag{1.7}$$

where B is a constant, u is the fluid velocity in the jet direction, x, ρ is the gas density, p is the pressure and A is the transverse area. The last equation has been obtained by using a polytropic relation between ρ and p. This relation implies $\frac{dp}{dx} = c_s^2\frac{d\rho}{dx}$ where c_s is the sound speed (e.g. Charbonneau, 2016). Substituting the Euler equation in the differentiated continuity equation and using the Mach number definition, $\mathcal{M} = \frac{u}{c_s}$, we obtain:

$$\frac{(1-\mathcal{M})}{u}\frac{du}{dx} = -\frac{1}{A}\frac{dA}{dx} \tag{1.8}$$

This equation implies that the outflow reaches the sound speed at the narrowest part of the jets. A schematic representation of the model is shown in Figure 1.3. The Blandford

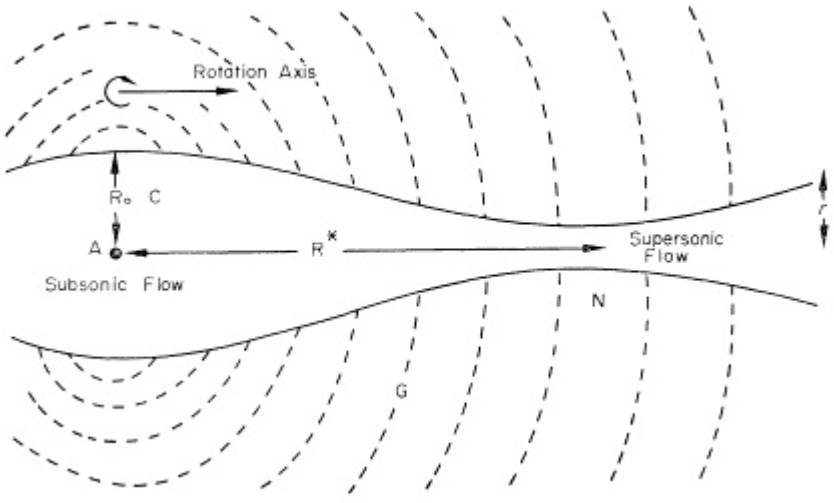

Figure 1.3 Diagram from Blandford and Rees (1974) illustrating the model. Outflow is accelerated continuously from the centre of the galaxy to the jet end. It reaches the sound speed at the narrowest part of the jets.

and Rees (1974) model suffers from several problems, including the lack of magnetics fields (e.g. Choudhuri, 1998). So, later, Blandford and Payne (1982) developed a new magnetohydrodynamic model, based on an axisymmetric and autosimilar development.

This model links the accretion disk to the jets, suggesting that, to launch the jet matter, the magnetic field lines should be at an angle of $\alpha < 60^o$ (e.g. Blandford and Payne, 1982; Choudhuri, 1998) with respect to the accretion disk. Choudhuri (1998) presented a schematic version of this computation based on a thin disk following a keplerian rotation. Figure 1.4 illustrates such a disk, at an angle α to a magnetic field line. Choudhuri (1998) computed the gravitational and centrifugal potential at the point R, obtaining:

$$\Phi = -\frac{GM}{s_0}\left[\frac{1}{2}\left(1+\frac{s_1}{s_0}\right)^2 + \frac{s_0}{((s_0+s_1)^2+z^2)^{\frac{1}{2}}}\right] \tag{1.9}$$

where s_0 is the distance between M (the black hole position) and P (where the magnetic field line is intersecting the accretion disk), s_1 is the projection of the distance between P and R in the direction parallel to the disk and z is the projection of this distance in the vertical direction ($s_0 \gg s_1$ and $s_0 \gg z$). Using a binomial approximation for the gravitational term and keeping only terms of second order or lower, this leads to:

$$\Phi = -\frac{GM}{s_0}\left[\frac{3}{2}+\frac{3}{2}\left(\frac{s_1}{s_0}\right)^2 - \frac{1}{2}\left(\frac{z}{s_0}\right)^2\right] \tag{1.10}$$

$$F_{r_l} = \frac{GMr_l}{s_0^3}[(3\cos^2(\alpha) - \sin^2(\alpha)] \tag{1.11}$$

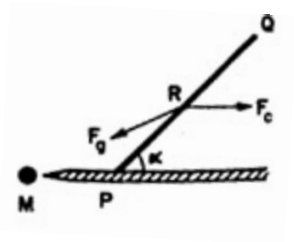

Figure 1.4 Geometry (not at the scale) used for the demonstration of the particle ejection from the accretion disk. Diagram from Choudhuri (1998).

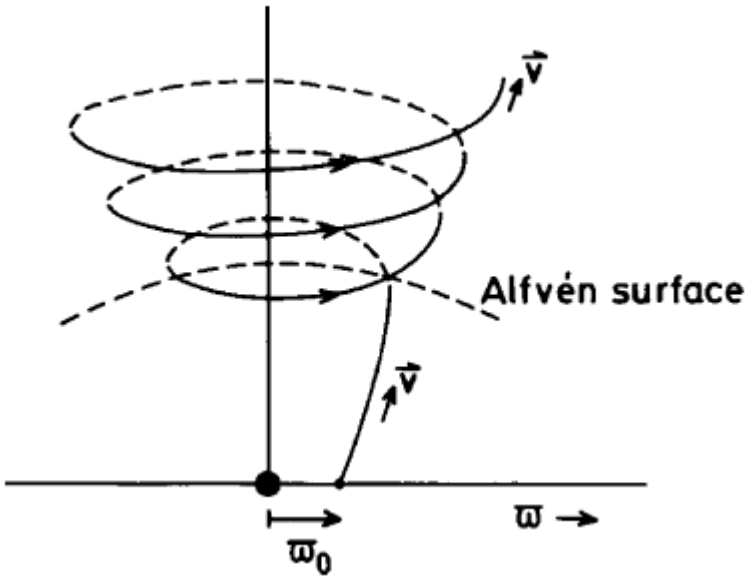

Figure 1.5 Schematic view of the magnetic field lines of a jet. Diagram from Belloni (2010).

where F_{r_l} is the component of $-\nabla\Phi$ along the magnetic field line (coordinate r_l) and has been obtained using $z = r_l \sin(\alpha)$ and $s_1 = r_l \cos(\alpha)$. Clearly, a particle moving along the line will be ejected of the disk only if $\alpha < 60$.

This mechanism extracts angular momentum from the accretion disk, allowing non-ejected matter to infall. The ejected matter is collimated by the toroidal component of the magnetic field which becomes important at large distances (e.g. Blandford and Payne, 1982; Belloni, 2010). A schematic illustration of the magnetic field is presented in Figure 1.5.

Today, the presence of a toroidal magnetic field is commonly invoked to explain collimation (e.g. Mignone et al., 2010; Tchekhovskoy and Bromberg, 2016), but several authors suggest than an additional factor may play a role in the collimation of some jets (e.g. Beskin, 2010; Belloni, 2010). Simulations show that the stability of the magnetic field toroidal component is a major concern (e.g. McKinney and Blandford, 2009; Mignone et al., 2010), as

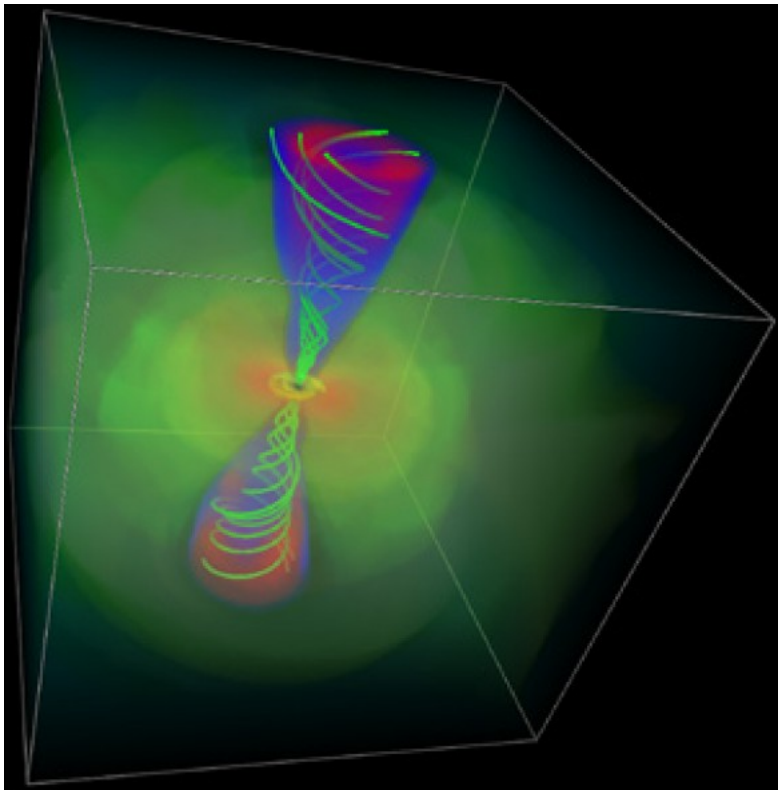

Figure 1.6 Simulation of a jet (in blue and red) using a dipolar magnetic field as an initial condition. The simulation shows the accretion disk (in yellow), the outer disk and wind (in green and orange) and the magnetic field lines (in green). Image from McKinney and Blandford (2009).

well as the large scale configuration of the magnetic field. McKinney and Blandford (2009) found that the magnetic field has to be mostly dipolar rather than of higher order to produce a highly relativistic jet. Figure 1.6 presents the jets obtained with a dipolar magnetic field at large scale by McKinney and Blandford (2009), with the magnetic field lines represented in green.

1.3.1.1. *Synchrotron radiation*

Most of the jet emission originates from synchrotron radiation. Usually in the radio domain, but sometimes in the optical or the X-ray domain, synchrotron radiation is emitted by charged particles rotating around magnetic field lines. For example, the angular frequency (ω_B) and the frequency (ν_B) of a rotating electron are given by (e.g. Condon and Ransom, 2016; Rybicki and Lightman, 2004; Courvoisier, 2013; Rosswog and Brüggen, 2007):

$$\omega_B = \frac{eB}{(\gamma m_e)c} \equiv \frac{\omega_L}{\gamma} \tag{1.12}$$

$$\nu_B = \frac{\omega_B}{2\pi} \equiv \frac{\nu_L}{\gamma} \tag{1.13}$$

where e is the elementary charge, B the norm of the magnetic field, $\gamma = \frac{1}{\sqrt{1-\beta}}$ with $\beta = \frac{v^2}{c^2}$ and v the speed. m_e is the electron mass and ω_L and ν_L are respectively defined as the gyro angular frequency and the gyro frequency. In the electron instantaneous rest frame, its synchrotron power is given by the Larmor equation, where $a'_\perp$ is the acceleration component perpendicular to the velocity in the rest frame (e.g. Condon and Ransom, 2016):

$$P' = \frac{2e^2(a'_\perp)^2}{3c^3} \tag{1.14}$$

$$P = \frac{2e^2(a_\perp)^2\gamma^4}{3c^3} \tag{1.15}$$

The emitted power is a relativistic invariant so $P = P'$. The additional γ^4 term in equation 1.15 is from the relation between acceleration in the rest frame and acceleration in the observer frame, $a_\perp = \frac{a'_\perp}{\gamma^2}$. Moreover, $a_\perp = \frac{eBv\sin(\alpha)}{\gamma m_e c}$ where α is the pitch angle (the angle between the velocity direction and the magnetic field). This equation, combined with the Thomson scattering cross section, $\sigma_T = \frac{8\pi}{3}\frac{e^4}{m_e^2c^4}$, and the magnetic energy density $U_B = \frac{B^2}{8\pi}$ leads to (e.g. Condon and Ransom, 2016):

$$P = 2\sigma_T\beta^2\gamma^2 cU_B\sin^2(\alpha) \tag{1.16}$$

$$P = \frac{4}{3}\sigma_T\beta^2\gamma^2 cU_B \tag{1.17}$$

where equation 1.17 has been obtained by averaging over all pitch angles (e.g. Condon and Ransom, 2016; Rybicki and Lightman, 2004; Courvoisier, 2013; Rosswog and Brüggen, 2007). It is possible to compute a characteristic time for the energy losses of the electron by dividing its rest mass energy ($E_e = \gamma m_e c^2$) by synchrotron power (e.g. Condon and Ransom, 2016; Rybicki and Lightman, 2004; Courvoisier, 2013; Rosswog and Brüggen, 2007). This time scale is called the synchrotron cooling time:

$$t_{sync} = \frac{3\gamma m_e c^2}{4\sigma_T\beta^2\gamma^2 cU_B} \tag{1.18}$$

For an optically thin electron distribution described by the power law $dN = N_0\gamma^{-p}d\gamma$, the power per frequency interval is $P_\nu = \frac{4}{3}\sigma_T\beta^2\gamma^2 cU_B\Phi(\gamma)$. Assuming that $\beta \simeq 1$ and that the unknown function Φ is strongly peaked around ω_B, Φ could be approximated by a Dirac delta function (e.g. Rybicki and Lightman, 2004; Courvoisier, 2013; Rosswog and Brüggen, 2007) and the power per unit frequency of the distribution is given by:

$$P_{\nu,tot} = \int P_\nu(\gamma)dN(\gamma) \tag{1.19}$$

$$P_{\nu,tot} = \frac{4}{3}N_0\sigma_T cU_B\int\gamma^{2-p}\delta(\nu-\nu_B)d\gamma \tag{1.20}$$

Making the substitution $\nu' = \gamma^2\nu_L$ (ν_L is given by equation 1.13) this becomes:

$$P = \frac{2N_0\sigma_T c U_B}{3\nu_L} \int \left(\frac{\nu'}{\nu_L}\right)^{\frac{-(p-1)}{2}} \delta(\nu - \nu') d\nu' \tag{1.21}$$

$$P = \frac{2N_0\sigma_T c U_B}{3\nu_L} \left(\frac{\nu}{\nu_L}\right)^{\frac{-(p-1)}{2}} \tag{1.22}$$

This result can be generalized to any charged particle distribution. So, a power law particle distribution of index p leads to a power spectrum described by a power law of index $\frac{-(p-1)}{2}$. Synchrotron power is greater for higher energy particles, so they tend to lose their energy first, as suggested by equation 1.18. This effect, called synchrotron ageing tends to deviate the high energy tail from the original power law (e.g. Rosswog and Brüggen, 2007; Heesen et al., 2014).

1.3.1.2. *Observationnal classification of jets*

Observationally, radiogalaxies harbouring jets were divided into two classes by Fanaroff and Riley (1974): Fanaroff-Riley type I and Fanaroff-Riley type II galaxies, often abbreviated as FR I and FR II galaxies. FR I galaxies have jets that are brighter in their centre than at their ends (e.g. Fanaroff and Riley, 1974; Rosswog and Brüggen, 2007) and have steeper spectra at their jet ends (e.g. Rosswog and Brüggen, 2007), while FR II have their brighter region further out than their fainter regions (e.g. Fanaroff and Riley, 1974; Rosswog and Brüggen, 2007). These galaxies often have more collimated and powerful jets, often showing bright spots at their ends, called hot spots (e.g. Rosswog and Brüggen, 2007). One example of an FR I galaxy is M87 (e.g. Hines et al., 1989; Tchekhovskoy and Bromberg, 2016) while Cygnus A is a classical example of an FR II galaxy (e.g. Tchekhovskoy and Bromberg, 2016). There is no consensus on the physical interpretation of this dichotomy (e.g. Rosswog and Brüggen, 2007; Tchekhovskoy and Bromberg, 2016), but Tchekhovskoy and Bromberg (2016) recently suggested that the less powerful jets could be subject to kink instabilities at a critical distance, forming FR I type jets, while more powerful jets are not sensitive to this instability and form FR II jets.

1.4. AGN Feedback in clusters of galaxies

As discussed in Section 1.2, heating by AGN feedback is the most probable mechanism that can offset cooling in the centre of cool core clusters. Energy in present and past outbursts (e.g. Rafferty et al., 2006; McDonald et al., 2015; McNamara and Nulsen, 2007) can be estimated with X-ray cavities. However, how energy is transferred to the ICM remains poorly understood. The proposed mechanisms are turbulent heating (e.g. Zhuravleva et al., 2014), sound waves (e.g. Fabian et al., 2017) and shock fronts (e.g. Markevitch and Vikhlinin, 2007; Randall et al., 2015).

1.4.1. Bubbles

Cavities appear as regions in clusters or groups of galaxies, depleted of X-ray emission,and correlated with radio emission from jets (e.g. McNamara and Nulsen, 2012; Rafferty et al., 2006). Compared with the surrounding ICM, cavities (also called bubbles) show $20-40\%$ less X-ray emission (e.g. McNamara and Nulsen, 2007) because they are less dense. Since jets are supersonic (e.g. Blandford and Rees, 1974), cavities initially expand supersonically. Once formed, they detach and rise under buoyant motion (e.g. McNamara and Nulsen, 2007; Bridle and Perley, 1984). During the initial stages of their life, bubbles are filled with synchrotron emission (e.g. Bridle and Perley, 1984), but when they detach and rise through the ICM, relativistic particles undergo ageing, so older bubbles are depleted of high frequency radio emission: they are called *ghost bubbles* (e.g. McNamara et al., 2001; Fabian et al., 2002; Clarke et al., 2005; Wise et al., 2007). Figure 1.7 shows NGC 5813 at X-ray wavelengths, which hosts these two kinds of bubbles.

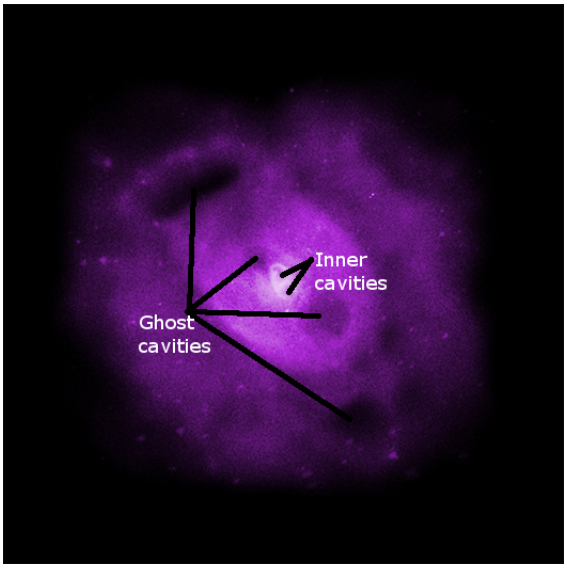

Figure 1.7 Deep Chandra X-ray image of the galaxy group NGC 5813, where the growing (inner) and the ghost cavities are labelled (image adapted from `http://chandra.harvard.edu/photo/2015/ngc5813/`).

One of the main interests of bubbles is that they are useful to estimate the jet power. To do this, the energy (labelled E_{cav} below) injected by the AGN in the ICM is needed. This energy is given by the enthalpy of the cavity, i.e

$$E_{cav} = E + pV = \frac{\Gamma}{\Gamma - 1} pV \tag{1.23}$$

where p is the pressure around the bubble, usually taken as an average (e.g. Churazov et al., 2002; Rafferty et al., 2006; McNamara and Nulsen, 2007, 2012). V is the volume of the cavity, assuming an elliptical or spherical shape, and Γ is the adiabatic index of the gas.

Non-relativistic gas ($\Gamma = \frac{5}{3}$) leads to $E_{cav} = 2.5pV$, while a relativistic one ($\Gamma = \frac{4}{3}$) leads to $E_{cav} = 4pV$.

There are three ways to estimate the age of a bubble (e.g. Churazov et al., 2002; McNamara and Nulsen, 2007). First, the refill time is an estimate for cavities still attached to the AGN. As its name suggests, the refill time is the time required to refill the bubble by gravity, leading to the equation:

$$t_r = 2\sqrt{\frac{r}{g}} \tag{1.24}$$

where g is the gravitational acceleration. r is the mean radius, given by $r = (ab)^{\frac{1}{2}}$ where a and b are the semi-axis parallel and perpendicular to the jet respectively. The factor 2 is there because the diameter is given by 2 radii.

A bubble rises supersonically when tied to its jets and then subsonically under the control of buoyant motion (e.g. McNamara and Nulsen, 2007). So, it is a reasonable assumption for rising bubbles to use the local sound speed as their mean speed, leading to the sonic time estimate

$$t_s = \frac{R}{c_s} \tag{1.25}$$

where R is the distance between the cluster centre and the cavity middle. Moreover, several measurements of the Mach number of shock fronts in different clusters give numbers all lying around $\mathcal{M} \simeq 1$ (e.g. Machacek et al., 2005; Mazzotta et al., 2003; O'Hara et al., 2004; Markevitch and Vikhlinin, 2007), which is another element to support the use of the sound speed as the mean speed.

Finally, the buoyancy time gives an upper limit on the cavity age. This estimate is particularly useful for bubbles which have risen for a sufficient amount of time to approach the terminal speed. This estimate is obtained by equating the buoyancy force $F_A = Vg(\rho_a - \rho_b)$, where ρ_b is the bubble density and ρ_a the surrounding one, to the drag force $F_D = \frac{C_D}{2} S v^2 \rho_a$ (e.g. McNamara and Nulsen, 2007), where $C_D = 0.75$ is the drag coefficient, S the cross-sectional area of the cavity and v its speed. This gives

$$t_b \simeq R\sqrt{\frac{SC_D}{2gV}} \tag{1.26}$$

where we neglected $\frac{\rho_b}{\rho_a}$ (the bubble density is much smaller than the surrounding density) and used $R = vt$. Comparing the latter with the buoyancy rise time, we obtain the terminal speed $v_{term} = \sqrt{\frac{2gV}{SC_D}}$.

The jet power can then be estimated as

$$P = \frac{E_{cav}}{t} \tag{1.27}$$

(e.g. Rafferty et al., 2006) where t is one of the time estimates discussed above. For clusters with multiple cavities, Rafferty et al. (2006) used the average time between outbursts to compute the mean jet power. Equation 1.27 may give only a lower estimate of the total outburst power since shocks may drive an amount of energy comparable to the cavity enthalpy into the ICM (e.g. Rafferty et al., 2006; McNamara and Nulsen, 2007; Wise et al., 2007).

However, cavity power is on average sufficient to stop cooling in clusters (Figure 1.8).

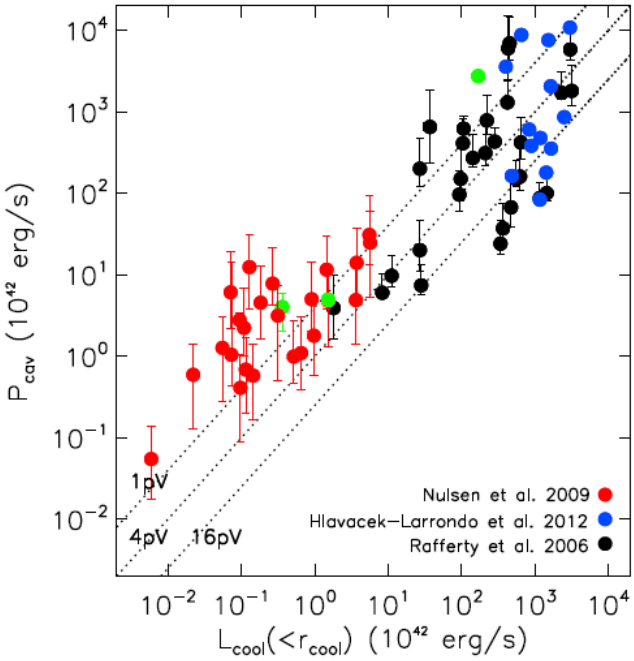

Figure 1.8 Cavity power versus the power needed to offset cooling within the cooling radius. Red dots are cavities mostly found in isolated elliptical galaxies or in groups. Black and blues dots are bubbles found in clusters. The three green dots are data taken from Jetha et al. (2008); Randall et al. (2009); Dunn and Fabian (2008) (Figure from Fabian, 2012).

1.4.2. Shocks and cold fronts

Shocks and cold fronts are sharp borders between two regions, appearing as bright rims in X-ray images. One way to differentiate them is to use the Rankine-Hugoniot relations; a shock front obeys them, while a cold front does not (e.g. Markevitch and Vikhlinin, 2007):

$$\mathcal{T} = \frac{\zeta + \mathcal{R}^{-1}}{\zeta - \mathcal{R}} \tag{1.28}$$

$$\mathcal{R}^{-1} = \left[\frac{1}{4}\zeta^2(\mathcal{T}-1)^2 + \mathcal{T}\right]^{\frac{1}{2}} - \frac{1}{2}\zeta(\mathcal{T}-1) \tag{1.29}$$

$$\mathcal{M} = \left[\frac{2\mathcal{R}}{\Gamma + 1 - \mathcal{R}(\gamma - 1)}\right]^{\frac{1}{2}} \tag{1.30}$$

where we defined $\mathcal{R} = \frac{\rho_1}{\rho_0}$ and $\mathcal{T} = \frac{T_1}{T_0}$ as the ratio of temperatures and densities on both sides of the shock front, with $\zeta = \frac{\Gamma+1}{\Gamma-1}$. Both types will create temperature and density discontinuities but unlike a shock, the pressure profile remains continuous across a cold front (e.g. Markevitch and Vikhlinin, 2007; Sanders et al., 2016; Ettori et al., 2013). Markevitch and Vikhlinin (2007) suggested that cold fronts are due to sloshing motions of the hot X-ray gas in the central potential well, while according to them, shock fronts are more likely to be associated with bubble formation (e.g. Randall et al., 2015).

1.5. BCGs

BCG usually refers to the dominant galaxy in mass and size of a cluster of galaxies (e.g. Lidman et al., 2012; Von Der Linden et al., 2007; Stott et al., 2008; Webb et al., 2015b,a), but some authors (e.g. Von Der Linden et al., 2007) use it also for the central galaxies of galaxy groups, usually called Brightest Group Galaxy (BGG). These galaxies are among the largest and most massive in the Universe (e.g. Lidman et al., 2012) so, not surprisingly, they exhibit the morphology of giant elliptical galaxies (e.g. Loubser et al., 2016; Von Der Linden et al., 2007; Stott et al., 2008) and are often cD galaxies (e.g. Von Der Linden et al., 2007). BCGs are located near the gravitational centre of their clusters: Lin and Mohr (2004) found that 70% of the BCGs in a sample of 93 galaxy clusters and groups in the 2MASS survey (Two Micron All Sky Survey) are off their cluster X-ray peak at most 5% of r_{200}. The proportion becomes 80% for BCGs that are located at most 10% of r_{200} off their cluster X-ray peak (Lin and Mohr, 2004). Due to their large masses and positions near the centre of potential wells (e.g. Von Der Linden et al., 2007), these galaxies present different properties than field giant elliptical galaxies, which hints to a different evolutionary path (e.g. De Lucia and Blaizot, 2007; Von Der Linden et al., 2007).

1.5.1. The distinct properties of BCG

BCGs have distinct properties from field elliptical galaxies. One of them is that BCGs have distinct surface brightness and luminosity profiles (e.g. Tremaine and Richstone, 1977; Dressler, 1978; Schombert, 1986, 1987, 1988), compared to other elliptical galaxies. In particular, Bernardi et al. (2007) found that when a standard Sérsic or de Vaucouleurs profile is fitted to BCGs, they follow a $r \; \alpha \; L^{0.88}$ relation, where r is the radius and L the luminosity within that radius, in contrast with other elliptical galaxies where this relation is flatter: $r \; \alpha \; L^{0.68}$. Other authors (e.g. Seigar et al., 2007; Donzelli et al., 2011) find that 2-component fits usually better describe the surface brightness profiles of BCGs: one component for the inner galaxy and one component for the stellar envelope. This envelope is another of the BCG specificities (e.g. Oemler, 1976; Schombert, 1986, 1987, 1988). For the most extreme BCGs, it can extend out to 2 Mpc (Oemler, 1976).

Envelopes are not the only particularity of BCG surface brightness profiles: some BCGs have a less luminous core than what would be expected from the usual luminosity profile relations (e.g. Laine et al., 2003). This "missing light" is related to the mass of the central supermassive black hole (e.g. Lauer et al., 2007; McNamara et al., 2009). Moreover, Von Der Linden et al. (2007) found that the dynamical mass-to-light ratio does not vary with the BCG luminosity, in contrast to non-BCGs of similar masses, using a sample of 625 brightest group and cluster galaxies from the SDSS survey (Sloan Digital Sky Survey).

In addition to their surface brightness properties, BCGs have smaller velocity dispersions (σ; e.g. Bernardi et al., 2007) than other elliptical galaxies. Indeed, BCGs have $\sigma - L$ relationships that are shallower than other elliptical galaxies. They also tend to be more metal-rich (e.g. Loubser et al., 2009).

BCGs also have peculiar radio properties: using the same sample as Von Der Linden et al. (2007), Best et al. (2007) found that BCGs are an order of magnitude more likely to host radio-loud AGNs compared to other galaxies of stellar masses below 10^{11} $M_{\odot}$. However, for stellar masses above 5×10^{11} $M_{\odot}$, BCGs are only twice more likely to host radio-loud AGNs than other galaxies. However, the presence of a relaxed cool core in clusters also influences the radio properties of BCGs. For example, Kale et al. (2015) found that radio-loud BCGs seem to be more common in relaxed cool core clusters, while radio-quiet BCGs are more common in merging systems. Moreover, Hogan et al. (2015) found that line emitting BCGs (line emission is indicative of the presence of a strong cool core) generally host more powerful radio sources.

1.5.2. The classical evolution scenario of BCG

One of the first scenarios proposed for BCG formation was that giant galaxies grew by cannibalizing their neighbours and by accreting stars by the process of dynamical friction (Ostriker and Tremaine, 1975). White (1976) wrote that dynamical friction is sufficient to create cD galaxies but Merritt (1985) calculated that this mechanism is too slow to explain the luminosity of the present-epoch BCGs.

Another model was developed based on the idea that cooling flows could be responsible for the BCG formation (e.g. Silk, 1976; Von Der Linden et al., 2007; Fabian, 1994). However, important cooling flows were not observed in galaxy clusters (e.g. McNamara and O'Connell, 1989, , see Section 1.2). Moreover, according to this scenario, BCG stellar populations should be young and blue (e.g. Von Der Linden et al., 2007), while observations show mostly red populations. Nevertheless, several BCGs exhibit a blue core due to small cooling flows (e.g. Bildfell et al., 2008; Loubser et al., 2016, see Section 1.5.4.).

Eleven years ago, using simulations and semi-analytic techniques, De Lucia and Blaizot (2007) suggested that star formation occurred very early in the history of BCGs: at a redshift of $z \sim 5$, 50% of their stars are formed and at $z \sim 3$ this proportion is 80%. BCGs then

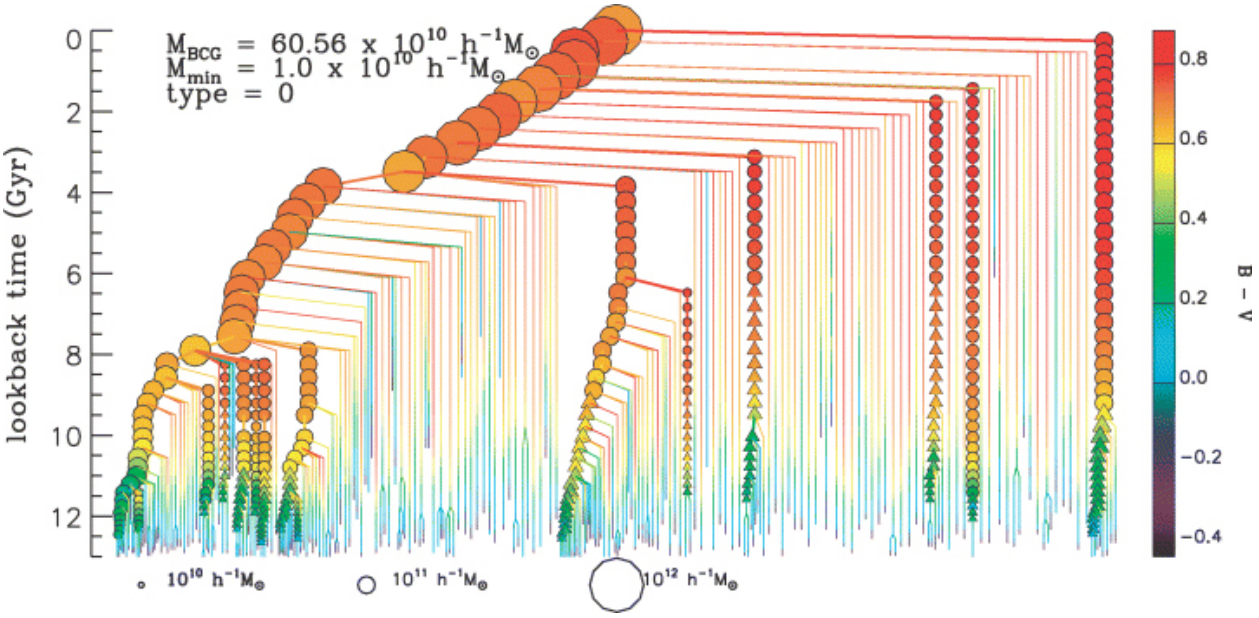

Figure 1.9 A diagram summarizing BCG history, according to De Lucia and Blaizot (2007). Each line corresponds to a BCG progenitor: only the most massive progenitors are shown by a symbol. The colour of the symbol indicates the galaxies B-V colour, more or less equivalent to the level or star formation: green is star forming, red is quiescent. Triangles indicate progenitors that have not yet reached the cluster core; circles are progenitors within the cluster core. According to this diagram, star formation stops early. BCG subsequent growth is due to dry mergers. During approximately one third of its history the BCG is not uniquely defined. From De Lucia and Blaizot (2007).

take form by mergers. As illustred in Figure 1.9, according to De Lucia and Blaizot (2007), BCGs grow mostly by minor dry mergers (a dry merger is a merger with little cold gas, which does not lead to significant star formation, in contrast to a wet merger) and very few major mergers. Also, in this model, the BCG is not uniquely defined before $z \sim 0.7$ and between $z = 1$ and the present epoch, the BCG experiences a mass growth of a factor ~ 3. More recently, Illustris simulations succeeded in creating a quiescent massive elliptical galaxy in the centre of a galaxy cluster (Vogelsberger et al., 2014), but to my knowledge no work has been done on BCGs evolution with the Illustris simulation.

Although each author obtains different constraints on redshift, they generally agree on the idea that most of the star formation occurs before $z = 2$ (e.g. Stott et al., 2008; Burke et al., 2000). The epoch of the BCG growth and the size of the mergers remain controversial. For example, Lidman et al. (2012) found that the stellar mass of BCGs increases by a factor 1.8 ± 0.3 between $z \sim 0.9$ and $z \sim 0.2$ and suggested that major dry mergers may play a significant role in build-ups. In contrast, Stott et al. (2011) found an increase of 30% in size between $z \sim 1$ and $z \sim 0.25$ and concluded that this modest growth may demonstrate that major merging is not an important process in BCGs' late evolution.

1.5.3. Alternative evolution scenarios

Within the last three years, some authors raised concerns with the dry merger evolution scenario based on the De Lucia and Blaizot (2007) simulations. In their high resolution simulations of a Virgo-like galaxy, Martizzi et al. (2012) found that the highest SFRs occur between $z \sim 2$ and $z \sim 1$ and then decreases toward $z \sim 0$.

On the observational side, McDonald et al. (2016) studied the specific star formation rates (sSFR; the star formation rate divided by the stellar mass) of 90 BCGs between $z \sim 0.25$ and $z \sim 1.25$ (see Figure 1.10). These authors suggest a hybrid scenario where BCGs are mostly quiescent at low to medium redshifts. Those that are not quiescent have star formation due to residual cooling flows (see Section 1.5.4). However, at high redshifts, BCG growth is dominated by wet mergers.

Webb et al. (2015b) find significant evidence for in-situ star formation in BCGs at $z \gtrsim 1$. According to them, above $z \sim 1$, BCGs may double their stellar masses by in-situ star formation. Below that redshift, BCGs growth seems dominated by dry mergers.

Although some of those works are exploratory, they suggest that BCG evolution might be more complex than we previously thought. Dry mergers are a dominant component of BCG evolution, but they are not necessarily the dominant process at all epochs.

1.5.4. Star formation in local BCGs

Even if most local BCGs are quiescent, several of them exhibit evidence of modest ongoing star formation (e.g. Bildfell et al., 2008; Pipino et al., 2009; O'Dea et al., 2010; Rawle et al., 2012; Donahue et al., 2011; O'Dea et al., 2008; Rafferty et al., 2008).

Typically, these BCGs harbour $\sim 1\%$ of very young stars, concentrated in a *blue core* (e.g. Bildfell et al., 2008; Pipino et al., 2009; Loubser et al., 2016). They are found in cool core clusters and their star formation is believed to be associated with cooling flows (e.g. Bildfell et al., 2008; Rafferty et al., 2008; Loubser et al., 2016). Specifically, Rafferty et al. (2008) found that star formation in BCGs seem to require an X-ray cooling luminosity superior to the cavity power (see Section 1.4.1), to allow the formation of a cooling flow.

One extreme example of star formation probably induced by a cooling flow is the BCG of the Phoenix cluster. Forming stars at a rate of 610 ± 50 $M_\odot$ yr^{-1} (e.g. McDonald et al., 2015), this BCG exhibits a complex morphology with not only a blue core, but also with star-forming filaments, the longest of them measuring ~ 100 kpc (McDonald et al., 2015, 2013a).

1.5.5. Evaluating the star formation rate

Several tracers exist for the presence of young stars in galaxies. One of them is the far ultraviolet emission (FUV; e.g. Heesen et al., 2014; Bell, 2002; Takeuchi et al., 2010). FUV

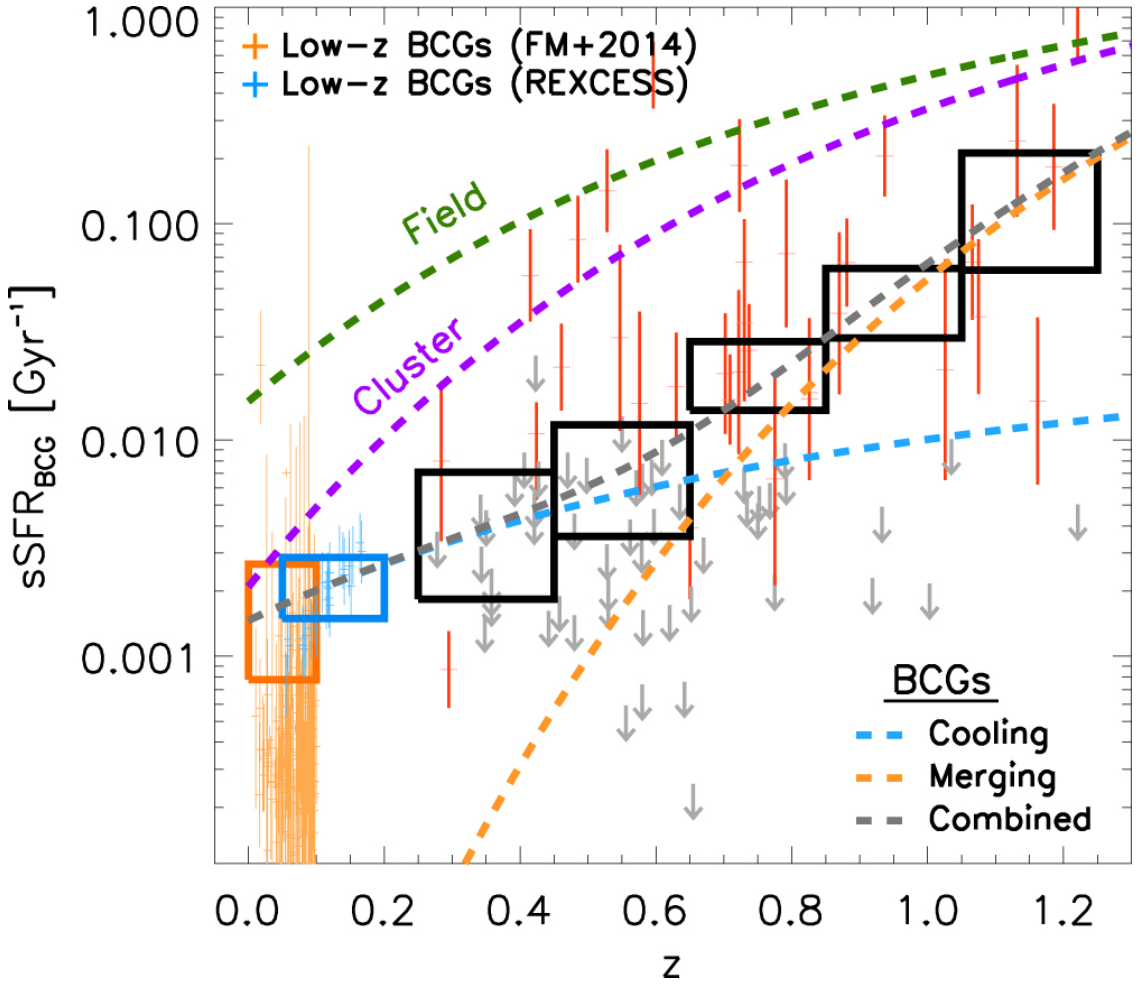

Figure 1.10 According to McDonald et al. (2016), BCGs evolve differently than non-BCG cluster members (purple curve) and field galaxies (green curve). Based on Fraser-McKelvie et al. (2014) (orange crosses) and Haarsma et al. (2010) (blue crosses) low-redshift samples, as well as their own sample (red crosses and grey arrows, black boxes representing the mean sSFR and its uncertainties for each redshift bin), these authors suggested that BCGs switched from wet-merger growth (orange curve) to cooling flow induced growth (blue curve) around z=0.7. From McDonald et al. (2016).

luminosity originates from massive stars, which are a good indicator of ongoing star formation because they are short-lived (e.g. Heesen et al., 2014; Takeuchi et al., 2010). However UV photons are affected by scattering and absorption by dust grains (e.g. Heesen et al., 2014; Takeuchi et al., 2010; Bell, 2002; Kennicutt et al., 2009). Dust grains re-emit absorbed light in the infrared, so FUV and middle or far infrared emission are jointly used in the star formation rate (SFR) estimation (e.g. Heesen et al., 2014; Takeuchi et al., 2010).

Another way of evaluating the star formation rate is by using synchrotron emission (see Section 1.3.1.1) from cosmic-ray electrons (CREs). These electrons are accelerated by supernova shockwaves and emit synchrotron emission in the interstellar medium (e.g. Heesen

et al., 2014; Condon, 1992), typically for $\sim 10^8$ yrs after the supernova explosion (e.g. Heesen et al., 2014). Therefore, CREs are tracers of SFR. Assuming that radio continuum is proportional to the CREs synchrotron emission, Condon et al. (2002) used previous results (Condon, 1992) to develop an empirical law relating the luminosity at 1.4 GHz ($L_{1.4GHz}$) to the star formation rate of an unresolved source (e.g. Heesen et al., 2014; Condon et al., 2002):

$$\frac{SFR}{\mathrm{M}_\odot\ \mathrm{yr}^{-1}} = 0.75 \times 10^{-21} \left(\frac{L_{1.4GHz}}{\mathrm{W\ Hz}^{-1}} \right) \tag{1.31}$$

Using $L_{1.4GHz} = 4\pi A I_{1.4GHz}$ where A is the observed area and $I_{1.4GHz}$ the intensity per unit area at 1.4 GHz, this relation can be modified to measure the SFR surface density in the plane of the sky, Σ'_{SFR} (e.g. Heesen et al., 2014):

$$\frac{\Sigma'_{SFR}}{\mathrm{M}_\odot\ \mathrm{yr}^{-1}\ \mathrm{kpc}^{-2}} = 8.8 \times 10^{-8} \left(\frac{I_{1.4GHz}}{\mathrm{J\ Ster}^{-1}} \right) \tag{1.32}$$

where the projection effect should be corrected using $\Sigma'_{SFR} \times \cos(i) = \Sigma_{SFR}$ (Σ_{SFR} is the corrected surface density), where i is the galaxy inclination angle. This technique has the advantage of being unaffected by dust attenuation (e.g. Heesen et al., 2014).

1.5.6. Cold and warm gas in BCGs

In addition to hot ICM gas, some BCGs contain substantial reservoirs of cold gas. Cold molecular gas (e.g. Edge, 2001; Salomé et al., 2006; McDonald et al., 2014; Russell et al., 2014, 2017) has been detected in BCGs in the centre of cool cores clusters. Nebula of warm ionized gas are sometimes found in systems with cold molecular gas (e.g. Conselice et al., 2001; McDonald et al., 2014). Correspondences are often observed between structures of cold, warm and host gas: for example, Russell et al. (2017) and Salomé et al. (2006) found cold molecular gas filaments wrapped around the X-ray cavities of the Phoenix and Perseus clusters respectively; cold gas filaments seems to be associated with warm gas filaments in the Perseus cluster (Salomé et al., 2006); McDonald et al. (2010) found a correlation between X-ray cooling flows and the Hα luminosity (related to the warm gas nebula) and so on. These connections suggest that the cold gas, the warm gas and the ICM are somehow linked (e.g. Salomé et al., 2006; McDonald et al., 2010; Gendron-Marsolais et al., 2018), although the nature of the link remains mysterious. A recent study unravelled a very complex velocity structure in the Perseus cluster nebula (Gendron-Marsolais et al., 2018), suggesting that the source of ionization might change across the warm gas nebula. Although several nebula of this type have been observed (e.g. McDonald et al., 2010; Gendron-Marsolais et al., 2018), these objects are very poorly understood.

1.6. The SpARCS survey

The acronym SpARCS stands for Spitzer Adaptation of the Red-sequence Clusters Survey. The goal of this survey is to find clusters of galaxies that have a redshift between 1 and 2, using the cluster red-sequence method (e.g. Wilson et al., 2006). This technique uses 2 filters, within a certain field-of-view, to find elliptical galaxies that live inside one predefined specific redshift bin (like $1 \lesssim z \lesssim 2$). The filters must be chosen in order to sample the spectral energy distribution (SED) before and after the so-called "4000 Å break," a dominant feature in quiescent galaxy spectra (e.g. Wilson et al., 2006).

To probe the SED before and after the 4000 Å break, in galaxies between $z \sim 1$ and $z \sim 2$, a good choice of blue filter is the z' filter (e.g. Wilson et al., 2006, 2009). However, to sample the SED red-ward of that feature, the SpARCS collaboration needed data around 3.6 μm, which is a wavelength not observable from the ground (e.g. Wilson et al., 2006). Therefore, the SpARCS collaboration made z'-band images of the fields previously covered by the Spitzer SWIRE survey (see Lonsdale et al., 2003, for a description of this survey) at 3.6, 4.5, 5.8, 8.0, 24, 70 and 160 μm (e.g. Wilson et al., 2006, 2009; Muzzin et al., 2009; Demarco et al., 2010).

The SpARCS survey uses the z'-3.6 μm colour to spot the largest overdensities in 6 fields. The 4 fields in the northern hemisphere, ELAIS-N1, ELAIS-N2, the Lockman Hole and XMM-LSS, were observed in the z' band by the MecaCam camera on the Canada-France-Hawaii Telescope (CFHT). In the southern hemisphere, ELAIS-S1 and Chandra-S fields were observed in z' band by the camera MOSAIC II on the Cerro Tololo Inter-American Observatory (CTIO; e.g. Wilson et al., 2009; Muzzin et al., 2009).

1.6.1. SpARCS1049

SpARCS104922.6+564032.5, hereafter abbreviated in SpARCS1049, is a rich galaxy cluster located at a redshift of $z = 1.7089$ (e.g. Webb et al., 2015a). This cluster has a mass about 3×10^{14} $M_\odot$ (Webb et al., 2017) and a richness of $N_{gal} = 30 \pm 8$ (see Webb et al., 2015a, in this study, the richness is defined as the number of galaxies which are one magnitude brighter or more than the characteristic magnitude at z=1.7, within a 500 kpc radius of the cluster centre). The complex morphology of the core (see the top panel of Figure 1.11), includes a tidal tail of diffuse emission and a *beads on a string* (as Webb et al., 2015a, call it) structure closer to the centre. These structures might be indicative of a major wet merger. They are associated with a SFR of 860 ± 130 $M_\odot$ yr^{-1} (Webb et al., 2015a) calculated by using templates-inferred infrared luminosities from Kirkpatrick et al. (2012) and Chary and Elbaz (2001). Moreover, data from the Spitzer Infrared Spectrograph (IRS) revealed the presence of an AGN in the centre of the BCG. The cluster is also associated with a strong 24 μm emission (Figure 1.11, bottom panel) which seems to originate from one of the beads.

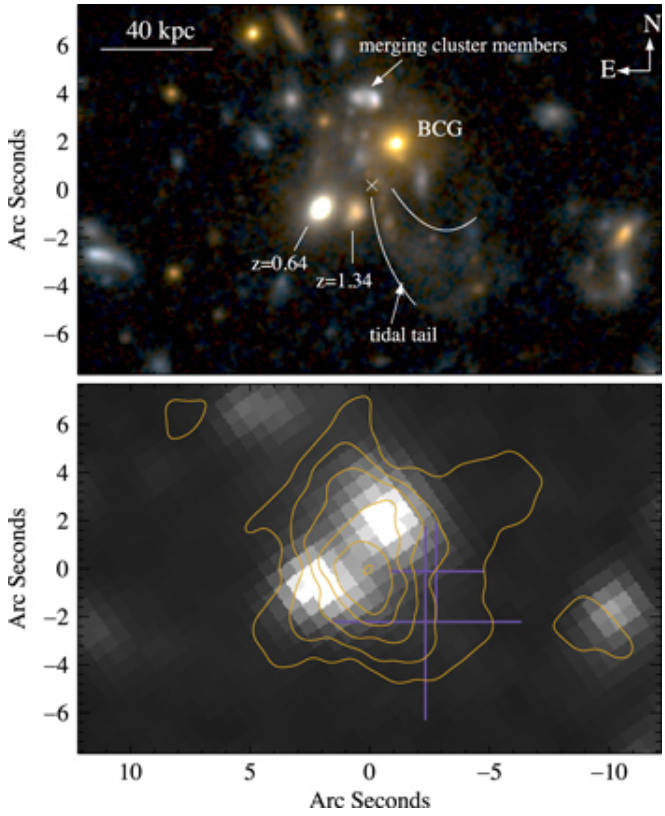

Figure 1.11 Top: A two color (F160W, F105W) image from the Hubble Space Telescope of the centre of SpARCS1049. This image reveals the presence of a tidal tail, prolongated in the cluster centre by a chain of clumps. Bottom: a 3.6 μm image of the same region, with flux contour of the 24 μm emission superimposed. The cross in the top panel shows the position of the centroid of the 24 μm emission. From Webb et al. (2015a).

Webb et al. (2017) found that SpARCS1049 has the largest gas reservoir ever detected in a BCG at $z > 1$: $1.1 \pm 0.1 \times 10^{11}$ $M_{\odot}$. This detection raises a problem with the major merger picture: how could such an amount of gas be deposited by a single major wet merger (e.g. Edge, 2001)? Therefore, additional scenarios have been invoked to explain the presence of this gas (Webb et al., 2017): gas stripping of several galaxies in the cluster centre or a displaced cooling flow.

Whatever is happening in the core of SpARCS1049, it is an indication that dry mergers might not be the only mechanism by which BCGs grow at high redshift. The purpose of this dissertation is to study the radio emission of SpARCS1049. More exactly this dissertation has three goals: study the central AGN in the context of a high-redshift cluster, better constrain the location, extent and intensity of the star formation in SpARCS1049 and see which of the aforementioned scenarios fits with the new radio data.

BIBLIOGRAPHY

Bell, E. F. 2002, Dust-induced Systematic Errors in Ultraviolet-derived Star Formation Rates, *The Astrophysical Journal*, vol. 577, doi:10.1086/342127, p. 150–154, ISSN 0004-637X. URL `http://adsabs.harvard.edu/abs/2002ApJ...577..150B`.

Belloni, T., ed.. 2010, The jet paradigm: from microquasar to quasar, Springer-Verlag, Berlin Heidelberg, Germany.

Bernardi, M., J. B. Hyde, R. K. Sheth, C. J. Miller and R. C. Nichol. 2007, The Luminosities, Sizes, and Velocity Dispersions of Brightest Cluster Galaxies: Implications for Formation History, *The Astronomical Journal*, vol. 133, doi:10.1086/511783, p. 1741–1755, ISSN 0004-6256. URL `http://adsabs.harvard.edu/abs/2007AJ....133.1741B`.

Beskin, V. S. 2010, Magnetohydrodynamic models of astrophysical jets, *Physics-Uspekhi*, vol. 53, nº 12, doi:10.3367/UFNe.0180.201012b.1241, p. 1199–1233, ISSN 1063-7869, 1468-4780. URL `http://arxiv.org/abs/1103.3375`, arXiv: 1103.3375.

Best, P. N., A. von der Linden, G. Kauffmann, T. M. Heckman and C. R. Kaiser. 2007, On the prevalence of radio-loud active galactic nuclei in brightest cluster galaxies: implications for AGN heating of cooling flows, *Monthly Notices of the Royal Astronomical Society*, vol. 379, doi:10.1111/j.1365-2966.2007.11937.x, p. 894–908, ISSN 0035-8711. URL `http://adsabs.harvard.edu/abs/2007MNRAS.379..894B`.

Bildfell, C., H. Hoekstra, A. Babul and A. Mahdavi. 2008, Resurrecting the red from the dead: optical properties of BCGs in X-ray luminous clusters, *Monthly Notices of the Royal Astronomical Society*, vol. 389, doi:10.1111/j.1365-2966.2008.13699.x, p. 1637–1654, ISSN 0035-8711. URL `http://adsabs.harvard.edu/abs/2008MNRAS.389.1637B`.

Blandford, R. D. and D. G. Payne. 1982, Hydromagnetic flows from accretion discs and the production of radio jets, *Monthly Notices of the Royal Astronomical Society*, vol. 199, doi:10.1093/mnras/199.4.883, p. 883–903, ISSN 0035-8711. URL `http://adsabs.harvard.edu/abs/1982MNRAS.199..883B`.

Blandford, R. D. and M. J. Rees. 1974, A 'twin-exhaust' model for double radio sources, *Monthly Notices of the Royal Astronomical Society*, vol. 169, doi:10.1093/mnras/169.3.395, p. 395–415, ISSN 0035-8711. URL `http://adsabs.harvard.edu/abs/1974MNRAS.169..395B`.

Bridle, A. H. and R. A. Perley. 1984, Extragalactic Radio Jets, *Annual Review of Astronomy and Astrophysics*, vol. 22, doi:10.1146/annurev.aa.22.090184.001535, p. 319–358, ISSN 0066-4146. URL http://adsabs.harvard.edu/abs/1984ARA%26A..22..319B.

Burke, D. J., C. A. Collins and R. G. Mann. 2000, Cluster Selection and the Evolution of Brightest Cluster Galaxies, *The Astrophysical Journal Letters*, vol. 532, doi:10.1086/312579, p. L105–L108, ISSN 0004-637X. URL http://adsabs.harvard.edu/abs/2000ApJ...532L.105B.

Burns, J. O. 1990, The radio properties of cD galaxies in Abell clusters. I - an X-ray selected sample, *The Astronomical Journal*, vol. 99, doi:10.1086/115307, p. 14–30, ISSN 0004-6256. URL http://adsabs.harvard.edu/abs/1990AJ.....99...14B.

Charbonneau, P. 2016, PHY 6756, Fluides astrophysiques, Notes de cours, URL http://www.astro.umontreal.ca/~paulchar/phy6756/phy6756.pdf.

Chary, R. and D. Elbaz. 2001, Interpreting the Cosmic Infrared Background: Constraints on the Evolution of the Dust-enshrouded Star Formation Rate, *The Astrophysical Journal*, vol. 556, doi:10.1086/321609, p. 562–581, ISSN 0004-637X. URL http://adsabs.harvard.edu/abs/2001ApJ...556..562C.

Chen, Y., T. H. Reiprich, H. Böhringer, Y. Ikebe and Y.-Y. Zhang. 2007, Statistics of X-ray observables for the cooling-core and non-cooling core galaxy clusters, *Astronomy and Astrophysics*, vol. 466, doi:10.1051/0004-6361:20066471, p. 805–812, ISSN 0004-6361. URL http://adsabs.harvard.edu/abs/2007A%26A...466..805C.

Choudhuri, A. R. 1998, The physics of fluids and plasmas, Cambridge University Press, Cambridge, United Kingdom.

Churazov, E., R. Sunyaev, W. Forman and H. Böhringer. 2002, Cooling flows as a calorimeter of active galactic nucleus mechanical power, *Monthly Notices of the Royal Astronomical Society*, vol. 332, doi:10.1046/j.1365-8711.2002.05332.x, p. 729–734, ISSN 0035-8711. URL http://adsabs.harvard.edu/abs/2002MNRAS.332..729C.

Clarke, T. E., C. L. Sarazin, E. L. Blanton, D. M. Neumann and N. E. Kassim. 2005, Low-Frequency Radio Observations of X-Ray Ghost Bubbles in A2597: A History of Radio Activity in the Core, *The Astrophysical Journal*, vol. 625, doi:10.1086/429717, p. 748–753, ISSN 0004-637X. URL http://adsabs.harvard.edu/abs/2005ApJ...625..748C.

Condon, J. J. 1992, Radio emission from normal galaxies, *Annual Review of Astronomy and Astrophysics*, vol. 30, doi:10.1146/annurev.aa.30.090192.003043, p. 575–611, ISSN 0066-4146. URL http://adsabs.harvard.edu/abs/1992ARA%26A..30..575C.

Condon, J. J., W. D. Cotton and J. J. Broderick. 2002, Radio Sources and Star Formation in the Local Universe, *The Astronomical Journal*, vol. 124, doi:10.1086/341650, p. 675–689, ISSN 0004-6256. URL http://adsabs.harvard.edu/abs/2002AJ....124..675C.

Condon, J. J. and S. M. Ransom. 2016, Essential radio astronomy, URL https://science.nrao.edu/opportunities/courses/era.

Conselice, C. J., J. S. Gallagher, III and R. F. G. Wyse. 2001, On the Nature of the NGC 1275 System, *The Astronomical Journal*, vol. 122, doi:10.1086/323534, p. 2281–2300, ISSN 0004-6256. URL http://adsabs.harvard.edu/abs/2001AJ....122.2281C.

Courvoisier, T. J.-L. 2013, High energy astrophysics, an introduction, Springer-Verlag, Berlin Heidelberg, Germany.

De Lucia, G. and J. Blaizot. 2007, The hierarchical formation of the brightest cluster galaxies, *Monthly Notices of the Royal Astronomical Society*, vol. 375, doi:10.1111/j.1365-2966.2006.11287.x, p. 2–14, ISSN 0035-8711. URL http://adsabs.harvard.edu/abs/2007MNRAS.375....2D.

Demarco, R., G. Wilson, A. Muzzin, M. Lacy, J. Surace, H. K. C. Yee, H. Hoekstra, K. Blindert and D. Gilbank. 2010, Spectroscopic Confirmation of Three Red-sequence Selected Galaxy Clusters at z = 0.87, 1.16, and 1.21 from the SpARCS Survey, *The Astrophysical Journal*, vol. 711, doi:10.1088/0004-637X/711/2/1185, p. 1185–1197, ISSN 0004-637X. URL http://adsabs.harvard.edu/abs/2010ApJ...711.1185D.

Donahue, M., G. E. de Messières, R. W. O'Connell, G. M. Voit, A. Hoffer, B. R. McNamara and P. E. J. Nulsen. 2011, Polycyclic Aromatic Hydrocarbons, Ionized Gas, and Molecular Hydrogen in Brightest Cluster Galaxies of Cool-core Clusters of Galaxies, *The Astrophysical Journal*, vol. 732, doi:10.1088/0004-637X/732/1/40, p. 40, ISSN 0004-637X. URL http://adsabs.harvard.edu/abs/2011ApJ...732...40D.

Donzelli, C. J., H. Muriel and J. P. Madrid. 2011, The Luminosity Profiles of Brightest Cluster Galaxies, *The Astrophysical Journal Supplement Series*, vol. 195, doi:10.1088/0067-0049/195/2/15, p. 15, ISSN 0067-0049. URL http://adsabs.harvard.edu/abs/2011ApJS..195...15D.

Dressler, A. 1978, A comprehensive study of 12 very rich clusters of galaxies. I - Photometric technique and analysis of the luminosity function, *The Astrophysical Journal*, vol. 223, doi:10.1086/156310, p. 765–775, ISSN 0004-637X. URL http://adsabs.harvard.edu/abs/1978ApJ...223..765D.

Dunn, R. J. H. and A. C. Fabian. 2008, Investigating heating and cooling in the BCS and B55 cluster samples, *Monthly Notices of the Royal Astronomical Society*, vol. 385, doi:10.1111/j.1365-2966.2008.12898.x, p. 757–768, ISSN 0035-8711. URL http://adsabs.harvard.edu/abs/2008MNRAS.385..757D.

Edge, A. C. 2001, The detection of molecular gas in the central galaxies of cooling flow clusters, *Monthly Notices of the Royal Astronomical Society*, vol. 328, doi:10.1046/j.1365-8711.2001.04802.x, p. 762–782, ISSN 0035-8711. URL http://adsabs.harvard.edu/abs/2001MNRAS.328..762E.

Ettori, S., F. Gastaldello, M. Gitti, E. O'Sullivan, M. Gaspari, F. Brighenti, L. David and A. C. Edge. 2013, Cold fronts and metal anisotropies in the X-ray cool core of the galaxy cluster Zw 1742+3306, *Astronomy and Astrophysics*, vol. 555, doi:10.1051/0004-6361/201321107, p. A93, ISSN 0004-6361. URL http://adsabs.harvard.edu/abs/2013A%26A...555A..93E.

Fabian, A. C. 1994, Cooling Flows in Clusters of Galaxies, *Annual Review of Astronomy and Astrophysics*, vol. 32, doi:10.1146/annurev.aa.32.090194.001425, p. 277–318, ISSN 0066-4146. URL http://adsabs.harvard.edu/abs/1994ARA%26A..32..277F.

Fabian, A. C. 2012, Observational Evidence of AGN Feedback, *Annual Review of Astronomy and Astrophysics*, vol. 50, nº 1, doi:10.1146/annurev-astro-081811-125521, p. 455–489, ISSN 0066-4146, 1545-4282. URL http://arxiv.org/abs/1204.4114, arXiv: 1204.4114.

Fabian, A. C., A. Celotti, K. M. Blundell, N. E. Kassim and R. A. Perley. 2002, The properties of the X-ray holes in the intracluster medium of the Perseus cluster, *Monthly Notices of the Royal Astronomical Society*, vol. 331, doi:10.1046/j.1365-8711.2002.05182.x, p. 369–375, ISSN 0035-8711. URL http://adsabs.harvard.edu/abs/2002MNRAS.331..369F.

Fabian, A. C., S. A. Walker, H. R. Russell, C. Pinto, J. S. Sanders and C. S. Reynolds. 2017, Do sound waves transport the AGN energy in the Perseus Cluster?, *Monthly Notices of the Royal Astronomical Society: Letters*, vol. 464, nº 1, doi:10.1093/mnrasl/slw170, p. L1–L5, ISSN 1745-3925, 1745-3933. URL http://arxiv.org/abs/1608.07088, arXiv: 1608.07088.

Fanaroff, B. L. and J. M. Riley. 1974, The morphology of extragalactic radio sources of high and low luminosity, *Monthly Notices of the Royal Astronomical Society*, vol. 167, doi:10.1093/mnras/167.1.31P, p. 31P–36P, ISSN 0035-8711. URL http://adsabs.harvard.edu/abs/1974MNRAS.167P..31F.

Fraser-McKelvie, A., M. J. I. Brown and K. A. Pimbblet. 2014, The rarity of star formation in brightest cluster galaxies as measured by WISE, *Monthly Notices of the Royal Astronomical Society*, vol. 444, doi:10.1093/mnrasl/slu117, p. L63–L67, ISSN 0035-8711. URL http://adsabs.harvard.edu/abs/2014MNRAS.444L..63F.

Gendron-Marsolais, M., J. Hlavacek-Larrondo, T. B. Martin, L. Drissen, M. McDonald, A. C. Fabian, A. C. Edge, S. L. Hamer, B. McNamara and G. Morrison. 2018, Revealing the velocity structure of the filamentary nebula in NGC 1275 in its entirety, *arXiv:1802.00031 [astro-ph]*. URL http://arxiv.org/abs/1802.00031, arXiv: 1802.00031.

Gendron-Marsolais, M., J. Hlavacek-Larrondo, R. J. van Weeren, T. Clarke, A. C. Fabian, H. T. Intema, G. B. Taylor, K. M. Blundell and J. S. Sanders. 2017, Deep 230-470 MHz VLA Observations of the mini-halo in the Perseus Cluster, *Monthly Notices of the Royal Astronomical Society*, vol. 469, nº 4, doi:10.1093/mnras/stx1042, p. 3872–3880, ISSN 0035-8711, 1365-2966. URL http://arxiv.org/abs/1701.03791, arXiv: 1701.03791.

Haarsma, D. B., L. Leisman, M. Donahue, S. Bruch, H. Böhringer, J. H. Croston, G. W. Pratt, G. M. Voit, M. Arnaud and D. Pierini. 2010, Brightest Cluster Galaxies and Core Gas Density in REXCESS Clusters, *The Astrophysical Journal*, vol. 713, doi:10.1088/0004-637X/713/2/1037, p. 1037–1047, ISSN 0004-637X. URL http://adsabs.harvard.edu/abs/2010ApJ...713.1037H.

Heesen, V., E. Brinks, A. K. Leroy, G. Heald, R. Braun, F. Bigiel and R. Beck. 2014, The Radio Continuum-Star Formation Rate Relation in WSRT SINGS Galaxies, *The Astronomical Journal*, vol. 147, doi:10.1088/0004-6256/147/5/103, p. 103, ISSN 0004-6256. URL http://adsabs.harvard.edu/abs/2014AJ....147..103H.

Hines, D. C., J. A. Eilek and F. N. Owen. 1989, Filaments in the radio lobes of M87, *The Astrophysical Journal*, vol. 347, doi:10.1086/168163, p. 713–726, ISSN 0004-637X. URL http://adsabs.harvard.edu/abs/1989ApJ...347..713H.

Hlavacek-Larrondo, J. 2012, Extreme AGN Feedback in Highly-Luminous Clusters of Galaxies, Ph.D. Thesis, University of Cambridge, United-Kingdom.

Hlavacek-Larrondo, J., S. W. Allen, G. B. Taylor, A. C. Fabian, R. E. A. Canning, N. Werner, J. S. Sanders, C. K. Grimes, S. Ehlert and A. von der Linden. 2013, Probing the Extreme Realm of Active Galactic Nucleus Feedback in the Massive Galaxy Cluster, RX J1532.9+3021, *The Astrophysical Journal*, vol. 777, doi:10.1088/0004-637X/777/2/163, p. 163, ISSN 0004-637X. URL http://adsabs.harvard.edu/abs/2013ApJ...777..163H.

Hogan, M. T., A. C. Edge, J. Hlavacek-Larrondo, K. J. B. Grainge, S. L. Hamer, E. K. Mahony, H. R. Russell, A. C. Fabian, B. R. McNamara and R. J. Wilman. 2015, A Comprehensive Study of the Radio Properties of Brightest Cluster Galaxies, *Monthly Notices of the Royal Astronomical Society*, vol. 453, n° 2, doi:10.1093/mnras/stv1517, p. 1201–1222, ISSN 0035-8711, 1365-2966. URL http://arxiv.org/abs/1507.03019, arXiv: 1507.03019.

Hudson, D. S., R. Mittal, T. H. Reiprich, P. E. J. Nulsen, H. Andernach and C. L. Sarazin. 2010, What is a cool-core cluster? a detailed analysis of the cores of the X-ray flux-limited HIFLUGCS cluster sample, *Astronomy and Astrophysics*, vol. 513, doi:10.1051/0004-6361/200912377, p. A37, ISSN 0004-6361. URL http://adsabs.harvard.edu/abs/2010A%26A...513A..37H.

Jetha, N. N., M. J. Hardcastle, A. Babul, E. O'Sullivan, T. J. Ponman, S. Raychaudhury and J. Vrtilek. 2008, The nature of the ghost cavity in the NGC 741 group, *Monthly Notices of the Royal Astronomical Society*, vol. 384, doi:10.1111/j.1365-2966.2007.12829.x, p. 1344–1354, ISSN 0035-8711. URL http://adsabs.harvard.edu/abs/2008MNRAS.384.1344J.

Kale, R., T. Venturi, R. Cassano, S. Giacintucci, S. Bardelli, D. Dallacasa and E. Zucca. 2015, Brightest cluster galaxies in the extended GMRT radio halo cluster sample. Radio properties and cluster dynamics, *Astronomy and Astrophysics*, vol. 581, doi:10.1051/0004-6361/201526341, p. A23, ISSN 0004-6361. URL http://adsabs.harvard.edu/abs/2015A%26A...581A..23K.

Kennicutt, R. C., Jr., C.-N. Hao, D. Calzetti, J. Moustakas, D. A. Dale, G. Bendo, C. W. Engelbracht, B. D. Johnson and J. C. Lee. 2009, Dust-corrected Star Formation Rates of Galaxies. I. Combinations of Hα and Infrared Tracers, *The Astrophysical Journal*, vol. 703, doi:10.1088/0004-637X/703/2/1672, p. 1672–1695, ISSN 0004-637X. URL http://adsabs.harvard.edu/abs/2009ApJ...703.1672K.

Kirkpatrick, A., A. Pope, D. M. Alexander, V. Charmandaris, E. Daddi, M. Dickinson, D. Elbaz, J. Gabor, H. S. Hwang, R. Ivison, J. Mullaney, M. Pannella, D. Scott, B. Altieri, H. Aussel, F. Bournaud, V. Buat, D. Coia, H. Dannerbauer, K. Dasyra, J. Kartaltepe, R. Leiton, L. Lin, G. Magdis, B. Magnelli, G. Morrison, P. Popesso and I. Valtchanov. 2012, GOODS-Herschel: Impact of Active Galactic Nuclei and Star Formation Activity on Infrared Spectral Energy Distributions at High Redshift, *The Astrophysical Journal*, vol. 759, doi:10.1088/0004-637X/759/2/139, p. 139, ISSN 0004-637X. URL http://adsabs.harvard.edu/abs/2012ApJ...759..139K.

Laine, S., R. P. van der Marel, T. R. Lauer, M. Postman, C. P. O'Dea and F. N. Owen. 2003, Hubble Space Telescope Imaging of Brightest Cluster Galaxies, *The Astronomical Journal*, vol. 125, doi:10.1086/345823, p. 478–505, ISSN 0004-6256. URL http://adsabs.harvard.edu/abs/2003AJ...125..478L.

Lauer, T. R., S. M. Faber, D. Richstone, K. Gebhardt, S. Tremaine, M. Postman, A. Dressler, M. C. Aller, A. V. Filippenko, R. Green, L. C. Ho, J. Kormendy, J. Magorrian and J. Pinkney. 2007, The Masses of Nuclear Black Holes in Luminous Elliptical Galaxies and Implications for the Space Density of the Most Massive Black Holes, *The Astrophysical Journal*, vol. 662, doi: 10.1086/518223, p. 808–834, ISSN 0004-637X. URL http://adsabs.harvard.edu/abs/2007ApJ...662..808L.

Lidman, C., J. Suherli, A. Muzzin, G. Wilson, R. Demarco, S. Brough, A. Rettura, J. Cox, A. DeGroot, H. K. C. Yee, D. Gilbank, H. Hoekstra, M. Balogh, E. Ellingson, A. Hicks, J. Nantais, A. Noble, M. Lacy, J. Surace and T. Webb. 2012, Evidence for significant growth in the stellar mass of brightest cluster galaxies over the past 10 billion years, *Monthly Notices of the Royal Astronomical Society*, vol. 427, doi:10.1111/j.1365-2966.2012.21984.x, p. 550–568, ISSN 0035-8711. URL http://adsabs.harvard.edu/abs/2012MNRAS.427..550L.

Lin, Y.-T. and J. J. Mohr. 2004, K-band Properties of Galaxy Clusters and Groups: Brightest Cluster Galaxies and Intracluster Light, *The Astrophysical Journal*, vol. 617, doi:10.1086/425412, p. 879–895, ISSN 0004-637X. URL http://adsabs.harvard.edu/abs/2004ApJ...617..879L.

Lonsdale, C. J., H. E. Smith, M. Rowan-Robinson, J. Surace, D. Shupe, C. Xu, S. Oliver, D. Padgett, F. Fang, T. Conrow, A. Franceschini, N. Gautier, M. Griffin, P. Hacking, F. Masci, G. Morrison, J. O'Linger, F. Owen, I. Pérez-Fournon, M. Pierre, R. Puetter, G. Stacey, S. Castro, M. d. C. Polletta, D. Farrah, T. Jarrett, D. Frayer, B. Siana, T. Babbedge, S. Dye, M. Fox, E. Gonzalez-Solares, M. Salaman, S. Berta, J. J. Condon, H. Dole and S. Serjeant. 2003, SWIRE: The SIRTF Wide-Area Infrared Extragalactic Survey, *Publications of the Astronomical Society of the Pacific*, vol. 115, doi:10.1086/376850, p. 897–927, ISSN 0004-6280. URL http://adsabs.harvard.edu/abs/2003PASP..115..897L.

Loubser, S. I., A. Babul, H. Hoekstra, A. Mahdavi, M. Donahue, C. Bildfell and G. M. Voit. 2016, The regulation of star formation in cool-core clusters: imprints on the stellar populations of brightest cluster galaxies, *Monthly Notices of the Royal Astronomical Society*, vol. 456, nº 2, doi:10.1093/mnras/stv2784, p. 1565–1578, ISSN 0035-8711, 1365-2966. URL http://arxiv.org/abs/1511.07884, arXiv: 1511.07884.

Loubser, S. I., P. Sánchez-Blázquez, A. E. Sansom and I. K. Soechting. 2009, Stellar populations in the centres of brightest cluster galaxies, *Monthly Notices of the Royal Astronomical Society*, vol. 398, doi:10.1111/j.1365-2966.2009.15171.x, p. 133–156, ISSN 0035-8711. URL http://adsabs.harvard.edu/abs/2009MNRAS.398..133L.

Machacek, M., A. Dosaj, W. Forman, C. Jones, M. Markevitch, A. Vikhlinin, A. Warmflash and R. Kraft. 2005, Infall of the Elliptical Galaxy NGC 1404 into the Fornax Cluster, *The Astrophysical Journal*, vol. 621, doi:10.1086/427548, p. 663–672, ISSN 0004-637X. URL http://adsabs.harvard.edu/abs/2005ApJ...621..663M.

Markevitch, M. and A. Vikhlinin. 2007, Shocks and cold fronts in galaxy clusters, *Physics Reports*, vol. 443, nº 1, doi:10.1016/j.physrep.2007.01.001, p. 1–53, ISSN 03701573. URL http://arxiv.org/abs/astro-ph/0701821, arXiv: astro-ph/0701821.

Martizzi, D., R. Teyssier and B. Moore. 2012, The formation of the brightest cluster galaxies in cosmological simulations: the case for active galactic nucleus feedback, *Monthly Notices of the Royal Astronomical Society*, vol. 420, doi:10.1111/j.1365-2966.2011.19950.x, p. 2859–2873, ISSN 0035-8711. URL http://adsabs.harvard.edu/abs/2012MNRAS.420.2859M.

Mazzotta, P., A. C. Edge and M. Markevitch. 2003, A Chandra Study of the Complex Structure in the Core of 2a 0335+096, *The Astrophysical Journal*, vol. 596, doi:10.1086/377633, p. 190–203, ISSN 0004-637X. URL http://adsabs.harvard.edu/abs/2003ApJ...596..190M.

McDonald, M., B. Benson, S. Veilleux, M. W. Bautz and C. L. Reichardt. 2013a, An HST/WFC3-UVIS View of the Starburst in the Cool Core of the Phoenix Cluster, *The Astrophysical Journal Letters*, vol. 765, doi:10.1088/2041-8205/765/2/L37, p. L37, ISSN 0004-637X. URL http://adsabs.harvard.edu/abs/2013ApJ...765L..37M.

McDonald, M., B. A. Benson, A. Vikhlinin, B. Stalder, L. E. Bleem, T. de Haan, H. W. Lin, K. A. Aird, M. L. N. Ashby, M. W. Bautz, M. Bayliss, S. Bocquet, M. Brodwin, J. E. Carlstrom, C. L. Chang, H. M. Cho, A. Clocchiatti, T. M. Crawford, A. T. Crites, S. Desai, M. A. Dobbs, J. P. Dudley, R. J. Foley, W. R. Forman, E. M. George, D. Gettings, M. D. Gladders, A. H. Gonzalez, N. W. Halverson, F. W. High, G. P. Holder, W. L. Holzapfel, S. Hoover, J. D. Hrubes, C. Jones, M. Joy, R. Keisler, L. Knox, A. T. Lee, E. M. Leitch, J. Liu, M. Lueker, D. Luong-Van, A. Mantz, D. P. Marrone, J. J. McMahon, J. Mehl, S. S. Meyer, E. D. Miller, L. Mocanu, J. J. Mohr, T. E. Montroy, S. S. Murray, D. Nurgaliev, S. Padin, T. Plagge, C. Pryke, C. L. Reichardt, A. Rest, J. Ruel, J. E. Ruhl, B. R. Saliwanchik, A. Saro, J. T. Sayre, K. K. Schaffer, E. Shirokoff, J. Song, R. Šuhada, H. G. Spieler, S. A. Stanford, Z. Staniszewski, A. A. Stark, K. Story, A. van Engelen, K. Vanderlinde, J. D. Vieira, R. Williamson, O. Zahn and A. Zenteno. 2013b, The Growth of Cool Cores and Evolution of Cooling Properties in a Sample of 83 Galaxy Clusters at $0.3 < z < 1.2$ Selected from the SPT-SZ Survey, *The Astrophysical Journal*, vol. 774, doi:10.1088/0004-637X/774/1/23, p. 23, ISSN 0004-637X. URL http://adsabs.harvard.edu/abs/2013ApJ...774...23M.

McDonald, M., B. R. McNamara, R. J. van Weeren, D. E. Applegate, M. Bayliss, M. W. Bautz, B. A. Benson, J. E. Carlstrom, L. E. Bleem, M. Chatzikos, A. C. Edge, A. C. Fabian, G. P. Garmire, J. Hlavacek-Larrondo, C. Jones-Forman, A. B. Mantz, E. D. Miller, B. Stalder, S. Veilleux and J. A. ZuHone. 2015, Deep Chandra, HST-COS, and Megacam Observations of the Phoenix Cluster: Extreme Star Formation and AGN Feedback on Hundred Kiloparsec Scales, *The Astrophysical Journal*, vol. 811, doi:10.1088/0004-637X/811/2/111, p. 111, ISSN 0004-637X. URL http://adsabs.harvard.edu/abs/2015ApJ...811..111M.

McDonald, M., B. Stalder, M. Bayliss, S. W. Allen, D. E. Applegate, M. L. N. Ashby, M. Bautz, B. A. Benson, L. E. Bleem, M. Brodwin, J. E. Carlstrom, I. Chiu, S. Desai, A. H. Gonzalez, J. Hlavacek-Larrondo, W. L. Holzapfel, D. P. Marrone, E. D. Miller, C. L. Reichardt, B. R. Saliwanchik, A. Saro, T. Schrabback, S. A. Stanford, A. A. Stark, J. D. Vieira and A. Zenteno. 2016, Star-forming Brightest Cluster Galaxies at $0.25 < z < 1.25$: A Transitioning Fuel Supply, *The Astrophysical Journal*, vol. 817, doi:10.3847/0004-637X/817/2/86, p. 86, ISSN 0004-637X. URL http://adsabs.harvard.edu/abs/2016ApJ...817...86M.

McDonald, M., M. Swinbank, A. C. Edge, D. J. Wilner, S. Veilleux, B. A. Benson, M. T. Hogan, D. P. Marrone, B. R. McNamara, L. H. Wei, M. B. Bayliss and M. W. Bautz. 2014, The State of the Warm and Cold Gas in the Extreme Starburst at the Core of the Phoenix Galaxy Cluster (SPT-CLJ2344-4243), *The Astrophysical Journal*, vol. 784, doi:10.1088/0004-637X/784/1/18, p. 18, ISSN 0004-637X. URL `http://adsabs.harvard.edu/abs/2014ApJ...784...18M`.

McDonald, M., S. Veilleux, D. S. N. Rupke and R. Mushotzky. 2010, On the Origin of the Extended Hα Filaments in Cooling Flow Clusters, *The Astrophysical Journal*, vol. 721, doi:10.1088/0004-637X/721/2/1262, p. 1262–1283, ISSN 0004-637X. URL `http://adsabs.harvard.edu/abs/2010ApJ...721.1262M`.

McKinney, J. C. and R. D. Blandford. 2009, Stability of relativistic jets from rotating, accreting black holes via fully three-dimensional magnetohydrodynamic simulations, *Monthly Notices of the Royal Astronomical Society*, vol. 394, doi:10.1111/j.1745-3933.2009.00625.x, p. L126–L130, ISSN 0035-8711. URL `http://adsabs.harvard.edu/abs/2009MNRAS.394L.126M`.

McNamara, B. R., F. Kazemzadeh, D. A. Rafferty, L. Bîrzan, P. E. J. Nulsen, C. C. Kirkpatrick and M. W. Wise. 2009, An Energetic AGN Outburst Powered by a Rapidly Spinning Supermassive Black Hole or an Accreting Ultramassive Black Hole, *The Astrophysical Journal*, vol. 698, doi:10.1088/0004-637X/698/1/594, p. 594–605, ISSN 0004-637X. URL `http://adsabs.harvard.edu/abs/2009ApJ...698..594M`.

McNamara, B. R. and P. E. J. Nulsen. 2007, Heating Hot Atmospheres with Active Galactic Nuclei, *Annual Review of Astronomy and Astrophysics*, vol. 45, n^{o} 1, doi:10.1146/annurev.astro.45.051806.110625, p. 117–175, ISSN 0066-4146, 1545-4282. URL `http://arxiv.org/abs/0709.2152`, arXiv: 0709.2152.

McNamara, B. R. and P. E. J. Nulsen. 2012, Mechanical Feedback from Active Galactic Nuclei in Galaxies, Groups, and Clusters, *New Journal of Physics*, vol. 14, n^{o} 5, doi:10.1088/1367-2630/14/5/055023, p. 055 023, ISSN 1367-2630. URL `http://arxiv.org/abs/1204.0006`, arXiv: 1204.0006.

McNamara, B. R. and R. W. O'Connell. 1989, Star formation in cooling flows in clusters of galaxies, *The Astronomical Journal*, vol. 98, doi:10.1086/115275, p. 2018–2043, ISSN 0004-6256. URL `http://adsabs.harvard.edu/abs/1989AJ.....98.2018M`.

McNamara, B. R., M. W. Wise, P. E. J. Nulsen, L. P. David, C. L. Carilli, C. L. Sarazin, C. P. O'Dea, J. Houck, M. Donahue, S. Baum, M. Voit, R. W. O'Connell and A. Koekemoer. 2001, Discovery of Ghost Cavities in the X-Ray Atmosphere of Abell 2597, *The Astrophysical Journal Letters*, vol. 562, doi:10.1086/338326, p. L149–L152, ISSN 0004-637X. URL `http://adsabs.harvard.edu/abs/2001ApJ...562L.149M`.

Merritt, D. 1985, Relaxation and tidal stripping in rich clusters of galaxies. III - Growth of a massive central galaxy, *The Astrophysical Journal*, vol. 289, doi:10.1086/162860, p. 18–32, ISSN 0004-637X. URL `http://adsabs.harvard.edu/abs/1985ApJ...289...18M`.

Mignone, A., P. Rossi, G. Bodo, A. Ferrari and S. Massaglia. 2010, High-resolution 3d relativistic MHD simulations of jets, *Monthly Notices of the Royal Astronomical Society*, vol. 402, doi:10.

1111/j.1365-2966.2009.15642.x, p. 7–12, ISSN 0035-8711. URL http://adsabs.harvard.edu/abs/2010MNRAS.402....7M.

Muzzin, A., G. Wilson, H. K. C. Yee, H. Hoekstra, D. Gilbank, J. Surace, M. Lacy, K. Blindert, S. Majumdar, R. Demarco, J. P. Gardner, M. Gladders and C. Lonsdale. 2009, Spectroscopic Confirmation of Two Massive Red-Sequence-Selected Galaxy Clusters at z ~ 1.2 in the SpARCS-North Cluster Survey, *The Astrophysical Journal*, vol. 698, doi:10.1088/0004-637X/698/2/1934, p. 1934–1942, ISSN 0004-637X. URL http://adsabs.harvard.edu/abs/2009ApJ...698.1934M.

O'Dea, C. P., S. A. Baum, G. Privon, J. Noel-Storr, A. C. Quillen, N. Zufelt, J. Park, A. Edge, H. Russell, A. C. Fabian, M. Donahue, C. L. Sarazin, B. McNamara, J. N. Bregman and E. Egami. 2008, An Infrared Survey of Brightest Cluster Galaxies. II. Why are Some Brightest Cluster Galaxies Forming Stars?, *The Astrophysical Journal*, vol. 681, doi:10.1086/588212, p. 1035–1045, ISSN 0004-637X. URL http://adsabs.harvard.edu/abs/2008ApJ...681.1035O.

O'Dea, K. P., A. C. Quillen, C. P. O'Dea, G. R. Tremblay, B. T. Snios, S. A. Baum, K. Christiansen, J. Noel-Storr, A. C. Edge, M. Donahue and G. M. Voit. 2010, Hubble Space Telescope Far-ultraviolet Observations of Brightest Cluster Galaxies: The Role of Star Formation in Cooling Flows and BCG Evolution, *The Astrophysical Journal*, vol. 719, doi:10.1088/0004-637X/719/2/1619, p. 1619–1632, ISSN 0004-637X. URL http://adsabs.harvard.edu/abs/2010ApJ...719.1619O.

Oemler, A., Jr. 1976, The structure of elliptical and cD galaxies., *The Astrophysical Journal*, vol. 209, doi:10.1086/154769, p. 693–709, ISSN 0004-637X. URL http://adsabs.harvard.edu/abs/1976ApJ...209..693O.

O'Hara, T. B., J. J. Mohr and M. A. Guerrero. 2004, A Chandra Study of the Effects of a Major Merger on the Structure of A2319, *The Astrophysical Journal*, vol. 604, doi:10.1086/382063, p. 604–613, ISSN 0004-637X. URL http://adsabs.harvard.edu/abs/2004ApJ...604..604O.

Ostriker, J. P. and S. D. Tremaine. 1975, Another evolutionary correction to the luminosity of giant galaxies, *The Astrophysical Journal Letters*, vol. 202, doi:10.1086/181992, p. L113–L117, ISSN 0004-637X. URL http://adsabs.harvard.edu/abs/1975ApJ...202L.113O.

Oswalt, T. D. and W. C. Keel, eds.. 2013, Planets, stars and stellar systems volume 6: Extragalactic astronomy and cosmology, Springer.

Pipino, A., S. Kaviraj, C. Bildfell, A. Babul, H. Hoekstra and J. Silk. 2009, Evidence for recent star formation in BCGs: a correspondence between blue cores and UV excess, *Monthly Notices of the Royal Astronomical Society*, vol. 395, doi:10.1111/j.1365-2966.2009.14534.x, p. 462–471, ISSN 0035-8711. URL http://adsabs.harvard.edu/abs/2009MNRAS.395..462P.

Plionis, M., O. López-Cruz and D. Hughes, eds.. 2008, A pan-chromatic view of clusters of galaxies and the large-scale structure, Lecture notes in physics, 740, Springer, Dordrecht, ISBN 9781402069413.

Rafferty, D. A., B. R. McNamara and P. E. J. Nulsen. 2008, The Regulation of Cooling and Star Formation in Luminous Galaxies by Active Galactic Nucleus Feedback and the Cooling-Time/Entropy Threshold for the Onset of Star Formation, *The Astrophysical Journal*, vol. 687, doi:10.1086/591240, p. 899–918, ISSN 0004-637X. URL http://adsabs.harvard.edu/abs/2008ApJ...687..899R.

Rafferty, D. A., B. R. McNamara, P. E. J. Nulsen and M. W. Wise. 2006, The Feedback-regulated Growth of Black Holes and Bulges through Gas Accretion and Starbursts in Cluster Central Dominant Galaxies, *The Astrophysical Journal*, vol. 652, doi:10.1086/507672, p. 216–231, ISSN 0004-637X. URL http://adsabs.harvard.edu/abs/2006ApJ...652..216R.

Randall, S. W., C. Jones, M. Markevitch, E. L. Blanton, P. E. J. Nulsen and W. R. Forman. 2009, Gas Sloshing and Bubbles in the Galaxy Group NGC 5098, *The Astrophysical Journal*, vol. 700, doi:10.1088/0004-637X/700/2/1404, p. 1404–1414, ISSN 0004-637X. URL http://adsabs.harvard.edu/abs/2009ApJ...700.1404R.

Randall, S. W., P. E. J. Nulsen, C. Jones, W. R. Forman, E. Bulbul, T. E. Clarke, R. Kraft, E. L. Blanton, L. David, N. Werner, M. Sun, M. Donahue, S. Giacintucci and A. Simionescu. 2015, A Very Deep Chandra Observation of the Galaxy Group NGC 5813: AGN Shocks, Feedback, and Outburst History, *The Astrophysical Journal*, vol. 805, doi:10.1088/0004-637X/805/2/112, p. 112, ISSN 0004-637X. URL http://adsabs.harvard.edu/abs/2015ApJ...805..112R.

Rawle, T. D., A. C. Edge, E. Egami, M. Rex, G. P. Smith, B. Altieri, A. Fiedler, C. P. Haines, M. J. Pereira, P. G. Pérez-González, J. Portouw, I. Valtchanov, G. Walth, P. P. van der Werf and M. Zemcov. 2012, The Relation between Cool Cluster Cores and Herschel-detected Star Formation in Brightest Cluster Galaxies, *The Astrophysical Journal*, vol. 747, doi:10.1088/0004-637X/747/1/29, p. 29, ISSN 0004-637X. URL http://adsabs.harvard.edu/abs/2012ApJ...747...29R.

Rosswog, S. and M. Brüggen. 2007, Introduction to high-energy astrophysics, Cambridge University Press.

Russell, H. R., M. McDonald, B. R. McNamara, A. C. Fabian, P. E. J. Nulsen, M. B. Bayliss, B. A. Benson, M. Brodwin, J. E. Carlstrom, A. C. Edge, J. Hlavacek-Larrondo, D. P. Marrone, C. L. Reichardt and J. D. Vieira. 2017, Alma Observations of Massive Molecular Gas Filaments Encasing Radio Bubbles in the Phoenix Cluster, *The Astrophysical Journal*, vol. 836, doi:10.3847/1538-4357/836/1/130, p. 130, ISSN 0004-637X. URL http://adsabs.harvard.edu/abs/2017ApJ...836..130R.

Russell, H. R., B. R. McNamara, A. C. Edge, P. E. J. Nulsen, R. A. Main, A. N. Vantyghem, F. Combes, A. C. Fabian, N. Murray, P. Salomé, R. J. Wilman, S. A. Baum, M. Donahue, C. P. O'Dea, J. B. R. Oonk, G. R. Tremblay and G. M. Voit. 2014, Massive Molecular Gas Flows in the A1664 Brightest Cluster Galaxy, *The Astrophysical Journal*, vol. 784, doi:10.1088/0004-637X/784/1/78, p. 78, ISSN 0004-637X. URL http://adsabs.harvard.edu/abs/2014ApJ...784...78R.

Rybicki, G. B. and A. P. Lightman. 2004, Radiative processes in astrophysics, Wiley-VCH.

Salomé, P., F. Combes, A. C. Edge, C. Crawford, M. Erlund, A. C. Fabian, N. A. Hatch, R. M. Johnstone, J. S. Sanders and R. J. Wilman. 2006, Cold molecular gas in the Perseus cluster core. Association with X-ray cavity, Hα filaments and cooling flow, *Astronomy and Astrophysics*, vol. 454, doi:10.1051/0004-6361:20054745, p. 437–445, ISSN 0004-6361. URL http://adsabs.harvard.edu/abs/2006A%26A...454..437S.

Sanders, J. S., A. C. Fabian, G. B. Taylor, H. R. Russell, K. M. Blundell, R. E. A. Canning, J. Hlavacek-Larrondo, S. A. Walker and C. K. Grimes. 2016, A very deep Chandra view of metals, sloshing and feedback in the Centaurus cluster of galaxies, *Monthly Notices of the Royal Astronomical Society*, vol. 457, n° 1, doi:10.1093/mnras/stv2972, p. 82–109, ISSN 0035-8711, 1365-2966. URL http://arxiv.org/abs/1601.01489, arXiv: 1601.01489.

Santos, J. S., P. Rosati, P. Tozzi, H. Böhringer, S. Ettori and A. Bignamini. 2008, Searching for cool core clusters at high redshift, *Astronomy and Astrophysics*, vol. 483, doi:10.1051/0004-6361:20078815, p. 35–47, ISSN 0004-6361. URL http://adsabs.harvard.edu/abs/2008A%26A...483...35S.

Santos, J. S., P. Tozzi, P. Rosati and H. Böhringer. 2010, The evolution of cool-core clusters, *Astronomy and Astrophysics*, vol. 521, doi:10.1051/0004-6361/201015208, p. A64, ISSN 0004-6361. URL http://adsabs.harvard.edu/abs/2010A%26A...521A..64S.

Schombert, J. M. 1986, The structure of brightest cluster members. I - Surface photometry, *The Astrophysical Journal Supplement Series*, vol. 60, doi:10.1086/191100, p. 603–693, ISSN 0067-0049. URL http://adsabs.harvard.edu/abs/1986ApJS...60..603S.

Schombert, J. M. 1987, The structure of brightest cluster members. II - Mergers, *The Astrophysical Journal Supplement Series*, vol. 64, doi:10.1086/191212, p. 643–666, ISSN 0067-0049. URL http://adsabs.harvard.edu/abs/1987ApJS...64..643S.

Schombert, J. M. 1988, The structure of brightest cluster members. III - cD envelopes, *The Astrophysical Journal*, vol. 328, doi:10.1086/166306, p. 475–488, ISSN 0004-637X. URL http://adsabs.harvard.edu/abs/1988ApJ...328..475S.

Seigar, M. S., A. W. Graham and H. Jerjen. 2007, Intracluster light and the extended stellar envelopes of cD galaxies: an analytical description, *Monthly Notices of the Royal Astronomical Society*, vol. 378, doi:10.1111/j.1365-2966.2007.11899.x, p. 1575–1588, ISSN 0035-8711. URL http://adsabs.harvard.edu/abs/2007MNRAS.378.1575S.

Silk, J. 1976, Accretion by galaxy clusters and the relationship between X-ray luminosity and velocity dispersion, *The Astrophysical Journal*, vol. 208, doi:10.1086/154645, p. 646–649, ISSN 0004-637X. URL http://adsabs.harvard.edu/abs/1976ApJ...208..646S.

Stott, J. P., C. A. Collins, C. Burke, V. Hamilton-Morris and G. P. Smith. 2011, Little change in the sizes of the most massive galaxies since z = 1, *Monthly Notices of the Royal Astronomical Society*, vol. 414, doi:10.1111/j.1365-2966.2011.18404.x, p. 445–457, ISSN 0035-8711. URL http://adsabs.harvard.edu/abs/2011MNRAS.414..445S.

Stott, J. P., A. C. Edge, G. P. Smith, A. M. Swinbank and H. Ebeling. 2008, Near-infrared evolution of brightest cluster galaxies in the most X-ray luminous clusters since z = 1, *Monthly Notices*

of the Royal Astronomical Society, vol. 384, doi:10.1111/j.1365-2966.2007.12807.x, p. 1502–1510, ISSN 0035-8711. URL http://adsabs.harvard.edu/abs/2008MNRAS.384.1502S.

Takeuchi, T. T., V. Buat, S. Heinis, E. Giovannoli, F.-T. Yuan, J. Iglesias-Páramo, K. L. Murata and D. Burgarella. 2010, Star formation and dust extinction properties of local galaxies from the AKARI-GALEX all-sky surveys . First results from the most secure multiband sample from the far-ultraviolet to the far-infrared, *Astronomy and Astrophysics*, vol. 514, doi:10.1051/0004-6361/200913476, p. A4, ISSN 0004-6361. URL http://adsabs.harvard.edu/abs/2010A%26A...514A..4T.

Tchekhovskoy, A. and O. Bromberg. 2016, Three-dimensional Relativistic MHD Simulations of Active Galactic Nuclei Jets: Magnetic Kink Instability and Fanaroff-Riley Dichotomy, *Monthly Notices of the Royal Astronomical Society: Letters*, vol. 461, nº 1, doi:10.1093/mnrasl/slw064, p. L46–L50, ISSN 1745-3925, 1745-3933. URL http://arxiv.org/abs/1512.04526, arXiv: 1512.04526.

Tremaine, S. D. and D. O. Richstone. 1977, A test of a statistical model for the luminosities of bright cluster galaxies, *The Astrophysical Journal*, vol. 212, doi:10.1086/155049, p. 311–316, ISSN 0004-637X. URL http://adsabs.harvard.edu/abs/1977ApJ...212..311T.

Vogelsberger, M., S. Genel, V. Springel, P. Torrey, D. Sijacki, D. Xu, G. Snyder, D. Nelson and L. Hernquist. 2014, Introducing the Illustris Project: simulating the coevolution of dark and visible matter in the Universe, *Monthly Notices of the Royal Astronomical Society*, vol. 444, doi:10.1093/mnras/stu1536, p. 1518–1547, ISSN 0035-8711. URL http://adsabs.harvard.edu/abs/2014MNRAS.444.1518V.

Voigt, L. M. and A. C. Fabian. 2004, Thermal conduction and reduced cooling flows in galaxy clusters, *Monthly Notices of the Royal Astronomical Society*, vol. 347, doi:10.1111/j.1365-2966.2004.07285.x, p. 1130–1149, ISSN 0035-8711. URL http://adsabs.harvard.edu/abs/2004MNRAS.347.1130V.

Von Der Linden, A., P. N. Best, G. Kauffmann and S. D. M. White. 2007, How special are brightest group and cluster galaxies?, *Monthly Notices of the Royal Astronomical Society*, vol. 379, doi:10.1111/j.1365-2966.2007.11940.x, p. 867–893, ISSN 0035-8711. URL http://adsabs.harvard.edu/abs/2007MNRAS.379..867V.

Webb, T., J. Lowenthal, M. Yun, A. G. Noble, A. Muzzin, G. Wilson, H. K. C. Yee and R. Cybulski. 2017, Detection of a Substantial Molecular Gas Reservoir in a brightest cluster galaxy at z = 1.7, *The Astrophysical Journal*, vol. 844, nº 2, doi:10.3847/2041-8213/aa7749, p. L17, ISSN 2041-8213. URL http://arxiv.org/abs/1706.01366, arXiv: 1706.01366.

Webb, T., A. Noble, A. DeGroot, G. Wilson, A. Muzzin, N. Bonaventura, M. Cooper, A. Delahaye, R. Foltz, C. Lidman, J. Surace, H. K. C. Yee, S. Chapman, L. Dunne, J. Geach, B. Hayden, H. Hildebrandt, J. Huang, A. Pope, M. W. L. Smith, S. Perlmutter and A. Tudorica. 2015a, An Extreme Starburst in the Core of a Rich Galaxy Cluster at z = 1.7, *The Astrophysical Journal*, vol. 809, doi:10.1088/0004-637X/809/2/173, p. 173, ISSN 0004-637X. URL http://adsabs.harvard.edu/abs/2015ApJ...809..173W.

Webb, T. M. A., A. Muzzin, A. Noble, N. Bonaventura, J. Geach, Y. Hezevah, C. Lidman, G. Wilson, H. K. C. Yee, J. Surace and D. Shupe. 2015b, The Star Formation History of BCGs to z = 1.8 from the SpARCS/SWIRE Survey: Evidence for Significant In Situ Star Formation at High Redshift, *The Astrophysical Journal*, vol. 814, doi:10.1088/0004-637X/814/2/96, p. 96, ISSN 0004-637X. URL `http://adsabs.harvard.edu/abs/2015ApJ...814...96W`.

White, S. D. M. 1976, Dynamical friction in spherical clusters, *Monthly Notices of the Royal Astronomical Society*, vol. 174, doi:10.1093/mnras/174.1.19, p. 19–28, ISSN 0035-8711. URL `http://adsabs.harvard.edu/abs/1976MNRAS.174...19W`.

Wilson, G., A. Muzzin, M. Lacy, H. Yee, J. Surace, C. Lonsdale, H. Hoekstra, S. Majumdar, D. Gilbank and M. Gladders. 2006, Clusters of Galaxies at $1 < z < 2$: The Spitzer Adaptation of the Red-Sequence Cluster Survey, *arXiv:astro-ph/0604289*. URL `http://arxiv.org/abs/astro-ph/0604289`, arXiv: astro-ph/0604289.

Wilson, G., A. Muzzin, H. K. C. Yee, M. Lacy, J. Surace, D. Gilbank, K. Blindert, H. Hoekstra, S. Majumdar, R. Demarco, J. P. Gardner, M. D. Gladders and C. Lonsdale. 2009, Spectroscopic Confirmation of a Massive Red-Sequence-Selected Galaxy Cluster at z = 1.34 in the SpARCS-South Cluster Survey, *The Astrophysical Journal*, vol. 698, doi:10.1088/0004-637X/698/2/1943, p. 1943–1950, ISSN 0004-637X. URL `http://adsabs.harvard.edu/abs/2009ApJ...698.1943W`.

Wise, M. W., B. R. McNamara, P. E. J. Nulsen, J. C. Houck and L. P. David. 2007, X-Ray Supercavities in the Hydra A Cluster and the Outburst History of the Central Galaxy's Active Nucleus, *The Astrophysical Journal*, vol. 659, doi:10.1086/512767, p. 1153–1158, ISSN 0004-637X. URL `http://adsabs.harvard.edu/abs/2007ApJ...659.1153W`.

Zhuravleva, I., E. Churazov, A. A. Schekochihin, S. W. Allen, P. Arevalo, A. C. Fabian, W. R. Forman, J. S. Sanders, A. Simionescu, R. Sunyaev, A. Vikhlinin and N. Werner. 2014, Turbulent Heating in Galaxy Clusters Brightest in X-rays, *Nature*, vol. 515, n^{o} 7525, doi:10.1038/nature13830, p. 85–87, ISSN 0028-0836, 1476-4687. URL `http://arxiv.org/abs/1410.6485`, arXiv: 1410.6485.

Chapter 2

RADIO ASTRONOMY

2.1. Why radio astronomy?

Astronomy uses a wide variety of wavelengths to study the sky. Each wavelength gives insight on particular phenomena. Unfortunately for astronomers (but maybe fortunately for life), most of the electromagnetic spectrum is blocked by the terrestrial atmosphere. Figure 2.1 shows at what wavelengths ground-based observations are possible: in visible light (marked by a rainbow), in several very narrow windows in the near infrared and in the radio. From the centimetre to the metre scale (approximately between 1 THz and 10 MHz in

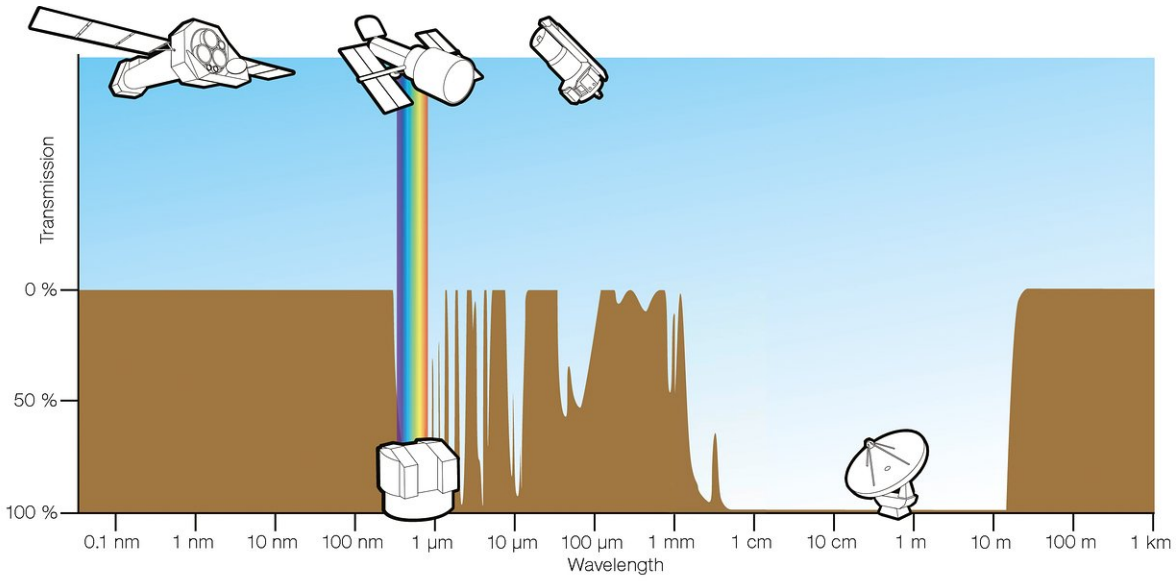

Figure 2.1 Schematic view of the atmospheric opacity as a function of the wavelength (brown curve, logarithmic scale), with several telescopes, outlined at the approximative wavelength at which they operate. The rainbow marks the visible light. From `https://www.eso.org/public/usa/images/atm_opacity/`.

terms of frequency, see e.g. Condon and Ransom, 2016), the atmospheric windows in radio domain is the largest window where ground-based observations are possible.

Radio waves are the least energetic waves of the electromagnetic spectrum. Therefore, for most celestial objects, extremely few radio waves are thermally emitted (e.g. Condon and Ransom, 2016), unless the object studied is very cold. So, why study the sky at radio wavelengths?

The answer is in the word *thermal*. A wide variety of processes in the Universe emit (or absorb) light non-thermally. At radio wavelengths, one of these processes is synchrotron radiation (see Section 1.3.1.1 for a mathematical description of synchrotron radiation), often associated with high-energy phenomena like supermassive black holes actively accreting or supernovae (e.g. Condon, 1992; Heesen et al., 2014; Condon and Ransom, 2016). So paradoxically, the low energy tail of the electromagnetic spectrum probes the high energy Universe.

The following 2 sections are largely based on Condon and Ransom (2016) and on Burke and Graham-Smith (2010). For a comprehensive review of radio astronomy, see Condon and Ransom (2016). For historical aspects or basic principles of instrumentation and interferometry, see Burke and Graham-Smith (2010).

2.2. Basic principles

Historically, astronomers have failed to develop radio astronomy. Knowing that thermal radio emission from stars would be very faint, they incorrectly assumed that no sources would be bright in radio. It is only in 1932, when Karl G. Jansky serendipitously discovered radio emission from our galaxy, that radio astronomy started. In his honour, the flux density unit used in radio astronomy is called a Jansky (Jy):

$$1 \text{ Jy} = 10^{-23} \text{ erg s}^{-1} \text{ cm}^{-2} \text{ Hz}^{-1} \tag{2.1}$$

$$1 \text{ Jy} = 10^{-26} \text{ W m}^{-2} \text{ Hz}^{-1} \tag{2.2}$$

However, early astronomers were not wrong about the faint emission of stars in the radio. The Sun emits very few radio waves, so there is no need to wait for the night to observe in the radio: the radio sky is always "dark". Another advantage of radio domain is its greater tolerance to clouds, compared with the optical. However, this advantage is limited: small drops of water in suspension in the atmosphere increase the atmospheric opacity to radio wavelengths, as well as a strong and wide water vapour spectral line at $\nu = 22.235$ GHz. Therefore, radio observatories tend to be in dry places.

Among the other limitations of radio astronomy there is the problem of technological pollution. Radio waves emitted by modern devices, such as cell phones, Wi-Fi, etc. are a significant source of corrupted data. These are called Radio Frequency Interferences (RFI;

e.g. Perreault, 2018) and affect mostly low-frequency observations. At higher frequency, there is generally less RFI, but they are still a concern. One of the longest steps in data reduction is the RFI excision.

2.3. Instrumental principles

The device transforming a radio electromagnetic waves into an electrical current is called the "feeding antenna". The simplest designs for a feeding antenna consist of two collinear short dipoles separated by a gap. Another simple design is a horn with a waveguide. The horn is a kind of gently narrowing pipe, prolonged by a waveguide of constant cross section. Waveguides are not exclusive to horn antennae: sometimes waveguides could be coupled with dipoles. However, since such systems are sensitive to a very narrow range of frequencies they are of limited interest. Exponential horns, bowties (pairs of triangular dipoles, mimicking the shape of a bow tie) or log-periodic arrays (collections of double dipoles, the decrease in their sizes described by a logarithmic curve) are adaptations of the basic horn and dipole designs to broader ranges of frequencies.

In addition to the feed antenna, most radio telescopes have one or two reflectors designed to concentrate the radio waves at the feed antenna. These reflectors follow the relation between resolution (θ), diameter (D) and wavelength (λ) :

$$\theta \approx \frac{\lambda}{D} \approx \frac{c}{\nu D} \tag{2.3}$$

where c is the speed of light and ν the frequency. Therefore, to have a high resolution we need extremely large radio telescopes. A large telescope often means a fixed reflector, which cannot easily track a source on the sky. However there is a way to bypass this problem: interferometry.

2.3.1. Interferometry

The idea behind aperture synthesis interferometry is to use several antennae to mimic the resolving power of a single large dish antenna that would have occupied the same area. If an interferometer is composed of N antennae, these antennae can be combined in $\frac{N(N-1)}{2}$ pairs. The distance between the two elements of a pair is called a baseline. The signal of 2 antennae combine either constructively or destructively, depending on the light path difference between them, and form fringed patterns. Therefore, an interferometer measures the Fourier transform of the source brightness distribution, which is called the complex visibility.

The complex visibility of a source can be measured on the $u - v$ plane, which is parallel to the plane of the sky at the source location. A baseline corresponds to a point in the $u - v$ plane. As the earth rotates, baselines start to draw curves on the $u - v$ plane. To achieve a good image reconstruction, one must have a sufficient coverage of the $u - v$ plane: gaps

in this plane imply a loss of Fourier components. Thus, to acquire a better coverage of the $u-v$ plane, one can either increase the number of antennae or the observing time.

2.4. Facilities

2.4.1. The Jansky Very Large Array

Figure 2.2 Left: The Very Large Array in D-configuration. Image courtesy of NRAO/AUI (`http://images.nrao.edu/90`). Right: One of the VLA antennae being moved during a configuration change. Image courtesy of NRAO/AUI/NSF (`https://public.nrao.edu/gallery/vla-antenna-on-transporter/`).

One of the facilities offering a good instantaneous coverage of the $u-v$ plane is the Karl G. Jansky Very Large Array (JVLA) with 27 antennae, each 25 metres in diameter, organized in a regular "Y-like" shape (e.g Burke and Graham-Smith, 2010, ; see Figure 2.2, left panel). Previously known as the Very Large Array (VLA), this interferometer has been recently upgraded and then took the name of Karl G.Jansky Very Large Array, although its old name is still widely used.

One of the main particularities of the JVLA is that its antennae are not fixed: they can be moved on rails, using an appropriate transporter (see Figure 2.2, right panel). There are 4 basic configurations, A, B, C and D, A being the most extended and D the most compact. The A configuration offers the largest diameter and thus the best resolution at a given wavelength. The drawback of this configuration is that the shortest baseline is rather long. Consequently, the very centre of the $u-v$ plane is not well populated and the missing Fourier modes are those needed to recover large scale or diffuse structures in the image (Burke and Graham-Smith, 2010). Conversely, the D configuration (on the left panel of Figure 2.2, the VLA is in D configuration) is better in detecting large scale structures but suffers from poor resolution. The B and C configurations represents 2 compromises between resolution and detection of large scale structures. The JVLA also offers hybrid configurations during

short periods. In these configurations, two "arms" of the Y are in a certain configuration (for example C) and the third "arm" is in a more extended configuration (B in our previous example). Since the resolution of a telescope is inversely proportional to the frequency (see equation 2.3), for a same configuration the JVLA achieves better resolutions at higher frequencies.

2.4.2. Future facilities

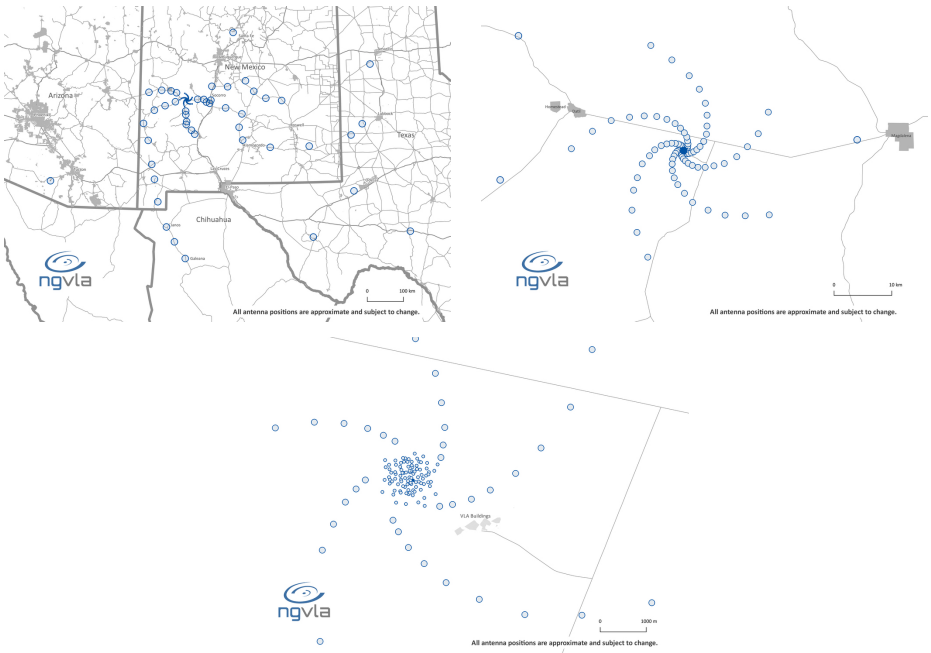

Figure 2.3 Top Left: The Next Generation Very Large Array will consist of 214 18-metre antennae scattered across the South West of United States and North of Mexico. Top Right: Zoom-in on the 36 kilometre-wide spiralled structure at the centre of the ngVLA. Bottom: Further zooming-in, showing the layout of the ngVLA core. All images come from the ngVLA website (`hhttp://ngvla.nrao.edu/images`).

The successor of the JVLA is called the Next Generation VLA (ngVLA). It will consist (the design is subject to change) of 214 antennae, each 18 metres in diameter, scattered across the South West of the United States and the North of Mexico. Figure 2.3 shows the 3 different parts of its current design: a compact core made of antennae randomly distributed, extended by antennae arranged in 5 spiral arms (spanning across a 36 km wide region) and on larger scales, asymmetrically distributed antennae (e.g. ngVLA team, 2018). Early science data are expected for 2028 and full array operations might begin in 2034.

On a shorter timescale, another project is the Square Kilometer Array located in Australia and South Africa. The SKA will be built in two phases: the construction of the first phase (SKA1) should start this year and early science starts in 2020, while the second phase of construction (SKA2) will require more than a decade (e.g. SKA team, 2018).

BIBLIOGRAPHY

Burke, B. F. and F. Graham-Smith. 2010, An Introduction to Radio Astronomy Third edition, Cambridge University Press.

Condon, J. J. 1992, Radio emission from normal galaxies, *Annual Review of Astronomy and Astrophysics*, vol. 30, doi:10.1146/annurev.aa.30.090192.003043, p. 575–611, ISSN 0066-4146. URL http://adsabs.harvard.edu/abs/1992ARA%26A..30..575C.

Condon, J. J. and S. M. Ransom. 2016, Essential radio astronomy, URL https://science.nrao.edu/opportunities/courses/era.

Heesen, V., E. Brinks, A. K. Leroy, G. Heald, R. Braun, F. Bigiel and R. Beck. 2014, The Radio Continuum-Star Formation Rate Relation in WSRT SINGS Galaxies, *The Astronomical Journal*, vol. 147, doi:10.1088/0004-6256/147/5/103, p. 103, ISSN 0004-6256. URL http://adsabs.harvard.edu/abs/2014AJ....147..103H.

Perreault, T. 2018, Radio frequency interferences, URL https://science.nrao.edu/facilities/vla/docs/manuals/obsguide/rfi.

SKA team. 2018, SKA Telescope Square Kilometer Array, URL https://www.skatelescope.org.

ngVLA team. 2018, ngVLA Next Generation Very Large Array, URL http://ngvla.nrao.edu.

Chapter 3

MULTIWAVELENGTH RADIO OBSERVATIONS OF A BRIGHTEST CLUSTER GALAXY AT Z=1.7

This article will be submitted to the periodic *The Astrophysical Journal*.

The main contributions of *Ariane Trudeau* to this article are presented.

— Data reduction and analysis for the VLA data

— Numerical calculations

— Writing of the manuscript

— Creation of the figures and tables

Multiwavelength radio observations of a brightest cluster galaxy at z=1.7

Ariane Trudeau
Département de physique, Université de Montréal, C.P. 6128, Succursale Centre-ville, Montréal, Canada H3C 3J7
Tracy Webb
Physics Department, McGill, Montréal, Canada H3A 2T8
Julie Hlavacek-Larrondo
Département de physique, Université de Montréal, C.P. 6128, Succursale Centre-ville, Montréal, Canada H3C 3J7
Allison Noble
Physics Department, McGill, Montréal, Canada H3A 2T8

Résumé

Nous présentons des observations radio profondes multi-longueurs d'onde de SpARCS104922.6+564032.5, un amas de galaxies à $z = 1.7$ avec un sursaut de formation d'étoiles en son coeur. Les observations ont été faites par le Karl G. Jansky Very Large Array (JVLA) en 3 bandes : 1-2 GHz, 4-8 GHz et 8-12 GHz. Nous avons détecté un AGN dans la BCG, laquelle est bien modélisée par une loi de puissance ayant $\alpha = -0.44 \pm 0.29$, même si la distribution spectrale de l'énergie (SED) est mal contrainte. Nous avons aussi détecté des émissions radios provenant de 2 des 27 membres spectroscopiquement confirmés de l'amas, mais nous n'avons pas détecté d'émission diffuse relative à la formation d'étoiles. En utilisant des données d'archive infrarouges, nous avons calculé un taux de formation d'étoiles (SFR) de 950 ± 100 $M_\odot$ an^{-1} en bon accord avec les estimations précédentes (Webb et al., 2015a). Nous avons aussi trouvé un écart entre les SED radio et infrarouge, que nous avons interprété comme une indication que la formation d'étoiles a lieu dans les environs de la BCG, mais pas en elle. Une comparaison entre la limite supérieure radio et le flux infrarouge lointain montre que la région de formation d'étoiles est probablement étendue ou constituée de plusieurs grumeaux d'étoiles. Nous suspectons

donc que la morphologie complexe du coeur de l'amas en proche infrarouge ne s'explique probablement pas par une seule fusion majeure de galaxies riches en gaz, mais plutôt par plusieurs petites galaxies dépouillées de leur gaz ou par le déplacement d'un flot de gaz refroidi, même si davantage de données sont nécessaires pour confirmer l'un ou l'autre de ces scénarios. Ces résultats montrent la pertinence de combiner l'imagerie radio et infrarouge, mais aussi la nécessité d'avoir un interféromètre radio plus sensible pour explorer l'univers à haut décalage vers le rouge.

Keywords : continuum radio : galaxies, galaxies : active, galaxies : amas : individuel (SpARCS104922.6+564032.5), galaxies : évolution, galaxies : interactions, galaxies : sursaut de formation d'étoiles

Abstract

We present deep, multiwavelength radio observations of SpARCS104922.6+564032.5, a $z = 1.7$ galaxy cluster with a starbusting core. Observations were made with the Karl G. Jansky Very Large Array (JVLA) in 3 bands: 1-2 GHz, 4-8 GHz and 8-12 GHz. We detected an AGN in the BCG, which is best fitted by a power law with $\alpha = -0.44 \pm 0.29$, although the radio Spectral Energy Distribution (SED) is poorly constrained. We also detected radio emission in 2 of the 27 spectroscopically confirmed cluster members, but we found no diffuse emission related to star formation. Using infrared archival data, we computed a star formation rate (SFR) of 950 ± 100 $M_\odot$ yr^{-1}, in good agreement with the previous estimates (Webb et al., 2015a). We also found a discrepancy between radio and infrared SEDs, which we interpreted as an indication that the star formation happens in the BCG vicinity, but not within. A comparison between the radio upper limit and the SED-estimated far infrared flux shows that the star-forming region might be extended or made of several clumps. Thus, we suspect that the complex near-infrared morphology in the cluster core might not be explained by a single major wet merger, but rather by several small galaxies stripped of their gas or by a displaced cooling flow, although more data are needed to confirm any of those scenarios. These results illustrate the pertinence of combining radio and infrared imaging, but also show the need for a more sensitive radio interferometer to explore star formation in the high-redshift Universe.

Keywords: galaxies: active, galaxies: clusters: individual (SpARCS104922.6+564032.5), galaxies: evolution, galaxies: interactions, galaxies: starburst, radio continuum: galaxies

3.1. Introduction

The most massive galaxies in the Universe sit at the centre of galaxy clusters. In comparison with field objects, these galaxies, called Brightest Cluster Galaxies (BCGs), exhibit

unique properties such as distinct luminosity and surface brightness profiles (e.g. Dressler, 1978; Oemler, 1976; Tremaine and Richstone, 1977). We still do not understand the origin of these distinct properties, but they are likely due to environmental effects as well as to their distinct formation histories.

On larger scales, the clusters in which BCGs reside can generally be divided into two categories: cool core clusters, which exhibit very peaked surface brightness distributions at X-ray wavelengths and non cool core clusters, with similar overall X-ray luminosities but with smoother, less peaked X-ray surface brightness distributions. Some authors (e.g. Hudson et al., 2010; Santos et al., 2010) define an intermediate category called moderate or weak cool core clusters. Since cool core clusters have short radiative cooling timescales on the order of 10^8 years in their centres (e.g. Voigt and Fabian, 2004; McNamara and Nulsen, 2012, 2007; Hlavacek-Larrondo et al., 2012), starbursts are expected to be common at the centre of such clusters. Indeed, the central cool gas in these clusters should condense onto the BCG, forming stars at rates of hundreds of solar masses per year (e.g. Fabian, 1994). However, most BCGs are relatively quiescent. Those that do show evidence of star formation tend to have star formation rates (SFRs) on the order of $1-150$ $\mathrm{M_\odot\ yr^{-1}}$ (e.g. Bildfell et al., 2008; Donahue et al., 2007; O'Dea et al., 2008, 2010; Rawle et al., 2012). However, there are some exceptions; perhaps the most extreme of them is the BCG in the Phoenix cluster, with a SFR of 610 ± 50 $\mathrm{M_\odot\ yr^{-1}}$ (e.g. McDonald et al., 2015, 2012, 2013a, 2014; Russell et al., 2017).

This mismatch between expected and observed SFRs, known as the cooling flow problem, is thought to be caused by Active Galactic Nuclei (AGN) feedback processes from the BCG. Indeed, AGNs can release copious amounts of energy into the intracluster medium (ICM) through many ways, including via jetted outflows that inflate cavities, weak shocks or sound waves in the ICM (e.g. McNamara and Nulsen, 2007, 2012; Markevitch and Vikhlinin, 2007; Fabian et al., 2017). Alone, the energy released by jetted outflows appears to be on the same order as the energy needed to offset cooling (e.g. Rafferty et al., 2006; McNamara and Nulsen, 2007; Hlavacek-Larrondo et al., 2012), therefore suggesting that AGN feedback is a good candidate for solving the cooling flow problem.

According to semi-analytic models (e.g. De Lucia and Blaizot, 2007) it has been proposed that star formation occurs very early in BCG history (mostly before $z \sim 3$) and is quickly suppressed by AGN feedback (e.g. Croton et al., 2006). Later, BCGs are thought to be built-up by dry mergers, without significant star formation. This scenario is supported by several mass growth measurements of BCGs below $z \sim 1$ (e.g. Stott et al., 2008, 2011; Lidman et al., 2012), although authors disagree on the time scale of the mass growth.

At $z > 1$, however, there are growing divergences between observations and this scenario: McDonald et al. (2016) and Webb et al. (2015b) both find evidence of significant in-situ star formation in BCGs at $z \gtrsim 1$. The triggering mechanism is not known for sure, but several

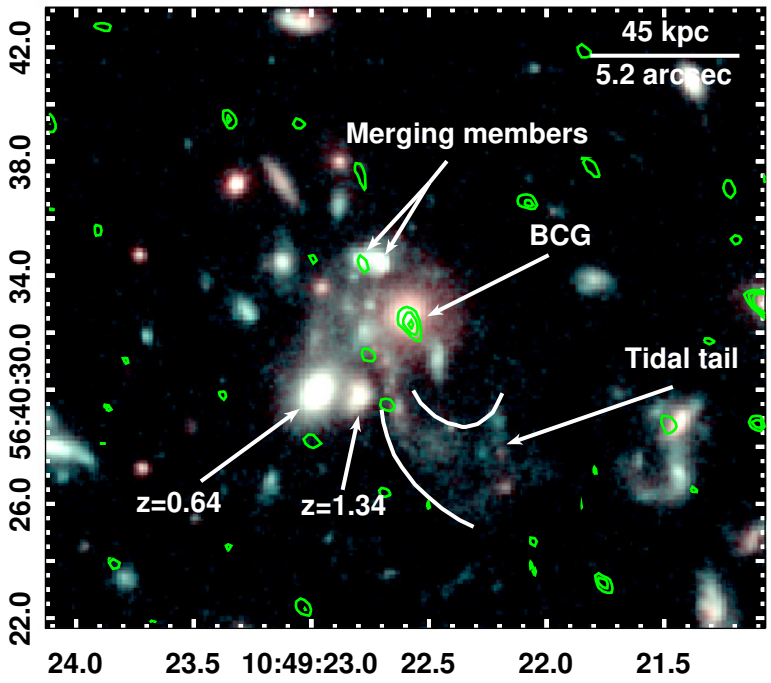

Figure 3.1 A composite Hubble Space Telescope (HST) infrared image (F105W in blue and green, F160W in red) of the central regions of SpARCS1049, with 6 GHz radio contours overplotted in green. We highlight the merging members, 2 foreground galaxies, the tidal tail and the BCG.

clues point toward galaxy-galaxy interactions. For example, according to McDonald et al. (2016), star-forming BCGs seem to preferentially lie in dynamically unrelaxed, non-cool core clusters.

SpARCS104922.6+564032.5 (hereafter referred as SpARCS1049), located at $z = 1.7089$, provides additional evidence for this scenario. It is one of the most distant spectroscopically confirmed clusters known to date and was discovered by the Spitzer Adaptation of the Red-sequence Cluster Survey (SpARCS) collaboration (e.g. Muzzin et al., 2009; Wilson et al., 2009; Demarco et al., 2010). This survey combines deep z'-band imaging with the Canada-France-Hawaii Telescope (CFHT; for the Northern fields) and the Cerro Tololo Inter-American Observatory (CTIO; for the Southern fields) to pre-existing images of the Spitzer Wide Infrared Extragalatic Legacy Survey (SWIRE; Lonsdale et al., 2003) at 3.6 μm to find $z > 1$ clusters of galaxies.

The complex morphology of the BCG in SpARCS1049, revealed by the Hubble Space Telescope in Figure 3.1, suggests that this BCG has been caught in the final stages of a major wet merger (Webb et al., 2015a). The single, large backward J-like tidal tail and the chain of clumps are reminiscent of "shrimp-like" interacting galaxies, as defined by Elmegreen

et al. (2007). The clump chain seems to originate from within the stellar halo of the BCG and has a linear extent of $\sim$ 60 kpc. The cluster core, including the BCG and a pair of interacting cluster members (highlighted in Figure 3.1), is embedded in diffuse infrared emission. Assuming all the infrared emission comes from the BCG, Webb et al. (2015a) calculated the level of far-infrared emission by fitting Spectral Energy Distributions (SEDs) to the BCG, and used it to find the AGN-corrected star formation rate. They found a value of 860 ± 130 $M_\odot$ yr^{-1}, largely surpassing what is seen in local BCGs. However, the archival data used to calculate the SFR and build the SED suffer from poor spatial resolution (several arcsec), and moreover, the centroid of the 24 μm MIPS data used in this calculation is located approximately 15 kpc to the South-East of the BCG centre. Therefore, it is still unclear how extended, clumpy and where exactly is the star formation in the core of SpARCS1049. Hereafter, we will refer to this region of star formation as the star formation in the vicinity of the BCG.

Recently, a large reservoir of cold molecular gas ($M_{H_2} = 1.1 \pm 0.1 \times 10^{11}$ $M_\odot$) was discovered in the central region of SpARCS1049 (Webb et al., 2017), although the beam, with a FWHM of 25 arcsec, is too wide to constrain more precisely the gas location and extent. This gas could be fuelling the star formation, but the lack of multiple velocity peaks, as might be expected in a major merger, as well as the immense amount of molecular gas, opens the door to other scenarios. For example, the core morphology and the gas reservoir could have been produced by the stripping of several small galaxies in the cluster centre. Another explanation is that a collision with an infalling galaxy disrupted the heating process in the BCG, triggering a cooling flow.

In this article, we present deep, multiwavelength Karl G. Jansky Very Large Array (JVLA) observations of SpARCS1049. We focus our analysis on the BCG and its vicinity. In Section 3.2, we present the observations and data reduction of the JVLA datasets, as well as archival observations from the Hubble Space Telescope (HST) and Spitzer Space Telescope. Detected cluster members are presented in Section 3.3. Section 3.4 discusses the results. Finally, we present a summary in Section 3.5. Throughout this paper, we assume $H_0 = 69.6$ km s^{-1} Mpc^{-1}, $\Omega_M = 0.286$ and $\Omega_\Lambda = 0.714$. At the redshift of the source ($z = 1.7089$, Webb et al., 2015a), 1 arcsec corresponds to 8.610 kpc.

3.2. Observations and data reduction

3.2.1. VLA observations and data reduction

In 2016, we were awarded 6.5 hours of observations on the JVLA (project 16A-283, PI Hlavachek-Larrondo). Observations, array configurations and on-source time are presented in Table 3. I. Centred on the BCG in SpARCS1049, the observations consisted of 2 hours in

Table 3. I. VLA observations

Date	Frequency (Band) (GHz)	Bandwidth (GHz)	Configuration	On-source time (min)	Flag percentage (%)	RMS [a] μJy beam^{-1}
19 Nov 2016	1.5 (L)	1	A	80	60	11
20 & 21 May 2016	6 (C)	4	B	54	45	3[b]
21 May 2016	6 (C)	4	B	54	52	
21 May 2016	10 (X)	4	B	54	28	4

[a]Local noise level.

[b]Local noise level for the merged image at 6 GHz

L band (1-2 GHz), two observations of 1.5 hours each in C band (4-8 GHz) and 1.5 hours in X band (8-12 GHz).

Data reduction was performed with CASA (Common Astronomy Software Application, McMullin et al., 2007) following the steps described below. Most of the data reduction was performed with CASA 4.7.2, but final imaging in X band was made with version 5.1.2.

First, corrupted antennae listed in the operator logs were removed. Then, prior to the automatic RFI flagging procedure, data were pre-calibrated using the tasks GAINCAL, BANDPASS and APPLYCAL. For each antenna, we examined the amplitude versus frequency plot with PLOTCAL and flagged any abnormally low or high visibilities. We then proceeded with automatic RFI excision using the RFLAG and EXTEND modes of the task FLAGDATA. The TFCROP mode was used on the most RFI affected spectral windows and further flagging was made with the MANUAL mode. After calibration, target data were split.

Images were made with the task CLEAN, using a W-projection algorithm (mode WIDEFIELD) and 480 w-planes to correct the sky curvature across the field of view (Cornwell et al., 2008). We used Briggs weighing and a robustness parameter of 0, although we test other parameters in Section 3.2.1.1. To ensure a sufficient sampling of the respective beams, we used a pixel size of 0.25 arcsec in L band, 0.20 arcsec in C bands and 0.15 arcsec in X band. For each band, the first clean was performed using the interactive mode, which allowed the creation of a customised cleaning mask. We then applied a self-calibration procedure to the initial image. This procedure consists of deriving phase corrections with GAINCAL, applying them to the data using APPLYCAL and then making a new image. We tested several time solution intervals and solving procedures, and varied the number of self-calibrations performed. The deepest images were obtained with one round of self-calibration and a T Jones solving procedure applied to an infinite time solution interval. The two datasets in C band were imaged, self-calibrated and then re-imaged separately. Then, they were merged using the task CLEAN, self-calibrated and merged anew. We used 100 000 iterations for merging and final cleans, except in X band where the final clean was performed with 45 000 iterations.

The last column of Table 3. I summarizes the local noise level reached in each image. Essentially, considering the exposure times and percentage of flagged data, we were able to reach the thermal noise in each of the images. No extended emission associated with the BCG is detected in all 3 frequency bands. The only sources we detect are a point source that coincides with the BCG and two other point sources associated with cluster members (see Section 3.3.1). The BCG detection is shown in Figure 3.2.

3.2.1.1. *Additional imaging of the VLA datasets*

To further search for evidence of extended radio emission (which might be related with star formation associated with the BCG), we made additional images using different resolutions and Briggs parameters. First, we produced images with identical pixel sizes (0.25 arcsec) and beams for all frequencies (L, C and X bands). We set the parameter RESTORINGBEAM to be identical to the default beam. We then compared the fluxes pixel by pixel. We find no traces of faint or diffuse emission beyond the detected point sources.

Our second test consisted in degrading the resolution of the L band image, in order to better capture faint, extended emission. We applied the same imaging procedure as in Section 3.2.1, except for the last clean, where the resolution was changed to 2 arcsec per pixel. We also made two other tests in L band, this time changing the Briggs robustness parameter. In one test, the robust parameter was set to -2, which is equivalent to a uniform weighting (i.e. faint and bright emission have the same weight in the image). In the other case, the robustness parameter was set to 2, equivalent to natural weighting (no enhancement of the fainter emission). None of these additional images show conclusive traces of extended emission beyond the BCG point source. This remains the case if we apply similar procedures to the C and X band images.

Finally, because we were able to reach a very low noise level in the C band merged image at 6 GHz, in addition to clearly detecting the BCG, we decided to split the 2 original datasets (those presented in Table 3. I). Each dataset, spanning from 4 GHz to 8 GHz, was divided into 2 sub-datasets: one spanning from 4 to 6 GHz and another spanning from 6 to 8 GHz. Following the procedure explained in the last section, we merged datasets with identical frequencies and produced two images: one centred at 5 GHz and another centred at 7 GHz. Such decomposition allows us to better study the flux variations of the sources with frequency. Signal-to-noise ratios in L and X band were judged insufficient to proceed with such a decomposition. From now on, we will specify the frequency when referring to a C band image, to avoid any confusion.

3.2.2. Hubble Space Telescope observations

Near infrared imaging of the cluster centre was obtained with the Wide Field Camera 3 (WFC3) onboard HST using the F160W and F105W filters in Cycle 22 (PI Webb). These

observations were obtained over nine separate visits, with total exposure times of 9237 s for the F160W filter and 8543 s for the F105W filter. The data were processed using standard HST data reduction techniques. See Webb et al. (2015a) for a complete description of the data reduction and mosaic composition of the HST data. The resulting composite HST image is shown in Figures 3.1 and 3.2 (left panel).

3.3. Results

3.3.1. Cluster members

3.3.1.1. *Detection criteria*

As mentioned in Section 3.2.1, using our new VLA observations, we have detected 3 point sources associated with SpARCS1049: the BCG (see Figure 3.2) and two known cluster members located to the East of the BCG.

Here, we only consider the BCG and the galaxies that have been identified as cluster members by Webb et al. (2015a). Indeed, these authors identified a total of 27 spectroscopic members, using the near-infrared multi-object spectrograph MOSFIRE on the W. M. Keck I Telescope. We apply the following criteria to consider that a cluster member is detected in radio wavelengths:

1. The galaxy should be detected above $3\sigma_{\rm RMS}$ in at least 2 frequency bands, or above $5\sigma_{\rm RMS}$ in at least one frequency band. A $3\sigma_{\rm RMS}$ ($5\sigma_{\rm RMS}$) detection corresponds to an integrated flux within one beam of 31.5 μJy (52.5 μJy) in L band, 9.6 μJy (16.0 μJy) in C band at 6 GHz, which is the deepest image obtained in C band, and 11.1 μJy (18.5 μJy) in X band.
2. The spectroscopic position of the cluster member should be within the $3\sigma_{\rm RMS}$ contours for each radio detection.

3.3.1.2. *Detections*

Applying these criteria at radio wavelengths, we find that only the BCG and two spectroscopically confirmed cluster members are detected. One of the non-BCG cluster members is located to the South East of the BCG and the other is located to the North-East. The BCG and the other detected galaxies respectively sit at $10:49:22.60\ +56:40:32.50$, at $10:49:26.40\ +56:40:14.98$ and at $10:49:32.25\ +56:40:51.53$. Since none of the detected cluster members are resolved, to calculate the flux, the peak and their uncertainties, we used the task IMFIT. Results are given in Table 3. II. To compute the upper limits presented in this Table, we simply calculated the $3\sigma_{\rm RMS}$ levels in the C band 5 GHz and X band images.

In this paper, from now on, we will focus on the radio observations of the BCG and its vicinity. Figure 3.2 presents the VLA images of this sources and its HST counterpart. The BCG is detected as a point source in all radio image. Therefore, we only show L and X band images (1.5 and 10 GHz respectively) in Figure 3.2.

Table 3. II. Detected cluster members

Frequency	BCG		Second member		Third member		RMS	Beam	PA[a]
	Flux	Peak	Flux	Peak	Flux	Peak			
(GHz)	(μJy)	(μJy beam^{-1})	(μJy)	(μJy beam^{-1})	(μJy)	(μJy beam^{-1})	(μJy beam^{-1})	(arcsec×arcsec)	(deg)
1.5	50 ± 21	42 ± 11	76 ± 19	70.3 ± 9.3	49 ± 20	43 ± 10	11	1.27×0.85	-81
5	29.1 ± 9.8	20.6 ± 4.1	42.5 ± 8.7	37.4 ± 4.5	< 14[b]	–	5	1.25×0.90	40
6	28.4 ± 8.7	14.8 ± 3.0	36.6 ± 5.8	34.3 ± 3.1	13.1 ± 5.1	14.4 ± 3.0	3	1.04×0.73	38
7	23.5 ± 8.7	21.8 ± 4.7	32.4 ± 9.1	27.1 ± 4.2	18.6 ± 7.4	20.7 ± 4.3	5	0.95×0.33	37
10	21.9 ± 6.5	21.5 ± 3.6	28 ± 11	13.0 ± 3.7	< 11[b]	–	4	0.72×0.46	81

[a]Position angle measured counter-clockwise from North to East.

[b]Upper limit on the flux of a potential point source, corresponding to 3 times the RMS of one beam

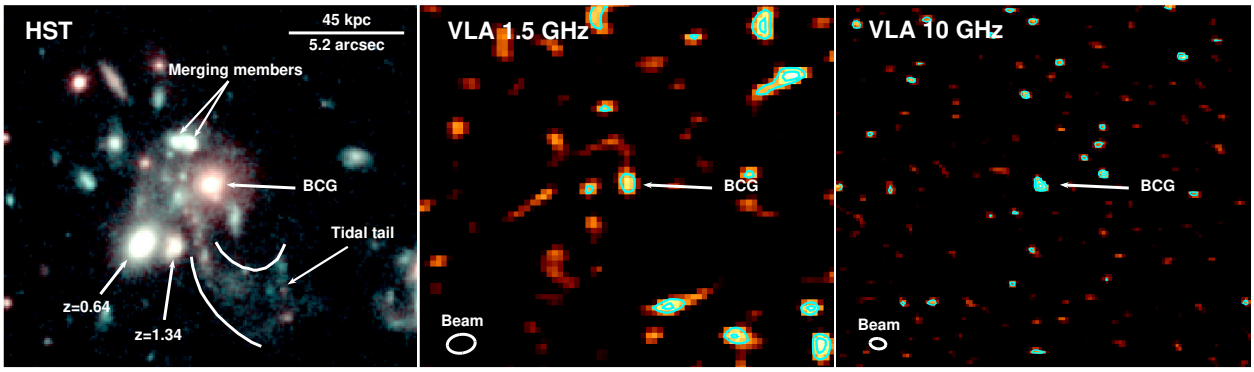

Figure 3.2 Deep VLA images of the BCG in SpARCS1049 and its HST counterpart. Left: Zoom-in of Figure 3.1. Middle: 1.5 GHz VLA image of the same area (RMS of 10.5 μJy beam^{-1}, $3\sigma_{\rm RMS}$ = 31.5 μJy beam^{-1}). Right: 10 GHz VLA image (RMS of 3.7 μJy beam^{-1}, $3\sigma_{\rm RMS}$ = 11.1 μJy beam^{-1}). No extended emission is detected. The scale is indicated in the top right corner of the HST image. The VLA beams are shown in the lower left corners and the radio contours (3, 4 and 5$\sigma_{\rm RMS}$ levels) are displayed in cyan.

The BCG is detected above a $3\sigma_{\rm RMS}$ level at 1.5 GHz in L band. At 5 and 7 GHz, the BCG is detected at a $4\sigma_{\rm RMS}$ level and at 6 and 10 GHz, it is detected at a $5\sigma_{\rm RMS}$ level. This suggests that the level of radio activity in the BCG is relatively mild. Moreover, no conclusive traces of extended emission have been detected in the BCG vicinity.

3.3.1.3. *Analysis*

To further understand the origin of the radio emission, we analysed the radio spectrum of the BCG (see Figure 3.3). We base our calculations on the Hogan et al. (2015) SED models since these models were developed for a variety of radio AGN including BCGs. These authors developed 4 schematic models, in which A_i is a constant to be determined and α_i is the spectral index. These models consist of:

$$S_{model} = A\nu^{\alpha} \tag{3.1}$$

a simple power law, appropriate for core or jet emission, depending on the spectral index;

$$S_{model} = A_1\nu^{\alpha_1} + A_2\nu^{\alpha_2} \tag{3.2}$$

a split power law, for a two component fit (jets and core emission);

$$S_{model} = A_0\nu^{\alpha_0}\left(1 - A_1 e^{\frac{-\nu_0}{\nu}}\right) \tag{3.3}$$

a "dropline" model, to illustrate synchrotron ageing of a jet;

$$\ln\left(S_{model}\right) = A_0 + \ln\left(\nu\right)\left(A_1 + A_2\ln\left(\nu\right)\right) \tag{3.4}$$

and a gigahertz peaked source (GPS) model, which illustrates the synchrotron self-absorption of the core emission of an actively accreting AGN. We applied the Hogan et al. (2015) fitting procedure to our data and discuss the results in Section 3.4.1. The most likely fit for the BCG is shown in Figure 3.3.

3.3.2. Star formation in the vicinity of the BCG

3.3.2.1. *Detection criteria*

The BCG in SpARCS1049 is known to harbour an extreme starburst with a SFR of 860± 130 $M_\odot$ yr^{-1} (Webb et al., 2015a). However current observations do not have the resolution to determine the location of the star formation. The only pre-existing high resolution data are HST photometry, which do not have good enough wavelength coverage to determine local SFRs based on the continuum emission. Moreover, infrared wavelengths are more subject to dust attenuation than radio. One method of probing star formation in very dusty regions is through radio observations (e.g. Heesen et al., 2014).

Using our new VLA observations, we have searched for evidence of radio emission that would be associated with the star formation in the BCG of SpARCS1049. To account for the different sensitivities of our radio images to star formation and considering that no information is available for its exact location, we use a different set of criteria for star formation compared to member detection. At radio wavelengths, star formation is usually quantified using the flux at 1.4 GHz (e.g. Condon, 1992; Condon et al., 2002; Heesen et al., 2014). However, our C band image (at 5 and 6 GHz) are more sensitive than our L band images due to the lower noise levels reached even when assuming a typical star formation spectral index of -0.7 (e.g. Heesen et al., 2014) and considering the redshift of the source. 7 GHz C band images, as well as X band images, are less sensitive to radio emission associated to star formation. Therefore, radio emission related to star formation is considered as a detection when:

1. Emission is detected above a $3\sigma_{\rm RMS}$ level in at least L band and C band (5 and 6 GHz) images. C band 5 and 6 GHz images are the deepest, but we also request a L band detection because C band subsets are not independent and may have spatially coincident noise spots.
2. The detected radio emission should correspond to some emission seen in the HST images.

3.3.2.2. *Non detection*

Following the detection criteria in Section 3.3.2.1, we do not detect any potential star forming clumps within a radius of $\sim$ 65 kpc, centred on the BCG of SpARCS1049. Thus, we set upper limits on the radio emission associate with star formation in the BCG or in its

Table 3. III. SFR detection threshold for each image

Frequency (GHz)	$3\sigma_{\rm RMS}$ upper limit (μJy beam^{-1})	3σ SFR upper limit ($M_\odot$ yr^{-1} beam^{-1})	5σ SFR upper limit ($M_\odot$ yr^{-1} beam^{-1})
1.5	32	600	990
5	14	590	990
6	10	480	800
7	14	780	1310
10	11	790	1320

vicinity. We calculated individual $3\sigma_{\rm RMS}$ upper limits for each frequency band. These are shown in Table 3. III (column 2).

3.3.2.3. *Analysis*

For each of our 5 radio images (see Table 3. III), we can use the $3\sigma_{\rm RMS}$ upper limits derived at radio wavelengths to compute an upper limit to the SFR, i.e. the minimal SFR detectable in each image. First, we must convert the flux density upper limits displayed in the second column of Table 3. III into k-corrected 1.4 GHz luminosities using (e.g. van Weeren et al., 2014; Delhaize et al., 2017):

$$L_{1.4GHz} = \frac{4\pi D_L^2}{(1+z)^{\alpha+1}} \left(\frac{1.4}{\nu_{band}}\right)^{\alpha} S_{band} \tag{3.5}$$

where $L_{1.4GHz}$ is in W Hz^{-1}, D_L is the luminosity distance and α the spectral index. ν_{band} is the image frequency in GHz and S_{band} is the flux density in W Hz^{-1} m^{-2}. Here, we assume a spectral index of -0.7, typical for star-forming regions (e.g. Heesen et al., 2014) and a maximum flux equivalent to the upper limits computed in the previous section.

These $3\sigma_{\rm RMS}$ upper limits of the k-corrected 1.4 GHz luminosities can now be used to compute upper limits on the SFR within one beam, using the relation of Condon et al. (2002) :

$$SFR = 1.20 \times 10^{-21} L_{1.4GHz} \tag{3.6}$$

where SFR is in $M_\odot$ yr^{-1} and $L_{1.4GHz}$ is, as before, in W Hz^{-1}. We used a Salpeter initial mass function to scale the relation. Results are presented in the third column of Table 3. III, which also displays the results of a similar computation, starting this time with $5\sigma_{\rm RMS}$ upper limits on the radio emission associate with star formation.

While the C band image at 6 GHz places the strongest constraints on the SFR within one beam (480 $M_\odot$ yr^{-1} beam^{-1}; Table 3. III, column 3), to be conservative and consistent with our detection criteria in Section 3.3.2.1, we consider from now on that the upper limit on the SFR is given by the L band limit, i.e. 600 $M_\odot$ yr^{-1} beam^{-1}, corresponding to a $3\sigma_{\rm RMS}$ upper limit of 24.5 μJy at 1.4 GHz (rest frame). This is consistent with the Webb et al.

(2015a) star formation rate, since as long as the star formation region extent is equivalent to 2 beams or more, the star formation is not detectable.

3.4. Discussion

Relatively common in the Universe, starbursts are rare in the vicinity of BCGs. Our goal was to study one of the most star-forming BCGs known, using some of the deepest VLA observations ever made of a high-redshift cluster of galaxies. Here, we discuss the implications of our results. First, we focus on the BCG detection. We then discuss the non detection of star formation and its implications.

3.4.1. BCG detection

We detected radio emission coincident with the BCG optical centre, at or above $3\sigma_{\rm RMS}$ levels in each of our 5 radio image. In addition, out of the 27 spectroscopically confirmed members, two galaxies were detected. No detections are resolved. We found no evidence for extended or diffuse emission.

Although the point-like morphology of the BCG and its coincidence with the optical centre of its HST counterpart suggest that we detected an AGN, we do not exclude the possibility of a compact starburst. Indeed, compact starbursts are common in star-forming galaxies at $z \sim 2$ (e.g. Elbaz et al., 2011; Barro et al., 2013; Elbaz et al., 2017). In addition, several simulations of galaxy wet mergers (e.g. Hopkins et al., 2013; Di Matteo et al., 2007) found that the bulks of the post-merging starbursts occur at the centres of the newly formed galaxies. Since the BCG of SpARCS1049 might have experienced a major wet merger in a recent past (Webb et al., 2015a, 2017) its radio luminosity could be either powered by AGN activity or by star formation.

We use the Hogan et al. (2015) SED models highlighted in Section 3.3.1.3 to distinguish between the various possible origins for radio emission: jetted outflows or core emission from the AGN, which would respectively have very steep and flat spectral indexes, or starburst-dominated emission, with a typical spectral index between -0.7 and -0.8 (e.g. Heesen et al., 2014). Core emission from the AGN is not rare: about 60% of the line-emitting BCGs (line-emitting BCGs, usually found in col core clusters, host generally more powerful sources ; e.g. Hogan et al., 2015) have a strong core component.

3.4.1.1. *Basic model fitting*

First, we fitted the 4 basic SED models that are outlined in Section 3.3.1.3 (Eq. 3.3.1.3, 3.3.1.3, 3.3.1.3 and 3.3.1.3) to the BCG. We let the coefficients, the spectral indexes, and the parameter ν_0 (in the "dropline" model only) free to vary. We did not restrain the range of possible values, although those models imply coefficients greater than 0. We then based

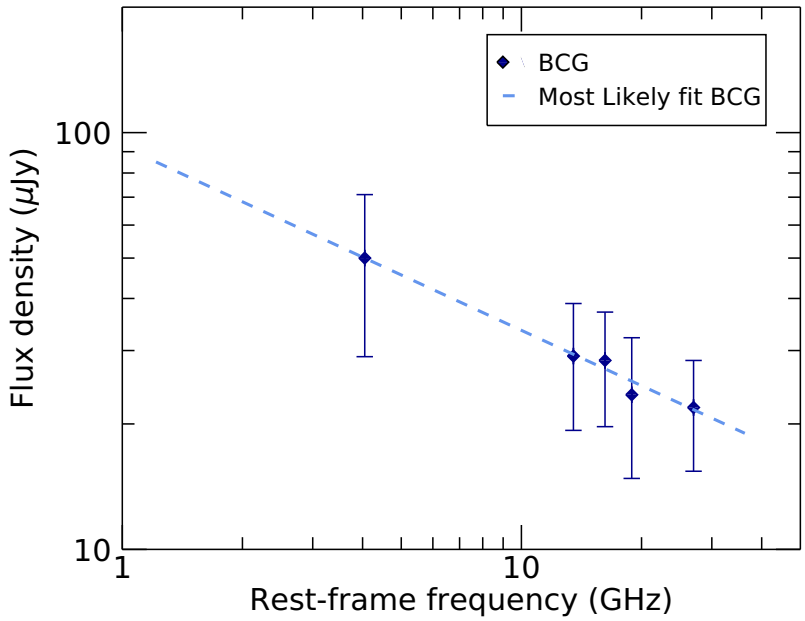

Figure 3.3 Radio SEDs for the BCG radio detection. The dashed lines illustrates the best fit when considering a simple power law.

Table 3. IV. Best model for the BCG.

Object	Best model	χ^2_ν
BCG	$S = (93 \pm 71)\nu^{(-0.44\pm0.29)}$	0.022

our evaluation of the fit on its physical plausibility and on the reduced χ^2_ν. By physical plausibility, we mean that:

1. A_i coefficients must be greater than 0.
2. Spectral index values must be between -3 and 1.

We then computed the χ^2_ν of the remaining models. The most likely fit is the model with the χ^2_ν value nearest 1. We found that the most likely fit consists of a simple power law (see Figure 3.3) with a spectral index of -0.44 ± 0.29 (see Table 3. IV). Radio emission related to star formation tends to be steeper, with spectral indexes between -0.7 and -0.8 (e.g. Heesen et al., 2014). However, since uncertainties are large, we can not determine decisively the origin, core emission, jets or star formation, of the radio emission.

Nevertheless, the 24 μm emission, used by Webb et al. (2015a) as a tracer of the star formation, and the CO emission, which traces the cold gas (e.g. Webb et al., 2017), have centroids located to the South-East ($\sim$ 15 kpc from the BCG optical centre), rather than on the BCG optical centre. Conversely, since our radio detection is a point source located

at the BCG optical centre, we suspect that the BCG radio emission is not related to star formation and more likely comes from the AGN only. For now on, we therefore consider that radio emission is due to AGN activity in the BCG only.

Core and non core models are not exclusive: Hogan et al. (2015) add a simple power law to a core or non-core model to describe the radio emission of several BCGs in their sample. To explore the possible presence of a core component and jets in the same time, we tested several of these hybrid models on the BCG. However, since our radio SED is poorly constrained, results were non-physical or irrelevant.

3.4.1.2. *Comparison to other BCGs*

We compared the radio emission from our BCG with the radio luminosities of the lower redshift BCGs from the Hogan et al. (2015) line-emitting sample. They determined the properties of about 250 $z \lesssim 0.4$ BCGs, half of them line-emitting, to explore if and how the radio properties of BCG hosted by relaxed clusters differ from those of the BCGs in more disturbed clusters. These authors use the presence or absence of emission lines (especially Hα and [NII]) as a proxy to distinguish between clusters with strong cool cores and those with weak or no cool cores. Given the intense star formation detected by Webb et al. (2015a), we suspect the presence of a cool core in SpARCS1049.

Since the steep, non core component usually dominates the overall BCG radio emission at low frequencies, Hogan et al. (2015) use the 1 GHz emission to characterize the non-core component. Conversely, the flat, core component usually dominates the BCG radio emission at higher frequencies. These author use the 10 GHz emission to characterize the core component. Figure 3.4 presents the core and non core luminosities of the line-emitting BCGs in Hogan et al. (2015) sample. The colours and shapes of the symbols indicate the various models used by Hogan et al. (2015) to perform the luminosity decompositions.

Since the exact origin and decomposition of the radio emission of SpARCS1049 BCG remain unclear, we tested two limiting cases. We first assumed that all the emission we observed in the BCG comes from AGN jets and follow the spectral index computed in Section 3.4.1.1. Based on the emission level at 1.5 GHz in the observer frame, we computed the k-corrected jet emission at 1 GHz. Then based on the k-corrected jet emission at 10 GHz, we computed an upper limit for the core emission. The result is shown in cyan on Figure 3.4.

We then assumed that all the observed emission in the BCG comes from the AGN core. Following a similar procedure, we computed a k-corrected core emission at 10 GHz and an upper limit for the jet emission at 1 GHz. The result is shown in magenta on Figure 3.4.

Figure 3.4 shows that the BCG in SpARCS1049 lies in the middle of the dot cloud, no matter how the emission is distributed between jets an core. Therefore, the BCG in

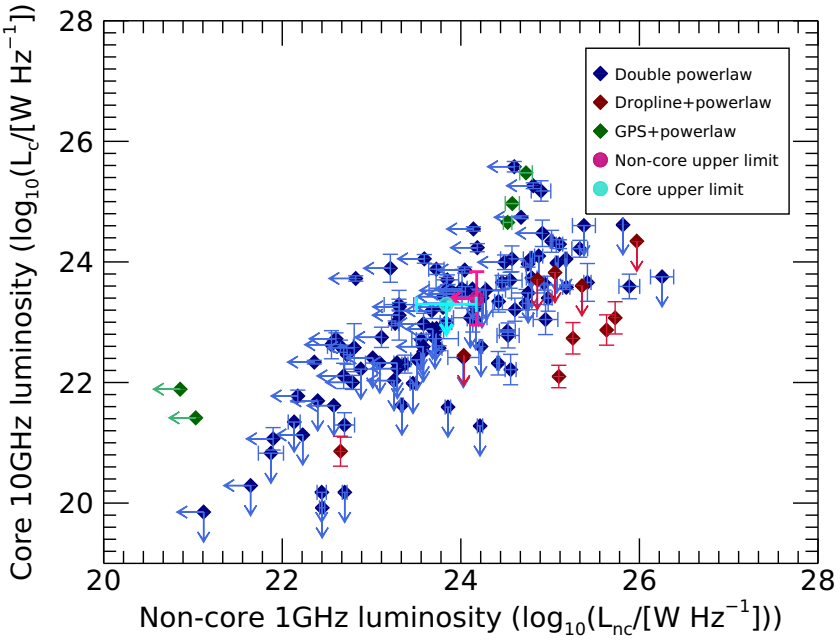

Figure 3.4 A comparison between core and a non-core powers of the Hogan et al. (2015) sample and 3 possibilities for SpARCS1049. Blue diamonds are Hogan et al. (2015) objects following a power law model for non-core and core emission, red diamonds non-core emission follow a "dropline" model, associated with a power law model for core emission. Green diamond models for non-core emission are power laws, but their core emission follow gigahertz peaked source (GPS) models. Assuming that most of the emission from SpARCS1049 BCG originates from one component, we derived an upper limit for the non-core component (magenta circle) and the core component (cyan circle).

SpARCS1049 has a radio luminosity typical of BCGs at $z \leq 0.4$, which is somewhat surprising. Since SpARCS1049 hosts an huge molecular gas reservoir (Webb et al., 2017), and radio AGN tend to be more common and more luminous at $z \sim 1.5$ (Smolcic et al., 2017), we expected the BCG of SpARCS1049 to lie among the luminous BCGs of Hogan et al. (2015) sample.

More quantitatively, assuming the simple power law model computed in Section 3.4.1.1, the BCG in SpARCS1049 has a rest frame 1.5 GHz luminosity of $(5.75 \pm 2.93) \times 10^{23}$ W Hz^{-1}, slightly below the threshold of 10^{24} W Hz^{-1}, set by Best et al. (2014) to distinguish between luminous and less luminous AGN.

Therefore, the black hole at the centre of the BCG might have a modest accretion rate. This normality suggests that something may prevent or partially block inflows from the molecular gas reservoir. Among the possible culprits: an efficient star formation or an offset between the gas reservoir and the BCG.

3.4.2. Star formation in the vicinity of the BCG

After a tentative characterization of the detected AGN, we need to constrain the other component of the BCG in SpARCS1049: the starburst. Although we did not detect it, the star formation location can be constrained with SED fitting and its extent can be constrained with radio upper limits. Thus, combining these 2 constraints, we can also constrain the triggering mechanism of the star formation.

3.4.2.1. *The infrared star formation rate*

Webb et al. (2015a) computed an AGN-corrected star formation rate (SFR) of 860 ± 130 $M_\odot$ yr^{-1}, based on the far infrared emission (FIR), computed from the SED fitting. To make our own SFR estimate, we used Chary and Elbaz (2001) SED templates which cover radio wavelengths up to 0.3 m (1 GHz) in the BCG rest frame.

To compute the best fit, the SFR and their uncertainties, we followed the Webb et al. (2015a) method, altering only the computation of the amplitude of the fit. Instead of using a range of amplitudes for each template, we computed the multiplication factors needed to adjust a template to each single data point. Then, the fitting amplitude of this template was obtained by calculating the weighted mean of these factors, with the inverse square of the uncertainties as weights.

We computed two different fits. First, we made a fit similar to the Webb et al. (2015a) fit, to insure that the alterations we made to the calculations do not significantly change the resulting SED fits. Then, we performed a second fit, including our new VLA observations, in addition to the data mentioned above. Hereafter, we will refer to these fits as the IR fit and the all-data fit respectively. This is to verify if we are able to fit all the observed fluxes with a single SED, even though the FIR and radio emission could be distinct spatially. Results are presented in Table 3. V and in Figure 3.5.

For the IR fit, the AGN-corrected SFR is 952 ± 103 $M_\odot$ yr^{-1}, in good agreement with the Webb et al. (2015a) value. However, including the radio data from the AGN detection lowers the amount of FIR emission in the resulting fit. The AGN-removed SFR computed from this fit is also significantly lower: 620 ± 59 $M_\odot$ yr^{-1}.

An examination of Figure 3.5 reveals that the measured radio fluxes are significantly below the expected values in both fits. For example, at 1.5 GHz (L band), the observed emission level is 50 ± 21 μJy, below the expected 86 ± 8 μJy and 142 ± 11 μJy for the all-data fit and IR fit respectively. Also, the expected spectral indexes, both around -0.7, are steeper than the observed index, -0.44 ± 0.29. To check if a different Chary and Elbaz (2001) SED model could better describe the radio data, we tried to do a radio-only fit. However, all the resulting fits are poor and none of the SED templates yield to a significantly better χ^2_ν than the others.

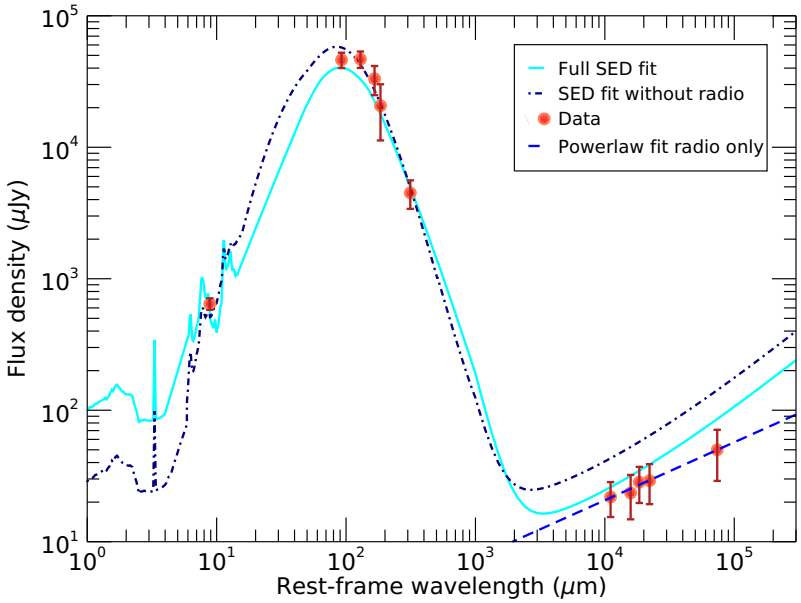

Figure 3.5 Best-fitted Chary and Elbaz (2001) templates. The best-fit template for all the existing data, infrared and radio, is in cyan. The dash-dotted navy template is the best fit for the pre-existing infrared data only. For comparison, the best fitted power law for radio data is shown by the blue dashed line.

Table 3. V. SED-based SFR

Fit	χ^2_ν	FIR luminosity ($L_\odot$)	Uncorrected SFR ($M_\odot$ yr^{-1})	SFR[a] ($M_\odot$ yr^{-1})	Expected flux in Lband (μJy)
All data	1.324	$(4.5 \pm 0.4) \times 10^{12}$	770 ± 70	620 ± 60	86 ± 8
Infrared data	1.006	$(6.9 \pm 0.7) \times 10^{12}$	1190 ± 130	950 ± 100	142 ± 11

[a]AGN-removed SFR, assuming 20% of the FIR luminosity comes from the AGN.

One explanation for the discrepancy between the SED models and the radio data is that the models assume a star-formation dominated radio emission, which has a typical spectral index of -0.7 (e.g. Heesen et al., 2014). However, as discussed in the previous section, the radio emission probably comes from the AGN. Therefore, we can treat this difference as an additional indication that the radio emission is AGN dominated with few (if any) contribution from the star formation.

Moreover, most of the mid and far-infrared measurements have resolutions of 5 arcsec or worse (one of the far infrared measurements has a resolution of 15 arcsec), while our biggest radio beam spans 1.27 arcsec $\times$ 0.85 arcsec. Keeping this in mind, we suggest that the star formation happens close to the BCG but not within it. If the star formation had been within

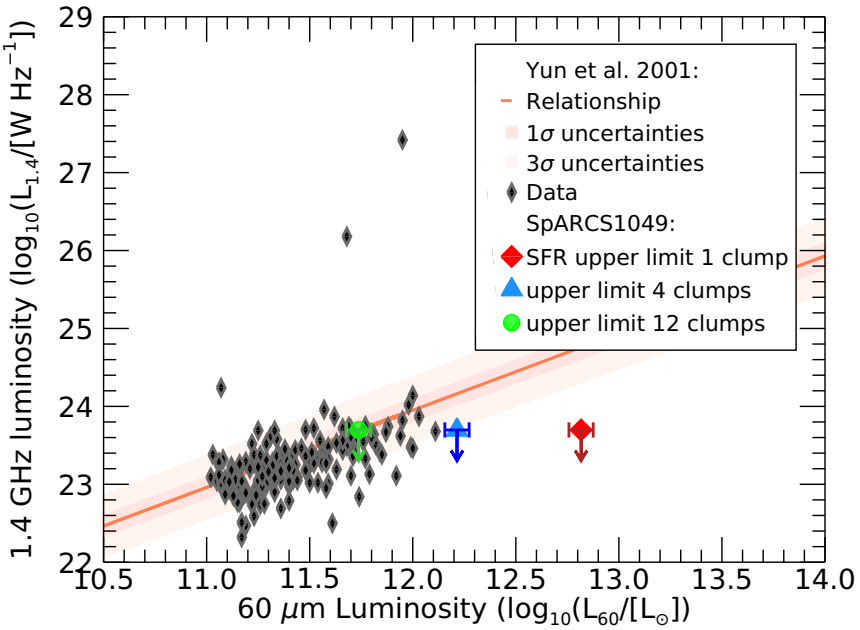

Figure 3.6 Comparison between Yun et al. (2001) and our upper limit for star formation detection, as calculated in Section 3.3.2.2. The three upper limits shows what happens when we vary the number of star formation "clumps", based on the assumption that these clumps could be resolved in radio (so the detection limit does not change in radio), but are all within one beam in the infrared. We also assume that all "clumps" contribute equally to the 60μm emission. The 60μm luminosity calculation is based on Chary and Elbaz (2001) best-fit for infrared data only. To be consistent with our SED-based star forming rates, the AGN far-infrared luminosity is subtracted to the FIR luminosities presented here, assuming a 20% contribution (Webb et al., 2015a).

the BCG, we would have detected it (the BCG is a point source) and the two SED fits would have been consistent.

3.4.2.2. *Implications of the radio limit*

After constraining the location of the star formation, the next step is to constrain the extent or "clumpiness" of the star-forming zone. We can do this with the radio flux upper limit, in combination with the far infrared luminosity inferred from the SED fitting presented in the last section.

We used the Yun et al. (2001) relation between far-infrared (60 μm) and 1.4 GHz luminosity. Figure 3.6 shows the Yun et al. (2001) data and relationship, with 3 overplotted upper limits. These upper limits show where 1, 4 or 12 star-forming "clumps," with similar star formation rates, would lie on that relation.

We used the SED "infrared best fit" to compute the 60 μm luminosities of those clumps, assuming that we do not have a sufficient resolution at 60 μm to resolve individuals clumps. Thus, if we have 4 clumps of equal star-forming rates, the infrared luminosity is divided by four and if we have 12 clumps, it is divided by twelve. In radio, we assume that resolution is sufficient to distinguish individual clumps, but not the sensitivity. Hence, the radio luminosity is set to an upper limit of 5.0×10^{23} W Hz^{-1}, which correspond to the 1.4 GHz rest frame luminosity of a SFR of 596 M$_\odot$ yr^{-1} per beam. Figure 3.6 shows that the 12 clumps upper limit is on the relation. The 4 clumps upper limit is on the edge of the 3σ region near the relation.

Our detection limit for star formation is 596 M$_\odot$ yr^{-1} beam^{-1} and the total SFR is 952 ± 103 M$_\odot$ yr^{-1}. Therefore, the conclusion is simple: star formation is not concentrated inside one beam, or we would have detected it. However, as long as the star formation extends to two beams or more, the star-forming zones would not have been detected, except if two thirds or more of the overall emission is concentrated within one beam. Moreover, Figure 3.6 suggests that the star-forming zones could be far more extended than 2 beams.

3.4.3. Implications for BCG formation scenarios

We can now say two things about the star formation: star-forming regions are in the BCG vicinity but not within; and the star formation is diffuse or divided into multiple clumps.

Based on that, we can constrain the evolutionary scenarios invoked to explain the characteristics of the BCG in SpARCS1049. There are three different scenarios: 1) a major wet merger, 2) several small galaxies stripped of their molecular gas by the BCG and 3) a dry merger induced offset between the BCG and the gravitational centre of the cluster, which would create a cooling flow responsible for the star formation (Webb et al., 2017).

The first scenario, involving a major wet merger, is disfavoured by our constrains on star formation: Hopkins et al. (2013) and Di Matteo et al. (2007) found that in the final stages of a wet merger (i.e. the coalescence), most of the resulting starburst occurs in the centre of the newly formed galaxy. The HST mosaic (see Figures 3.1 and 3.2) shows a morphology coherent with the final stage of a wet merger, but our SED fitting suggests that the bulk of the star formation is outside the BCG. The disturbed morphology could be due to an interaction excluding the BCG, but this situation is unlikely, since no members have been detected in radio in the vicinity of the BCG. Moreover, the AGN in the BCG isn't very active, but this is weak evidence against the first scenario: although major galaxy interactions can trigger radio-mode AGN (Ellison et al., 2015), galaxy interactions are not the main cause of AGN activity (Kocevski et al., 2012).

In the second scenario, star formation may occur in the near-infrared clumps. This is more likely, as long as the star-forming clumps are sufficiently dispersed to fill several beams. A rough estimate of the number of L band beams (the biggest) needed to cover the clump

region gives ~ 3.5 beams. This scenario implies no particular constrains for AGN activity in the BCG. Thus, the second scenario is plausible.

In the third scenario, a cooling flow could create a diffuse star-forming region. The cooling flow could trigger AGN activity, but the offset between the cluster centre and the BCG limits the amount of gas that reaches the AGN. It is unclear which effect would dominate. However, the presence of a large, $1.1 \pm 0.1 \times 10^{11}$ $M_\odot$ molecular gas reservoir with a single velocity component (Webb et al., 2015a), fits well with this scenario.

3.4.3.1. *A comparison with the Phoenix cluster*

To investigate the likeliness of the displaced cooling flow scenario, we compare the SpARCS1049 centre to the Phoenix cluster BCG. The Phoenix cluster hosts the only other well-studied high redshift BCG with a comparable SFR. At z=0.596, the BCG of the Phoenix cluster hosts a massive cooling flow of 3820 ± 530 $M_\odot$ yr^{-1} (McDonald et al., 2012), fuelled by a molecular gas reservoir (dihydrogen) of $(2.1 \pm 0.3) \times 10^{10}$ $M_\odot$ (McDonald et al., 2014; Russell et al., 2017). It forms stars at a rate of 610 ± 50 $M_\odot$ yr^{-1} (McDonald et al., 2015). By comparison, SpARCS1049 has a SFR of 952 ± 103 $M_\odot$ yr^{-1} and a molecular gas reservoir of $1.1 \pm 0.1 \times 10^{11}$ $M_\odot$.

SpARCS1049 and the Phoenix cluster central AGNs are very different. Assuming a simple power law model for the SpARCS1049 BCG radio emission, with a spectral index of -0.44, leads to a 10 MHz to 10 GHz integrated power of $(4.4 \pm 3.5) \times 10^{33}$ W. In contrast, the radio power emitted by the jets in the Phoenix cluster is ~ 1000 times stronger (3.6×10^{36} W; McDonald et al., 2015). Therefore, if both clusters harbour cooling flows of comparable amplitudes, only a small fraction of the inflowing gas reaches the centre of the BCG in SpARCS1049. Thus, if SpARCS1049 has a cooling flow, there might be some distance between the BCG and the gravitational centre of the cluster and/or a very efficient star formation. The molecular gas reservoir in the centre of SpARCS1049 is ~ 5 times more massive than the gas reservoir of the Phoenix cluster BCG, for similar star-forming rates.

However, cooling flows are closely related to the dynamics of cool core clusters (see Section 3.1). Moderate cool core clusters are found up to $z \sim 1.5$ (e.g. Santos et al., 2008; McDonald et al., 2013b), but the combination of a cool core and a recent major merger sufficiently powerful to displace the BCG away from the centre seems unlikely.

Although the optical morphology of the Phoenix cluster BCG is filamentary (McDonald et al., 2015), the majority of the star formation occurs within 15 kpc of the BCG centre (M. McDonald, private communication). If the SpARCS1049 star-forming region has a similar extent, then the size of the star-forming region would be consistent with a non-detection. Moreover, we found in Section 3.4.2.2 that the star-forming region might be about 12 beams wide to fall onto Yun et al. (2001) relationship between radio and infrared emission, assuming that each beam (or clump) contributes equally to far infrared emission.

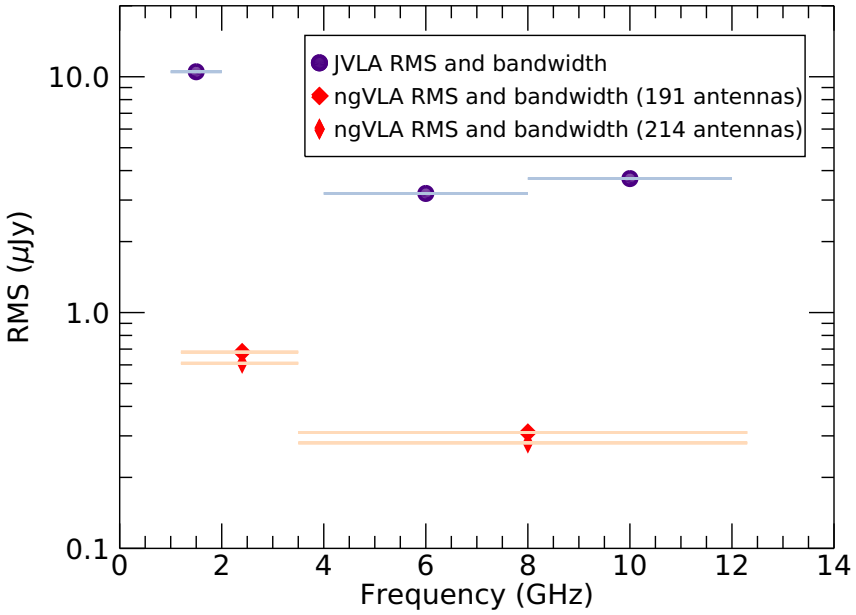

Figure 3.7 A comparison between the sensitivity reached by the actual Jansky VLA on SpARCS1049 observations and the planned sensitivity of the next generation VLA, assuming similar observations. Horizontal lines show the actual and planned bandwidths. For the ngVLA, we assumed 90 minutes of on-source time in each band, with 60 and 40% of the data flagged in 2.4 and 8 GHz bands respectively, and a robust weighting in the imaging algorithm (increase the RMS by a factor of 1.2 approximately). The thin diamonds show the ngVLA performances if all antennas are working properly, while the thick diamonds indicate what happens if $\frac{3}{28}$ of the antenna are flagged (a typical rate in SpARCS1049 Jansky VLA data), assuming the total flag percentage remains the same.

The diffuse infrared emission in the BCG vicinity (excluding the tidal tail seen in Figure 3.1) is consistent with a star-forming region with a radius of $\lesssim$ 2.5 arcsec. However, the near infrared morphology of the centre of SpARCS1049 shows no evidence of the filamentary structures presents in the Phoenix clusters.

The displaced cooling flow hypothesis can explain the diffuse morphology. However, it needs a merger sufficiently violent to displace the BCG but sufficiently smooth to keep an eventual cool core relaxed.

3.4.4. Implications for the future of the field

We lack information to understand what is taking place in SpARCS1049's core. X-ray observations of SpARCS1049 with the Chandra X-ray Observatory will be discussed in a future paper but for now, we need additional data to better constrain the location and extent of the star formation. Our new radio observations also show the limit of the current

VLA for exploring the high-redshift Universe. Thus, we are interested in the capacities of the VLA successor, the future next generation VLA (ngVLA). Through this section, we will use our VLA observations of SpARCS1049 as a model to explore the sensitivity of the future ngVLA in a realistic observing context.

To compare our current observations to the planned performance of the ngVLA, we calculated the theoretical RMS of the ngVLA in the 2.4 and 8 GHz bands (Selina and Murphy, 2017) [1]. To perform our computation, we assumed 90 minutes of on-source time in each band, with a level of RFI similar to what we found in our current data: 60% at 2.4 GHz band and 40% at 8 GHz band. Finally, we assume robust Briggs weighting in the imaging algorithm, which increase the RMS by a factor of 1.2 approximately.

For the number of working antennae, we tested 2 limiting cases, assuming that the overall flag percentage remains the same. We first assumed an ideal situation where each of the 214 planned antennae work properly. Conversely, in our data reduction, we found a mean of 3 antennae (out of 28) per observation with abnormal visibilities. We can reasonably assume that the ngVLA performance will be better. Thus, at worse, about $\frac{3}{28}$ of the antennae may have problems, which gives us a lower limit of 191 working antennae.

A comparison between the expected RMS for the ngVLA and the RMS reached by our actual VLA data is presented on Figure 3.7. The expected RMS for the ngVLA are approximately 10 times lower than the RMS level reached by the current VLA at similar frequencies. We note that the RMS reached with 191 and 214 antennae are relatively similar.

To push our analysis further, we computed the minimum SFR detectable with the ngVLA, following the method presented in Section 3.3.2.3. We compute a $3\sigma_{\rm RMS}$ detection limit for both bands. If 191 antennae are working, the detection thresholds are 2.04 μJy beam^{-1} at 2.4 GHz and 0.93 μJy beam^{-1} at 8 GHz. In the ideal case (214 antennae working), these thresholds are respectively 1.83 and 0.84 μJy beam^{-1}.

To be conservative and consistent with our work in Section 3.3.2, we want a $3\sigma_{\rm RMS}$ for a potential star-forming zone in both bands. Following the calculation presented in Section 3.3.2.3, if 191 (214) antennae are working, we found that the minimum detectable SFR is 57 (51) $M_\odot$ yr^{-1} beam^{-1}.

3.5. Summary

We presented deep, multiwavelength radio observation of SpARCS1049, one of the most distant objects ever studied in radio. SpARCS1049 is a cluster of galaxies with a starbursting core, displaying a complex morphology in the infrared (Webb et al., 2015a) and a immense

1. Updated SEFD values and bandwidths have been taken on the ngVLA project website, `http://ngvla.nrao.edu/page/refdesign`, Dec. 2017

$\sim 10^{11} M_\odot$ molecular gas reservoir (Webb et al., 2017). We detected the BCG and 2 galaxies among the 27 spectroscopically confirmed members, but we did not detect any diffuse emission or starbursting clump. Given that, we draw the following conclusions:

— The radio emission of the BCG likely comes from its AGN. It is best fitted by a simple power law, with a spectral index of -0.44 ± 0.29. However, more data are needed to better constrain the radio SED origin and shape.

— We found that the star-formation rate in the cluster core is 952 ± 103 $M_\odot$ yr^{-1}. However, our new infrared and radio SED fit suggest that star-forming regions are not embedded in the BCG. Combining the SED fit with our upper limit for the radio emission induced by star formation, we find that star forming regions are either made of numerous clumps, or very extended.

— We explored the possible origins of the BCG complex infrared morphology and of its gas reservoir. There is growing evidence against the single, major wet merger scenario initially developed by Webb et al. (2015a). Although the displaced cooling flow scenario fits well with our constraints on the star-forming regions, we will need X-ray data to distinguish between the 3 scenarios.

These results demonstrate the pertinence of combining infrared imaging with radio, but also show the limits of the current VLA and the need for a more sensitive radio interferometer (like the ngVLA) to explore the high-redshift Universe.

BIBLIOGRAPHY

Barro, G., S. M. Faber, P. G. Pérez-González, D. C. Koo, C. C. Williams, D. D. Kocevski, J. R. Trump, M. Mozena, E. McGrath, A. van der Wel, S. Wuyts, E. F. Bell, D. J. Croton, D. Ceverino, A. Dekel, M. L. N. Ashby, E. Cheung, H. C. Ferguson, A. Fontana, J. Fang, M. Giavalisco, N. A. Grogin, Y. Guo, N. P. Hathi, P. F. Hopkins, K.-H. Huang, A. M. Koekemoer, J. S. Kartaltepe, K.-S. Lee, J. A. Newman, L. A. Porter, J. R. Primack, R. E. Ryan, D. Rosario, R. S. Somerville, M. Salvato and L.-T. Hsu. 2013, CANDELS: The Progenitors of Compact Quiescent Galaxies at z ~ 2, *The Astrophysical Journal*, vol. 765, doi:10.1088/0004-637X/765/2/104, p. 104, ISSN 0004-637X. URL `http://adsabs.harvard.edu/abs/2013ApJ...765..104B`.

Best, P. N., L. M. Ker, C. Simpson, E. E. Rigby and J. Sabater. 2014, The cosmic evolution of radio-AGN feedback to z=1, *Monthly Notices of the Royal Astronomical Society*, vol. 445, n° 1, doi:10.1093/mnras/stu1776, p. 955–969, ISSN 0035-8711, 1365-2966. URL `http://arxiv.org/abs/1409.0263`, arXiv: 1409.0263.

Bildfell, C., H. Hoekstra, A. Babul and A. Mahdavi. 2008, Resurrecting the red from the dead: optical properties of BCGs in X-ray luminous clusters, *Monthly Notices of the Royal Astronomical Society*, vol. 389, doi:10.1111/j.1365-2966.2008.13699.x, p. 1637–1654, ISSN 0035-8711. URL `http://adsabs.harvard.edu/abs/2008MNRAS.389.1637B`.

Chary, R. and D. Elbaz. 2001, Interpreting the Cosmic Infrared Background: Constraints on the Evolution of the Dust-enshrouded Star Formation Rate, *The Astrophysical Journal*, vol. 556, doi:10.1086/321609, p. 562–581, ISSN 0004-637X. URL `http://adsabs.harvard.edu/abs/2001ApJ...556..562C`.

Condon, J. J. 1992, Radio emission from normal galaxies, *Annual Review of Astronomy and Astrophysics*, vol. 30, doi:10.1146/annurev.aa.30.090192.003043, p. 575–611, ISSN 0066-4146. URL `http://adsabs.harvard.edu/abs/1992ARA%26A..30..575C`.

Condon, J. J., W. D. Cotton and J. J. Broderick. 2002, Radio Sources and Star Formation in the Local Universe, *The Astronomical Journal*, vol. 124, doi:10.1086/341650, p. 675–689, ISSN 0004-6256. URL `http://adsabs.harvard.edu/abs/2002AJ....124..675C`.

Cornwell, T. J., K. Golap and S. Bhatnagar. 2008, The non-coplanar baselines effect in radio interferometry: The W-Projection algorithm, *IEEE Journal of Selected Topics in Signal Processing*, vol. 2, n° 5, doi:10.1109/JSTSP.2008.2005290, p. 647–657, ISSN 1932-4553. URL `http://arxiv.org/abs/0807.4161`, arXiv: 0807.4161.

Croton, D. J., V. Springel, S. D. M. White, G. De Lucia, C. S. Frenk, L. Gao, A. Jenkins, G. Kauffmann, J. F. Navarro and N. Yoshida. 2006, The many lives of active galactic nuclei: cooling flows, black holes and the luminosities and colours of galaxies, *Monthly Notices of the Royal Astronomical Society*, vol. 365, doi:10.1111/j.1365-2966.2005.09675.x, p. 11–28, ISSN 0035-8711. URL http://adsabs.harvard.edu/abs/2006MNRAS.365...11C.

De Lucia, G. and J. Blaizot. 2007, The hierarchical formation of the brightest cluster galaxies, *Monthly Notices of the Royal Astronomical Society*, vol. 375, doi:10.1111/j.1365-2966.2006.11287.x, p. 2–14, ISSN 0035-8711. URL http://adsabs.harvard.edu/abs/2007MNRAS.375....2D.

Delhaize, J., V. Smolcic, I. Delvecchio, M. Novak, M. Sargent, N. Baran, B. Magnelli, G. Zamorani, E. Schinnerer, E. J. Murphy, M. Aravena, S. Berta, M. Bondi, P. Capak, P. Ciliegi, F. Civano, O. Ilbert, A. Karim, C. Laigle, O. L. Fevre, S. Marchesi, H. J. McCracken, M. Salvato, N. Seymour and L. Tasca. 2017, VLA-COSMOS 3ghz Large Project: The infrared-radio correlation of star-forming galaxies and AGN to $z\lesssim6$, *Astronomy & Astrophysics*, vol. 602, doi:10.1051/0004-6361/201629430, p. A4, ISSN 0004-6361, 1432-0746. URL http://arxiv.org/abs/1703.09723, arXiv: 1703.09723.

Demarco, R., G. Wilson, A. Muzzin, M. Lacy, J. Surace, H. K. C. Yee, H. Hoekstra, K. Blindert and D. Gilbank. 2010, Spectroscopic Confirmation of Three Red-sequence Selected Galaxy Clusters at z = 0.87, 1.16, and 1.21 from the SpARCS Survey, *The Astrophysical Journal*, vol. 711, doi:10.1088/0004-637X/711/2/1185, p. 1185–1197, ISSN 0004-637X. URL http://adsabs.harvard.edu/abs/2010ApJ...711.1185D.

Di Matteo, P., F. Combes, A.-L. Melchior and B. Semelin. 2007, Star formation efficiency in galaxy interactions and mergers: a statistical study, *Astronomy and Astrophysics*, vol. 468, doi:10.1051/0004-6361:20066959, p. 61–81, ISSN 0004-6361. URL http://adsabs.harvard.edu/abs/2007A%26A...468...61D.

Donahue, M., A. Jordán, S. A. Baum, P. Côté, L. Ferrarese, P. Goudfrooij, D. Macchetto, S. Malhotra, C. P. O'Dea, J. E. Pringle, J. E. Rhoads, W. B. Sparks and G. M. Voit. 2007, Infrared Emission from the Nearby Cool Core Cluster Abell 2597, *The Astrophysical Journal*, vol. 670, doi:10.1086/522575, p. 231–236, ISSN 0004-637X. URL http://adsabs.harvard.edu/abs/2007ApJ...670..231D.

Dressler, A. 1978, A comprehensive study of 12 very rich clusters of galaxies. I - Photometric technique and analysis of the luminosity function, *The Astrophysical Journal*, vol. 223, doi:10.1086/156310, p. 765–775, ISSN 0004-637X. URL http://adsabs.harvard.edu/abs/1978ApJ...223..765D.

Elbaz, D., M. Dickinson, H. S. Hwang, T. Díaz-Santos, G. Magdis, B. Magnelli, D. Le Borgne, F. Galliano, M. Pannella, P. Chanial, L. Armus, V. Charmandaris, E. Daddi, H. Aussel, P. Popesso, J. Kartaltepe, B. Altieri, I. Valtchanov, D. Coia, H. Dannerbauer, K. Dasyra, R. Leiton, J. Mazzarella, D. M. Alexander, V. Buat, D. Burgarella, R.-R. Chary, R. Gilli, R. J. Ivison, S. Juneau, E. Le Floc'h, D. Lutz, G. E. Morrison, J. R. Mullaney, E. Murphy, A. Pope, D. Scott, M. Brodwin, D. Calzetti, C. Cesarsky, S. Charlot, H. Dole, P. Eisenhardt,

H. C. Ferguson, N. Förster Schreiber, D. Frayer, M. Giavalisco, M. Huynh, A. M. Koekemoer, C. Papovich, N. Reddy, C. Surace, H. Teplitz, M. S. Yun and G. Wilson. 2011, GOODS-Herschel: an infrared main sequence for star-forming galaxies, *Astronomy and Astrophysics*, vol. 533, doi:10.1051/0004-6361/201117239, p. A119, ISSN 0004-6361. URL http://adsabs.harvard.edu/abs/2011A%26A...533A.119E.

Elbaz, D., R. Leiton, N. Nagar, K. Okumura, M. Franco, C. Schreiber, M. Pannella, T. Wang, M. Dickinson, T. Diaz-Santos, L. Ciesla, E. Daddi, F. Bournaud, G. Magdis, L. Zhou and W. Rujopakarn. 2017, Starbursts in and out of the star-formation main sequence, *arXiv:1711.10047 [astro-ph]*. URL http://arxiv.org/abs/1711.10047, arXiv: 1711.10047.

Ellison, S. L., D. R. Patton and R. C. Hickox. 2015, Galaxy pairs in the Sloan Digital Sky Survey - XII. The fuelling mechanism of low-excitation radio-loud AGN, *Monthly Notices of the Royal Astronomical Society*, vol. 451, doi:10.1093/mnrasl/slv061, p. L35–L39, ISSN 0035-8711. URL http://adsabs.harvard.edu/abs/2015MNRAS.451L..35E.

Elmegreen, D. M., B. G. Elmegreen, T. Ferguson and B. Mullan. 2007, Smooth and Starburst Tidal Tails in the GEMS and GOODS Fields, *The Astrophysical Journal*, vol. 663, doi:10.1086/518715, p. 734–751, ISSN 0004-637X. URL http://adsabs.harvard.edu/abs/2007ApJ...663..734E.

Fabian, A. C. 1994, Cooling Flows in Clusters of Galaxies, *Annual Review of Astronomy and Astrophysics*, vol. 32, doi:10.1146/annurev.aa.32.090194.001425, p. 277–318, ISSN 0066-4146. URL http://adsabs.harvard.edu/abs/1994ARA%26A..32..277F.

Fabian, A. C., S. A. Walker, H. R. Russell, C. Pinto, J. S. Sanders and C. S. Reynolds. 2017, Do sound waves transport the AGN energy in the Perseus Cluster?, *Monthly Notices of the Royal Astronomical Society: Letters*, vol. 464, nº 1, doi:10.1093/mnrasl/slw170, p. L1–L5, ISSN 1745-3925, 1745-3933. URL http://arxiv.org/abs/1608.07088, arXiv: 1608.07088.

Heesen, V., E. Brinks, A. K. Leroy, G. Heald, R. Braun, F. Bigiel and R. Beck. 2014, The Radio Continuum-Star Formation Rate Relation in WSRT SINGS Galaxies, *The Astronomical Journal*, vol. 147, doi:10.1088/0004-6256/147/5/103, p. 103, ISSN 0004-6256. URL http://adsabs.harvard.edu/abs/2014AJ....147..103H.

Hlavacek-Larrondo, J., A. C. Fabian, A. C. Edge, H. Ebeling, J. S. Sanders, M. T. Hogan and G. B. Taylor. 2012, Extreme AGN feedback in the MAssive Cluster Survey: a detailed study of X-ray cavities at z>0.3, *Monthly Notices of the Royal Astronomical Society*, vol. 421, doi:10.1111/j.1365-2966.2011.20405.x, p. 1360–1384, ISSN 0035-8711. URL http://adsabs.harvard.edu/abs/2012MNRAS.421.1360H.

Hogan, M. T., A. C. Edge, J. Hlavacek-Larrondo, K. J. B. Grainge, S. L. Hamer, E. K. Mahony, H. R. Russell, A. C. Fabian, B. R. McNamara and R. J. Wilman. 2015, A Comprehensive Study of the Radio Properties of Brightest Cluster Galaxies, *Monthly Notices of the Royal Astronomical Society*, vol. 453, nº 2, doi:10.1093/mnras/stv1517, p. 1201–1222, ISSN 0035-8711, 1365-2966. URL http://arxiv.org/abs/1507.03019, arXiv: 1507.03019.

Hopkins, P. F., T. J. Cox, L. Hernquist, D. Narayanan, C. C. Hayward and N. Murray. 2013, Star formation in galaxy mergers with realistic models of stellar feedback and the interstellar medium,

Monthly Notices of the Royal Astronomical Society, vol. 430, doi:10.1093/mnras/stt017, p. 1901–1927, ISSN 0035-8711. URL http://adsabs.harvard.edu/abs/2013MNRAS.430.1901H.

Hudson, D. S., R. Mittal, T. H. Reiprich, P. E. J. Nulsen, H. Andernach and C. L. Sarazin. 2010, What is a cool-core cluster? a detailed analysis of the cores of the X-ray flux-limited HIFLUGCS cluster sample, *Astronomy and Astrophysics*, vol. 513, doi:10.1051/0004-6361/200912377, p. A37, ISSN 0004-6361. URL http://adsabs.harvard.edu/abs/2010A%26A...513A..37H.

Kocevski, D. D., S. M. Faber, M. Mozena, A. M. Koekemoer, K. Nandra, C. Rangel, E. S. Laird, M. Brusa, S. Wuyts, J. R. Trump, D. C. Koo, R. S. Somerville, E. F. Bell, J. M. Lotz, D. M. Alexander, F. Bournaud, C. J. Conselice, T. Dahlen, A. Dekel, J. L. Donley, J. S. Dunlop, A. Finoguenov, A. Georgakakis, M. Giavalisco, Y. Guo, N. A. Grogin, N. P. Hathi, S. Juneau, J. S. Kartaltepe, R. A. Lucas, E. J. McGrath, D. H. McIntosh, B. Mobasher, A. R. Robaina, D. Rosario, A. N. Straughn, A. van der Wel and C. Villforth. 2012, CANDELS: Constraining the AGN-Merger Connection with Host Morphologies at z ~ 2, *The Astrophysical Journal*, vol. 744, doi:10.1088/0004-637X/744/2/148, p. 148, ISSN 0004-637X. URL http://adsabs.harvard.edu/abs/2012ApJ...744..148K.

Lidman, C., J. Suherli, A. Muzzin, G. Wilson, R. Demarco, S. Brough, A. Rettura, J. Cox, A. DeGroot, H. K. C. Yee, D. Gilbank, H. Hoekstra, M. Balogh, E. Ellingson, A. Hicks, J. Nantais, A. Noble, M. Lacy, J. Surace and T. Webb. 2012, Evidence for significant growth in the stellar mass of brightest cluster galaxies over the past 10 billion years, *Monthly Notices of the Royal Astronomical Society*, vol. 427, doi:10.1111/j.1365-2966.2012.21984.x, p. 550–568, ISSN 0035-8711. URL http://adsabs.harvard.edu/abs/2012MNRAS.427..550L.

Lonsdale, C. J., H. E. Smith, M. Rowan-Robinson, J. Surace, D. Shupe, C. Xu, S. Oliver, D. Padgett, F. Fang, T. Conrow, A. Franceschini, N. Gautier, M. Griffin, P. Hacking, F. Masci, G. Morrison, J. O'Linger, F. Owen, I. Pérez-Fournon, M. Pierre, R. Puetter, G. Stacey, S. Castro, M. d. C. Polletta, D. Farrah, T. Jarrett, D. Frayer, B. Siana, T. Babbedge, S. Dye, M. Fox, E. Gonzalez-Solares, M. Salaman, S. Berta, J. J. Condon, H. Dole and S. Serjeant. 2003, SWIRE: The SIRTF Wide-Area Infrared Extragalactic Survey, *Publications of the Astronomical Society of the Pacific*, vol. 115, doi:10.1086/376850, p. 897–927, ISSN 0004-6280. URL http://adsabs.harvard.edu/abs/2003PASP..115..897L.

Markevitch, M. and A. Vikhlinin. 2007, Shocks and cold fronts in galaxy clusters, *Physics Reports*, vol. 443, nº 1, doi:10.1016/j.physrep.2007.01.001, p. 1–53, ISSN 03701573. URL http://arxiv.org/abs/astro-ph/0701821, arXiv: astro-ph/0701821.

McDonald, M., M. Bayliss, B. A. Benson, R. J. Foley, J. Ruel, P. Sullivan, S. Veilleux, K. A. Aird, M. L. N. Ashby, M. Bautz, G. Bazin, L. E. Bleem, M. Brodwin, J. E. Carlstrom, C. L. Chang, H. M. Cho, A. Clocchiatti, T. M. Crawford, A. T. Crites, T. de Haan, S. Desai, M. A. Dobbs, J. P. Dudley, E. Egami, W. R. Forman, G. P. Garmire, E. M. George, M. D. Gladders, A. H. Gonzalez, N. W. Halverson, N. L. Harrington, F. W. High, G. P. Holder, W. L. Holzapfel, S. Hoover, J. D. Hrubes, C. Jones, M. Joy, R. Keisler, L. Knox, A. T. Lee, E. M. Leitch, J. Lieu, M. Lueker, D. Luong-Van, A. Mantz, D. P. Marrone, J. J. McMahon, J. Mehl, S. S. Meyer, E. D. Miller, L. Mocanu, J. J. Mohr, T. E. Montroy, S. S. Murray, T. Natoli, S. Padin, T. Plagge,

C. Pryke, T. D. Rawle, C. L. Reichardt, A. Rest, M. Rex, J. E. Ruhl, B. R. Saliwanchik, A. Saro, J. T. Sayre, K. K. Schaffer, L. Shaw, E. Shirokoff, R. Simcoe, J. Song, H. G. Spieler, B. Stalder, Z. Staniszewski, A. A. Stark, K. Story, C. W. Stubbs, R. Suhada, A. van Engelen, K. Vanderlinde, J. D. Vieira, A. Vikhlinin, R. Williamson, O. Zahn and A. Zenteno. 2012, A Massive, Cooling-Flow-Induced Starburst in the Core of a Highly Luminous Galaxy Cluster, *Nature*, vol. 488, nº 7411, doi:10.1038/nature11379, p. 349–352, ISSN 0028-0836, 1476-4687. URL http://arxiv.org/abs/1208.2962, arXiv: 1208.2962.

McDonald, M., B. Benson, S. Veilleux, M. W. Bautz and C. L. Reichardt. 2013a, An HST/WFC3-UVIS View of the Starburst in the Cool Core of the Phoenix Cluster, *The Astrophysical Journal Letters*, vol. 765, doi:10.1088/2041-8205/765/2/L37, p. L37, ISSN 0004-637X. URL http://adsabs.harvard.edu/abs/2013ApJ...765L..37M.

McDonald, M., B. A. Benson, A. Vikhlinin, B. Stalder, L. E. Bleem, T. de Haan, H. W. Lin, K. A. Aird, M. L. N. Ashby, M. W. Bautz, M. Bayliss, S. Bocquet, M. Brodwin, J. E. Carlstrom, C. L. Chang, H. M. Cho, A. Clocchiatti, T. M. Crawford, A. T. Crites, S. Desai, M. A. Dobbs, J. P. Dudley, R. J. Foley, W. R. Forman, E. M. George, D. Gettings, M. D. Gladders, A. H. Gonzalez, N. W. Halverson, F. W. High, G. P. Holder, W. L. Holzapfel, S. Hoover, J. D. Hrubes, C. Jones, M. Joy, R. Keisler, L. Knox, A. T. Lee, E. M. Leitch, J. Liu, M. Lueker, D. Luong-Van, A. Mantz, D. P. Marrone, J. J. McMahon, J. Mehl, S. S. Meyer, E. D. Miller, L. Mocanu, J. J. Mohr, T. E. Montroy, S. S. Murray, D. Nurgaliev, S. Padin, T. Plagge, C. Pryke, C. L. Reichardt, A. Rest, J. Ruel, J. E. Ruhl, B. R. Saliwanchik, A. Saro, J. T. Sayre, K. K. Schaffer, E. Shirokoff, J. Song, R. Šuhada, H. G. Spieler, S. A. Stanford, Z. Staniszewski, A. A. Stark, K. Story, A. van Engelen, K. Vanderlinde, J. D. Vieira, R. Williamson, O. Zahn and A. Zenteno. 2013b, The Growth of Cool Cores and Evolution of Cooling Properties in a Sample of 83 Galaxy Clusters at $0.3 < z < 1.2$ Selected from the SPT-SZ Survey, *The Astrophysical Journal*, vol. 774, doi:10.1088/0004-637X/774/1/23, p. 23, ISSN 0004-637X. URL http://adsabs.harvard.edu/abs/2013ApJ...774...23M.

McDonald, M., B. R. McNamara, R. J. van Weeren, D. E. Applegate, M. Bayliss, M. W. Bautz, B. A. Benson, J. E. Carlstrom, L. E. Bleem, M. Chatzikos, A. C. Edge, A. C. Fabian, G. P. Garmire, J. Hlavacek-Larrondo, C. Jones-Forman, A. B. Mantz, E. D. Miller, B. Stalder, S. Veilleux and J. A. ZuHone. 2015, Deep Chandra, HST-COS, and Megacam Observations of the Phoenix Cluster: Extreme Star Formation and AGN Feedback on Hundred Kiloparsec Scales, *The Astrophysical Journal*, vol. 811, doi:10.1088/0004-637X/811/2/111, p. 111, ISSN 0004-637X. URL http://adsabs.harvard.edu/abs/2015ApJ...811..111M.

McDonald, M., B. Stalder, M. Bayliss, S. W. Allen, D. E. Applegate, M. L. N. Ashby, M. Bautz, B. A. Benson, L. E. Bleem, M. Brodwin, J. E. Carlstrom, I. Chiu, S. Desai, A. H. Gonzalez, J. Hlavacek-Larrondo, W. L. Holzapfel, D. P. Marrone, E. D. Miller, C. L. Reichardt, B. R. Saliwanchik, A. Saro, T. Schrabback, S. A. Stanford, A. A. Stark, J. D. Vieira and A. Zenteno. 2016, Star-forming Brightest Cluster Galaxies at $0.25 < z < 1.25$: A Transitioning Fuel Supply, *The Astrophysical Journal*, vol. 817, doi:10.3847/0004-637X/817/2/86, p. 86, ISSN 0004-637X. URL http://adsabs.harvard.edu/abs/2016ApJ...817...86M.

McDonald, M., M. Swinbank, A. C. Edge, D. J. Wilner, S. Veilleux, B. A. Benson, M. T. Hogan, D. P. Marrone, B. R. McNamara, L. H. Wei, M. B. Bayliss and M. W. Bautz. 2014, The State of the Warm and Cold Gas in the Extreme Starburst at the Core of the Phoenix Galaxy Cluster (SPT-CLJ2344-4243), *The Astrophysical Journal*, vol. 784, doi:10.1088/0004-637X/784/1/18, p. 18, ISSN 0004-637X. URL http://adsabs.harvard.edu/abs/2014ApJ...784...18M.

McMullin, J. P., B. Waters, D. Schiebel, W. Young and K. Golap. 2007, CASA Architecture and Applications, in *Astronomical Data Analysis Software and Systems XVI*, *ASP Conf. Ser.*, vol. 376, edit by R. A. Shaw, F. Hill and D. J. Bell, p. 127.

McNamara, B. R. and P. E. J. Nulsen. 2007, Heating Hot Atmospheres with Active Galactic Nuclei, *Annual Review of Astronomy and Astrophysics*, vol. 45, nº 1, doi:10.1146/annurev.astro.45.051806.110625, p. 117–175, ISSN 0066-4146, 1545-4282. URL http://arxiv.org/abs/0709.2152, arXiv: 0709.2152.

McNamara, B. R. and P. E. J. Nulsen. 2012, Mechanical Feedback from Active Galactic Nuclei in Galaxies, Groups, and Clusters, *New Journal of Physics*, vol. 14, nº 5, doi:10.1088/1367-2630/14/5/055023, p. 055 023, ISSN 1367-2630. URL http://arxiv.org/abs/1204.0006, arXiv: 1204.0006.

Muzzin, A., G. Wilson, H. K. C. Yee, H. Hoekstra, D. Gilbank, J. Surace, M. Lacy, K. Blindert, S. Majumdar, R. Demarco, J. P. Gardner, M. Gladders and C. Lonsdale. 2009, Spectroscopic Confirmation of Two Massive Red-Sequence-Selected Galaxy Clusters at z ~ 1.2 in the SpARCS-North Cluster Survey, *The Astrophysical Journal*, vol. 698, doi:10.1088/0004-637X/698/2/1934, p. 1934–1942, ISSN 0004-637X. URL http://adsabs.harvard.edu/abs/2009ApJ...698.1934M.

O'Dea, C. P., S. A. Baum, G. Privon, J. Noel-Storr, A. C. Quillen, N. Zufelt, J. Park, A. Edge, H. Russell, A. C. Fabian, M. Donahue, C. L. Sarazin, B. McNamara, J. N. Bregman and E. Egami. 2008, An Infrared Survey of Brightest Cluster Galaxies. II. Why are Some Brightest Cluster Galaxies Forming Stars?, *The Astrophysical Journal*, vol. 681, doi:10.1086/588212, p. 1035–1045, ISSN 0004-637X. URL http://adsabs.harvard.edu/abs/2008ApJ...681.1035O.

O'Dea, K. P., A. C. Quillen, C. P. O'Dea, G. R. Tremblay, B. T. Snios, S. A. Baum, K. Christiansen, J. Noel-Storr, A. C. Edge, M. Donahue and G. M. Voit. 2010, Hubble Space Telescope Far-ultraviolet Observations of Brightest Cluster Galaxies: The Role of Star Formation in Cooling Flows and BCG Evolution, *The Astrophysical Journal*, vol. 719, doi:10.1088/0004-637X/719/2/1619, p. 1619–1632, ISSN 0004-637X. URL http://adsabs.harvard.edu/abs/2010ApJ...719.1619O.

Oemler, A., Jr. 1976, The structure of elliptical and cD galaxies., *The Astrophysical Journal*, vol. 209, doi:10.1086/154769, p. 693–709, ISSN 0004-637X. URL http://adsabs.harvard.edu/abs/1976ApJ...209..693O.

Rafferty, D. A., B. R. McNamara, P. E. J. Nulsen and M. W. Wise. 2006, The Feedback-regulated Growth of Black Holes and Bulges through Gas Accretion and Starbursts in Cluster Central Dominant Galaxies, *The Astrophysical Journal*, vol. 652, doi:10.1086/507672, p. 216–231, ISSN 0004-637X. URL http://adsabs.harvard.edu/abs/2006ApJ...652..216R.

Rawle, T. D., A. C. Edge, E. Egami, M. Rex, G. P. Smith, B. Altieri, A. Fiedler, C. P. Haines, M. J. Pereira, P. G. Pérez-González, J. Portouw, I. Valtchanov, G. Walth, P. P. van der Werf and M. Zemcov. 2012, The Relation between Cool Cluster Cores and Herschel-detected Star Formation in Brightest Cluster Galaxies, *The Astrophysical Journal*, vol. 747, doi:10.1088/0004-637X/747/1/29, p. 29, ISSN 0004-637X. URL http://adsabs.harvard.edu/abs/2012ApJ...747...29R.

Russell, H. R., M. McDonald, B. R. McNamara, A. C. Fabian, P. E. J. Nulsen, M. B. Bayliss, B. A. Benson, M. Brodwin, J. E. Carlstrom, A. C. Edge, J. Hlavacek-Larrondo, D. P. Marrone, C. L. Reichardt and J. D. Vieira. 2017, Alma Observations of Massive Molecular Gas Filaments Encasing Radio Bubbles in the Phoenix Cluster, *The Astrophysical Journal*, vol. 836, doi:10.3847/1538-4357/836/1/130, p. 130, ISSN 0004-637X. URL http://adsabs.harvard.edu/abs/2017ApJ...836..130R.

Santos, J. S., P. Rosati, P. Tozzi, H. Böhringer, S. Ettori and A. Bignamini. 2008, Searching for cool core clusters at high redshift, *Astronomy and Astrophysics*, vol. 483, doi:10.1051/0004-6361:20078815, p. 35–47, ISSN 0004-6361. URL http://adsabs.harvard.edu/abs/2008A%26A...483..35S.

Santos, J. S., P. Tozzi, P. Rosati and H. Böhringer. 2010, The evolution of cool-core clusters, *Astronomy and Astrophysics*, vol. 521, doi:10.1051/0004-6361/201015208, p. A64, ISSN 0004-6361. URL http://adsabs.harvard.edu/abs/2010A%26A...521A..64S.

Selina, R. and E. Murphy. 2017, ngVLA Reference Design Development & Performance Estimates, *ngVLA Memo Series*, vol. 17, p. 7. URL http://library.nrao.edu/public/memos/ngvla/NGVLA_17.pdf.

Smolcic, V., M. Novak, I. Delvecchio, L. Ceraj, M. Bondi, J. Delhaize, S. Marchesi, E. Murphy, E. Schinnerer, E. Vardoulaki and G. Zamorani. 2017, The VLA-COSMOS 3~GHz Large Project: Cosmic evolution of radio AGN and implications for radio-mode feedback since z~5, *Astronomy & Astrophysics*, vol. 602, doi:10.1051/0004-6361/201730685, p. A6, ISSN 0004-6361, 1432-0746. URL http://arxiv.org/abs/1705.07090, arXiv: 1705.07090.

Stott, J. P., C. A. Collins, C. Burke, V. Hamilton-Morris and G. P. Smith. 2011, Little change in the sizes of the most massive galaxies since z = 1, *Monthly Notices of the Royal Astronomical Society*, vol. 414, doi:10.1111/j.1365-2966.2011.18404.x, p. 445–457, ISSN 0035-8711. URL http://adsabs.harvard.edu/abs/2011MNRAS.414..445S.

Stott, J. P., A. C. Edge, G. P. Smith, A. M. Swinbank and H. Ebeling. 2008, Near-infrared evolution of brightest cluster galaxies in the most X-ray luminous clusters since z = 1, *Monthly Notices of the Royal Astronomical Society*, vol. 384, doi:10.1111/j.1365-2966.2007.12807.x, p. 1502–1510, ISSN 0035-8711. URL http://adsabs.harvard.edu/abs/2008MNRAS.384.1502S.

Tremaine, S. D. and D. O. Richstone. 1977, A test of a statistical model for the luminosities of bright cluster galaxies, *The Astrophysical Journal*, vol. 212, doi:10.1086/155049, p. 311–316, ISSN 0004-637X. URL http://adsabs.harvard.edu/abs/1977ApJ...212..311T.

Voigt, L. M. and A. C. Fabian. 2004, Thermal conduction and reduced cooling flows in galaxy clusters, *Monthly Notices of the Royal Astronomical Society*, vol. 347, doi:10.1111/j.1365-2966.2004.

07285.x, p. 1130–1149, ISSN 0035-8711. URL http://adsabs.harvard.edu/abs/2004MNRAS.347.1130V.

Webb, T., J. Lowenthal, M. Yun, A. G. Noble, A. Muzzin, G. Wilson, H. K. C. Yee and R. Cybulski. 2017, Detection of a Substantial Molecular Gas Reservoir in a brightest cluster galaxy at z = 1.7, *The Astrophysical Journal*, vol. 844, nº 2, doi:10.3847/2041-8213/aa7749, p. L17, ISSN 2041-8213. URL http://arxiv.org/abs/1706.01366, arXiv: 1706.01366.

Webb, T., A. Noble, A. DeGroot, G. Wilson, A. Muzzin, N. Bonaventura, M. Cooper, A. Delahaye, R. Foltz, C. Lidman, J. Surace, H. K. C. Yee, S. Chapman, L. Dunne, J. Geach, B. Hayden, H. Hildebrandt, J. Huang, A. Pope, M. W. L. Smith, S. Perlmutter and A. Tudorica. 2015a, An Extreme Starburst in the Core of a Rich Galaxy Cluster at z = 1.7, *The Astrophysical Journal*, vol. 809, doi:10.1088/0004-637X/809/2/173, p. 173, ISSN 0004-637X. URL http://adsabs.harvard.edu/abs/2015ApJ...809..173W.

Webb, T. M. A., A. Muzzin, A. Noble, N. Bonaventura, J. Geach, Y. Hezevah, C. Lidman, G. Wilson, H. K. C. Yee, J. Surace and D. Shupe. 2015b, The Star Formation History of BCGs to z = 1.8 from the SpARCS/SWIRE Survey: Evidence for Significant In Situ Star Formation at High Redshift, *The Astrophysical Journal*, vol. 814, doi:10.1088/0004-637X/814/2/96, p. 96, ISSN 0004-637X. URL http://adsabs.harvard.edu/abs/2015ApJ...814...96W.

van Weeren, R. J., H. T. Intema, D. V. Lal, F. Andrade-Santos, M. Brüggen, F. de Gasperin, W. R. Forman, M. Hoeft, C. Jones, S. E. Nuza, H. J. A. Röttgering and A. Stroe. 2014, A Distant Radio Mini-halo in the Phoenix Galaxy Cluster, *The Astrophysical Journal Letters*, vol. 786, doi:10.1088/2041-8205/786/2/L17, p. L17, ISSN 0004-637X. URL http://adsabs.harvard.edu/abs/2014ApJ...786L..17V.

Wilson, G., A. Muzzin, H. K. C. Yee, M. Lacy, J. Surace, D. Gilbank, K. Blindert, H. Hoekstra, S. Majumdar, R. Demarco, J. P. Gardner, M. D. Gladders and C. Lonsdale. 2009, Spectroscopic Confirmation of a Massive Red-Sequence-Selected Galaxy Cluster at z = 1.34 in the SpARCS-South Cluster Survey, *The Astrophysical Journal*, vol. 698, doi:10.1088/0004-637X/698/2/1943, p. 1943–1950, ISSN 0004-637X. URL http://adsabs.harvard.edu/abs/2009ApJ...698.1943W.

Yun, M. S., N. A. Reddy and J. J. Condon. 2001, Radio Properties of Infrared-selected Galaxies in the IRAS 2 Jy Sample, *The Astrophysical Journal*, vol. 554, doi:10.1086/323145, p. 803–822, ISSN 0004-637X. URL http://adsabs.harvard.edu/abs/2001ApJ...554..803Y.

Chapter 4

SECOND AND THIRD MEMBERS

4.1. Introduction

In the previous chapter, I presented three radio detections but focussed on the BCG detection. In this chapter, I will briefly present the two other detections. Figure 4.1, shows the location of the BCG (in yellow) and of the 27 spectroscopically confirmed members (Webb et al., 2015). Among those confirmed members, the non-detected members at radio

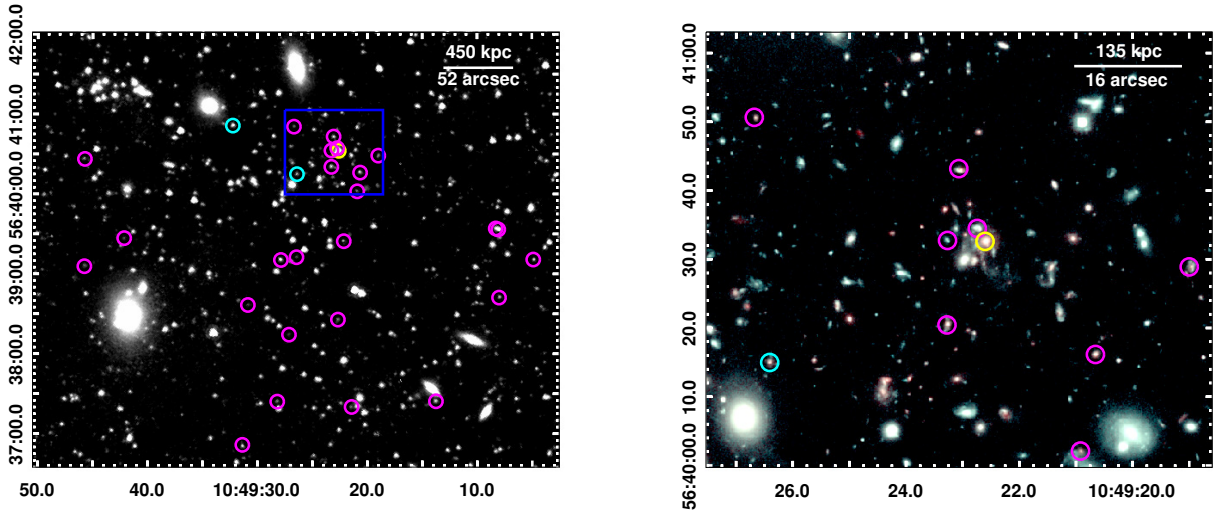

Figure 4.1 Large-scale view of SpARCS1049 and its 27 spectroscopically confirmed members (Webb et al., 2015). Left: 4.5 μm Spitzer archival IRAC image, spanning 3.4 Mpc by 2.8 Mpc. The blue box shows the part of the cluster displayed on the right panel. Right: Large-scale view of the HST image. The members with cyan circles are detected with our VLA observations, but the other members, in magenta, are not. The BCG is circled in yellow. The Spitzer image has been downloaded from `http://sha.ipac.caltech.edu/applications/Spitzer/SHA/`. The HST mosaïcs in the F160W and the F105W filters are a courtesy of Tracy Webb; see Webb et al. (2015).

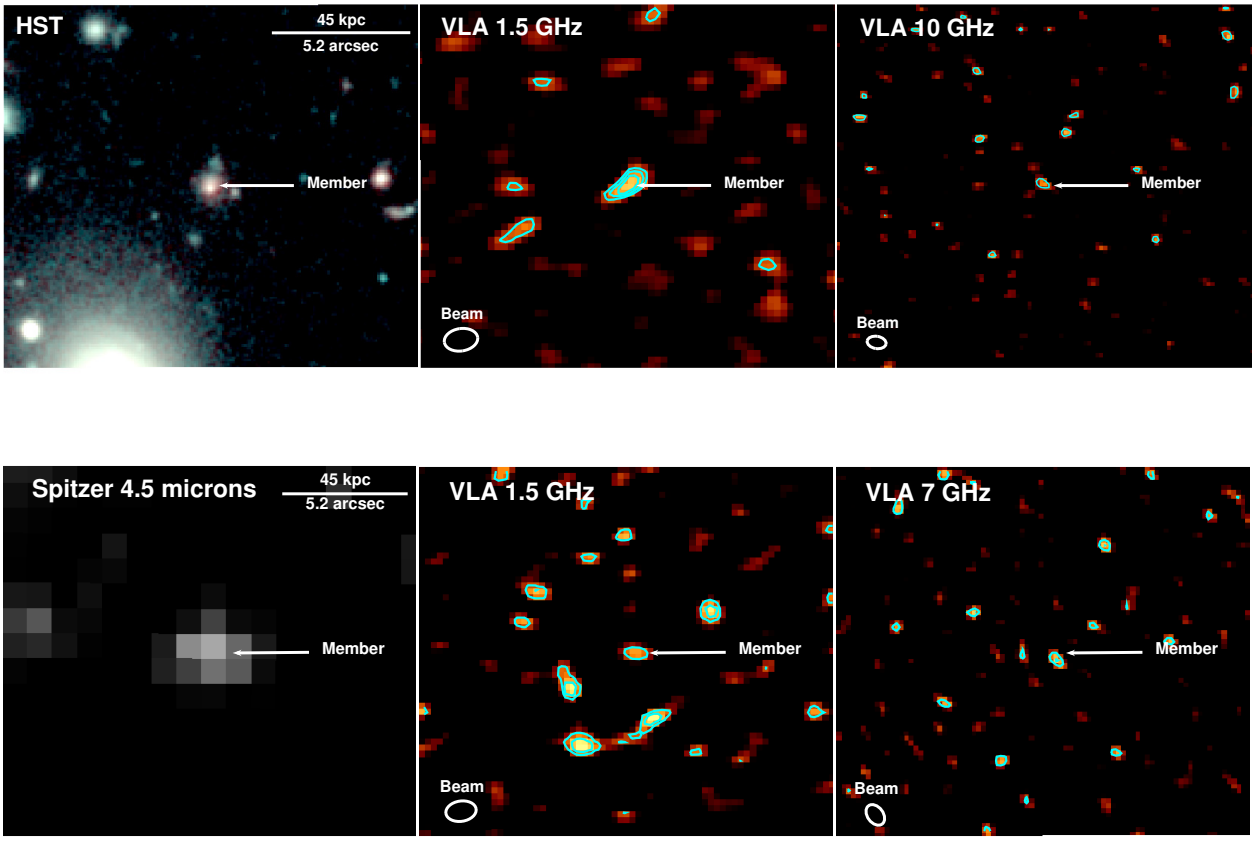

Figure 4.2 Deep VLA images of the non-BCG members in SpARCS1049 and their HST or Spitzer counterpart. Top-left: Zoom-in on the right panel of Figure 4.1. Top-middle: 1.5 GHz VLA image of the same area (RMS of 10.5 μJy beam^{-1}, $3\sigma_{\rm RMS} = 31.5$ μJy beam^{-1}). Top-right: 10 GHz VLA image (RMS of 3.7 μJy beam^{-1}, $3\sigma_{\rm RMS} = 11.1$ μJy beam^{-1}). Bottom-left: Zoom-in on the left panel of Figure 4.1. Bottom-middle: L band image of the third member. Bottom-right: C band 7 GHz image of the third member (there is no detection of this member in X band), with a RMS of 4.7 μJy beam^{-1}, $3\sigma_{\rm RMS} = 14.1$ μJy beam^{-1}. The scales are indicated in the top right corner of the HST images. The VLA beams are shown in the lower left corners and the radio contours (3, 4 and $5\sigma_{\rm RMS}$ levels) are displayed in cyan.

wavelengths are circled in magenta and the two detections in cyan. Hereafter, I will refer to the detected member sitting South-East of the BCG, at $10:49:26.40 \ +56:40:14.98$, as the second member. I will call third member the last detection, sitting at $10:49:32.25 \ +56:40:51.53$ to the North-East of the BCG.

Figure 4.2, shows these detections and their HST or Spitzer counterparts. Since both detections are point sources, I chose to display here only the edges of the radio spectrum: in L band at 1.5 GHz and in X band at 10 GHz. Since the third member is not detected in the X band, I replaced this image by its detection in the C band at 7 GHz. A multiwavelength radio view of each member is presented in Appendix A.

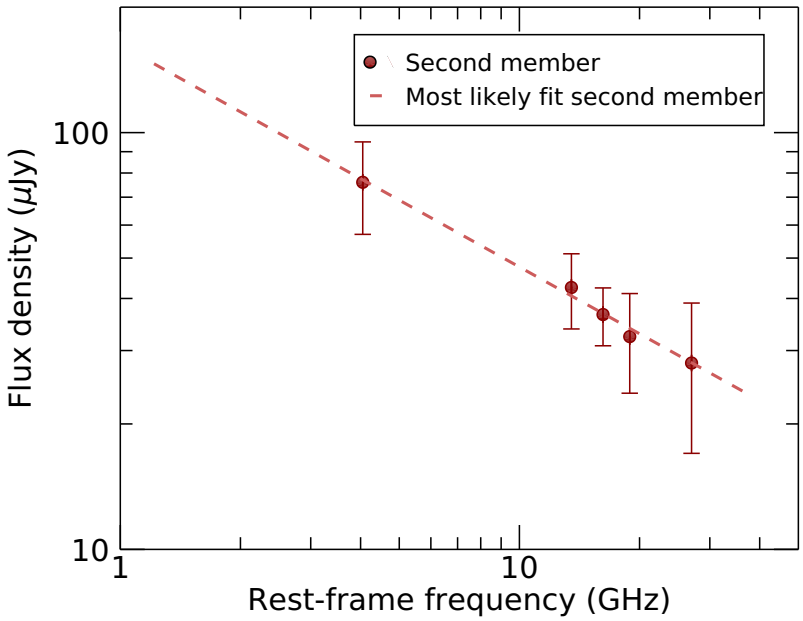

Figure 4.3 Radio SEDs for the second member detected with the VLA. The dashed lines illustrates the best fit when considering a simple power law. Since the SED of the third member is very poorly constrained, I choose not to display it here.

Table 4. I. Best model for the two spectroscopically confirmed detected members

Object	Best model	χ^2_ν
Second member	$S = (162 \pm 83)\nu^{(-0.53\pm0.19)}$	0.028
Third member	$S = (138 \pm 120)\nu^{(-0.76\pm0.35)}$	0.712

4.2. Tentative characterisation of the spectra

Following the method of Hogan et al. (2015) summarized in Section 3.3.1.3 of the previous chapter, I tried to determine the origin of the radio emission from the two members. Results are displayed in Table 4. I and in Figure 4.3. The second member is detected above $5\sigma_{\rm RMS}$ in every band, except for its $3\sigma_{\rm RMS}$ detection in the X band. Therefore, I was able to test each of the 4 basic models from Hogan et al. (2015). However, the only realistic fit is obtained with the simplest SED model: a power law with a spectral index of -0.53 ± 0.19 (presented in Figure 4.3). This spectral index suggests an AGN, since star formation tends to be steeper, with spectral indexes between -0.7 and -0.8 (e.g. Heesen et al., 2014). However uncertainties are too large to exclude the possibility of a star-forming origin.

Since the third member is only detected at $3\sigma_{\rm RMS}$ in 3 images (L band at 1.5 GHz, C band at 6 and 7 GHz), most of the SED models from Hogan et al. (2015) have too many

parameters to be tested. Fitting a simple power law to these 3 points yields to a spectral index of -0.76 ± 0.35, shown in Table 4. I. Since the fit is too uncertain, I chose not to display it in Figure 4.3.

BIBLIOGRAPHY

Heesen, V., E. Brinks, A. K. Leroy, G. Heald, R. Braun, F. Bigiel and R. Beck. 2014, The Radio Continuum-Star Formation Rate Relation in WSRT SINGS Galaxies, *The Astronomical Journal*, vol. 147, doi:10.1088/0004-6256/147/5/103, p. 103, ISSN 0004-6256. URL `http://adsabs.harvard.edu/abs/2014AJ....147..103H`.

Hogan, M. T., A. C. Edge, J. Hlavacek-Larrondo, K. J. B. Grainge, S. L. Hamer, E. K. Mahony, H. R. Russell, A. C. Fabian, B. R. McNamara and R. J. Wilman. 2015, A Comprehensive Study of the Radio Properties of Brightest Cluster Galaxies, *Monthly Notices of the Royal Astronomical Society*, vol. 453, nº 2, doi:10.1093/mnras/stv1517, p. 1201–1222, ISSN 0035-8711, 1365-2966. URL `http://arxiv.org/abs/1507.03019`, arXiv: 1507.03019.

Webb, T., A. Noble, A. DeGroot, G. Wilson, A. Muzzin, N. Bonaventura, M. Cooper, A. Delahaye, R. Foltz, C. Lidman, J. Surace, H. K. C. Yee, S. Chapman, L. Dunne, J. Geach, B. Hayden, H. Hildebrandt, J. Huang, A. Pope, M. W. L. Smith, S. Perlmutter and A. Tudorica. 2015, An Extreme Starburst in the Core of a Rich Galaxy Cluster at z = 1.7, *The Astrophysical Journal*, vol. 809, doi:10.1088/0004-637X/809/2/173, p. 173, ISSN 0004-637X. URL `http://adsabs.harvard.edu/abs/2015ApJ...809..173W`.

Chapter 5

CONCLUSION

SpARCS104922.6+564032.5, nicknamed SpARC1049, is a high redshift cluster of galaxies at $z = 1.7$. Discovered by the Spitzer Adaptation of the Red-sequence Cluster Survey (SpARCS), SpARCS1049 is relatively massive for its redshift, with a dynamic mass (M_{500}) of $3.3 \pm 1.2 \times 10^{14}$ $M_{\odot}$. SpARCS1049 has been the subject of two previous studies (Webb et al., 2015, 2017). The first used HST observations in the near infrared to unravel the complex morphology of the core of SpARCS1049. A chain of clumps seems to originate from the outskirts of the BCG and extends to ~ 60 kpc. This chain of clumps is prolonged by a tidal tail and the whole BCG complex is embedded in diffuse emission. Based on the infrared SED, Webb et al. (2015) calculated a frenetic SFR of 860 ± 130 $M_{\odot}yr^{-1}$. As a result, Webb et al. (2015) concluded that the BCG was experiencing an ongoing major gas-rich merger. Besides, Webb et al. (2015) spectroscopically confirmed the membership of 27 galaxies to SpARCS1049, in addition to the BCG.

Furthermore, Webb et al. (2017) discovered an immense gas reservoir of $1.1 \pm 0.1 \times 10^{11}$ $M_{\odot}$ in the central region of SpARCS1049, with a single velocity component. This reservoir is too large to originate from a single gas-rich merger only and it lacks the multiple velocity components created by a merger event. These authors invoked two alternative formation scenarios to explain the core morphology and the presence of a large gas reservoir in SpARCS1049: gas stripping of multiple small galaxies by the BCG or a displaced cooling flow.

BCG formation and evolution are poorly understood in high redshift clusters of galaxies. In this context, radio observations of SpARCS1049 are easy to justify. The aims of this dissertation are therefore to use multiwavelength radio observations of SpARCS1049 to study the supermassive black hole in the BCG, to constrain the location, extent and intensity of the star formation and to constrain the 3 possible formation scenarios aforementioned.

5.1. Radio observations of SpARCS1049

I reduced and analysed a total of 6.5 hours of data taken with the JVLA in L band (1.5 h), C band (2 sets of 1 h each) and X band (1 h). Radio Frequency Interferences (RFIs) were flagged, data calibrated, imaged, self-calibrated, re-imaged and, in the case of the two datasets in C band, merged. In order to achieve the best signal-to-noise ratio, special care was taken in choosing the parameters and the number of self-calibrations. I was able to reach the thermal noise in all images with one round of self-calibration.

I detected the BCG and 2 of the 27 spectroscopically confirmed members. Since both the BCG and one of the cluster members (called the second member) have 5σ detection levels in the merged original C band image (at 6 GHz), I split each C band dataset in two and re-imaged each part, making two additional images in the C band: one at 5 GHz and one at 7 GHz. The BCG and the second member are detected in every image, but the third member is only detected in 3 images (L band, 6 and 7 GHz in C band). Neither the images nor the radio SEDs show unambiguous traces of extended star formation in all the galaxies.

5.1.1. The black hole

The BCG and the two cluster members appeared as point sources in every image they are detected. A compact source is more likely to be powered by an AGN than by star formation, but a compact starburst is still a possibility. Following the method and models of Hogan et al. (2015), I tried to determine the origin (star formation, core or jetted outflows) of the radio emission of the 3 detected sources but since SEDs are poorly sampled (five integrated flux measurements, one per image, for two sources and only 3 measurements for one source), I cannot draw conclusions on the origin of the radio emission in the BCG nor in the two cluster members.

Assuming an AGN origin for the radio emission from the BCG, I derived an approximative value of the total radio power (core and jetted outflows) of the BCG. I found that, when compared to the Hogan et al. (2015) local sample of BCGs, SpARCS1049 BCG has an average radio power. So, despite the substantial molecular gas reservoir found in the centre of the cluster, the BCG black hole might only mildly accrete, which suggests that something prevents a part of the gas from reaching the black hole.

5.1.2. The star formation

I found no conclusive traces of star formation in the BCG vicinity. So, I calculated the minimum flux for a 3σ detection in each image and used these values to compute an upper limit on star formation. I found an upper limit of 596 $M_\odot$ yr^{-1} $beam^{-1}$, based on the conservative assumption that a potential star-forming zone should have been detected in 2 different bands to be confirmed. Such a limit means that, as long as a star-forming zone

spans across two beams or more, it could not be detected. However, a comparison between my radio flux upper limit and infrared emission, following the relation of Yun et al. (2001), suggests that the star-forming zone might be either more extended or made of multiple clumps.

In parallel, I made a new estimate of the infrared SFR, using the Chary and Elbaz (2001) SED templates to infer the flux density in the far infrared. I found an AGN-corrected SFR of $952 \pm 103\ M_{\odot}\ yr^{-1}$ in good agreement with the previous estimation of $860 \pm 130\ \mathrm{M}_{\odot}\ \mathrm{yr}^{-1}$ made by Webb et al. (2015). Therefore, star formation is detected in the BCG by infrared observations, but not by radio data. To solve this paradox, we invoke the poor resolution (several arcsecs) of the infrared data: there might be star formation in SpARCS1049's core, but not within the BCG. Thus, infrared data do not have the resolution to distinguish the BCG from its vicinity but detect star formation. Radio data have a sufficient resolution to isolate the BCG from the star-forming region, but insufficient sensitivity to detect the latter.

5.1.3. Toward a coherent formation scenario for the core of SpARCS1049

So far, my major conclusions can be summarized as follows: the black hole at the centre of the BCG is only mildly active, despite the large molecular gas reservoir previously found; the star-forming zone might be diffuse and is not located within the BCG. I can use this to constrain the 3 formation scenarios invoked by Webb et al. (2017): a major wet merger, gas stripping or multiple small galaxies or the displaced cooling flow.

The major wet merger hypothesis seems relatively unlikely, since in that case the bulk of star formation would be located in the core of the BCG. In addition, it does not fit well with the previous detection of molecular gas. The two other scenarios are more likely. More specifically, the displaced cooling flow scenario could explain the mild black hole activity by an offset between the black hole and its main feeding source, which may be a cooling flow. Similarly, the star formation would occur outside the BCG, where the cold gas is deposited.

5.2. Future work

However, no matter how attractive the displaced cooling flow scenario is, X-ray data are needed to distinguish between the two remaining scenarios. Chandra observations (PI Julie Hlavacek-Larrondo) have been awarded to my research group; they will provide evidence for the existence (or not) of a potential cooling flow in SpARCS1049. Additionally, they will give valuable insights on the intracluster medium physics of a high-redshift cluster.

Additionally, to trace more precisely the location and extent of the star formation, as well as study the state of the warm dust in the core of a high-redshift cluster, we plan to submit a proposal for the future James Webb Space Telescope (JWST). On a shorter timescale, we also plan to submit a proposal for snapshot observations with the JVLA, in order to study AGN activity in SpARCS clusters, especially for those at high redshift.

BIBLIOGRAPHY

Chary, R. and D. Elbaz. 2001, Interpreting the Cosmic Infrared Background: Constraints on the Evolution of the Dust-enshrouded Star Formation Rate, *The Astrophysical Journal*, vol. 556, doi: 10.1086/321609, p. 562–581, ISSN 0004-637X. URL http://adsabs.harvard.edu/abs/2001ApJ...556..562C.

Hogan, M. T., A. C. Edge, J. Hlavacek-Larrondo, K. J. B. Grainge, S. L. Hamer, E. K. Mahony, H. R. Russell, A. C. Fabian, B. R. McNamara and R. J. Wilman. 2015, A Comprehensive Study of the Radio Properties of Brightest Cluster Galaxies, *Monthly Notices of the Royal Astronomical Society*, vol. 453, nº 2, doi:10.1093/mnras/stv1517, p. 1201–1222, ISSN 0035-8711, 1365-2966. URL http://arxiv.org/abs/1507.03019, arXiv: 1507.03019.

Webb, T., J. Lowenthal, M. Yun, A. G. Noble, A. Muzzin, G. Wilson, H. K. C. Yee and R. Cybulski. 2017, Detection of a Substantial Molecular Gas Reservoir in a brightest cluster galaxy at z = 1.7, *The Astrophysical Journal*, vol. 844, nº 2, doi:10.3847/2041-8213/aa7749, p. L17, ISSN 2041-8213. URL http://arxiv.org/abs/1706.01366, arXiv: 1706.01366.

Webb, T., A. Noble, A. DeGroot, G. Wilson, A. Muzzin, N. Bonaventura, M. Cooper, A. Delahaye, R. Foltz, C. Lidman, J. Surace, H. K. C. Yee, S. Chapman, L. Dunne, J. Geach, B. Hayden, H. Hildebrandt, J. Huang, A. Pope, M. W. L. Smith, S. Perlmutter and A. Tudorica. 2015, An Extreme Starburst in the Core of a Rich Galaxy Cluster at z = 1.7, *The Astrophysical Journal*, vol. 809, doi:10.1088/0004-637X/809/2/173, p. 173, ISSN 0004-637X. URL http://adsabs.harvard.edu/abs/2015ApJ...809..173W.

Yun, M. S., N. A. Reddy and J. J. Condon. 2001, Radio Properties of Infrared-selected Galaxies in the IRAS 2 Jy Sample, *The Astrophysical Journal*, vol. 554, doi:10.1086/323145, p. 803–822, ISSN 0004-637X. URL http://adsabs.harvard.edu/abs/2001ApJ...554..803Y.

Appendix A

DETAILED VLA DATA REDUCTION

In 2016, we were awarded 6.5 hours of observations on the Karl G. Jansky Very Large Array (project 16A-283, PI Hlavachek-Larrondo), which are summarized in Table A. I. Observations, array configurations and on-source time are presented in Table A. I. Centred on the BCG in SpARCS1049, the observations consisted of 2 hours in L band (1-2 GHz), two observations of 1.5 hours each in C band (4-8 GHz) and 1.5 hours in X band (8-12 GHz). Data reduction was performed with CASA (Common Astronomy Software Application, McMullin et al. (2007)) following the steps described below. Most of the data reduction was performed with CASA 4.7.2, but final imaging in X band was made with version 5.1.2.

First, corrupted antennae listed in the operator logs were removed. Then, prior to the automatic RFI flagging procedure, data were pre-calibrated using the tasks GAINCAL, BANDPASS and APPLYCAL. For each antenna, we examined the amplitude versus frequency plot with PLOTCAL and flagged any abnormally low or high visibilities. We then proceeded with automatic RFI excision using the RFLAG and EXTEND modes of the task FLAGDATA. For the most RFI affected spectral windows in L band, additional flagging using the mode TFCROP was performed. Nevertheless, spectral windows 2, 4 and 8 of this band were so badly affected by RFI that we flagged them entirely. Spectral window 19 of C band was also entirely removed.

Table A. I. VLA observations

Date	Frequency (Band) (GHz)	Bandwidth (GHz)	Configuration	On-source time (min)	Flag percentage (%)	RMS [a] $\left(\frac{\mu Jy}{beam}\right)$
19 Nov 2016	1.5 (L)	1	A	80	60	11
20 & 21 May 2016	6 (C)	4	B	54	45	3[b]
21 May 2016	6 (C)	4	B	54	52	
21 May 2016	10 (X)	4	B	54	28	4

[a]Local noise level

[b]Local noise level for the merged image at 6GHz

We then examined the data using the task PLOTMS. Amplitude versus channels were carefully checked. Each spectral window was examined scan by scan, one spectral window at a time. For C and X band datasets, imaginary versus real corrected visibilities were examined as well, using the same systematic procedure. For C band only, target amplitudes versus UV distances were also verified. When most of the outliers were removed, data were calibrated. Then, target data were splitted (task SPLIT).

For C band datasets, several calibration problems occurred. They were solved by choosing a new reference antenna for calibration and by flagging two additional antennae in one of the datasets.

Images were made with the task CLEAN, using a W-projection algorithm (mode WIDE-FIELD) and 480 w-planes to correct the sky curvature across the field of view (Cornwell et al., 2008). We used Briggs weighing and a robustness parameter of 0. To ensure a sufficient sampling of the respective beams, we used a pixel size of 0.25 arcsec in L band, 0.20 arcsec in C bands and 0.15 arcsec in X band. For each band, the first clean was performed using the interactive mode, which allowed the creation of a customized cleaning mask. Subsequent cleans in the same band used the same mask, in the non-interactive mode. Both C band datasets were imaged with the same mask.

Since the BCG is very dim, we wanted to bring the noise down to the theoretical level. So, we applied a self-calibration procedure to the initial image. This procedure consists of deriving phase corrections with GAINCAL, applying them to the data using APPLYCAL and then making a new image. We tested several time solution intervals and solving procedures in L band, and varied the number of self-calibrations performed. The deepest images were obtained with one round of self-calibration and a T Jones solving procedure applied to an infinite time solution interval. Moreover, in order to attenuate artefacts, the threshold parameter in C and X band clean were set to approximately three times the RMS noise in initial images.

The two datasets in C band were imaged, self-calibrated and then re-imaged separately. Then, they were merged using the task CLEAN, individually self-calibrated using the procedure described above and finally re-merged in another clean. Both merging clean used 100 000 iteration, as well as the final clean in L band. In X band, we restrained ourselves to 45 000 iterations, because the clean seems unable to clean further. Other cleans were performed with 50 000 iterations. Final, reduced images are shown in Figures A.1, A.2 and A.3.

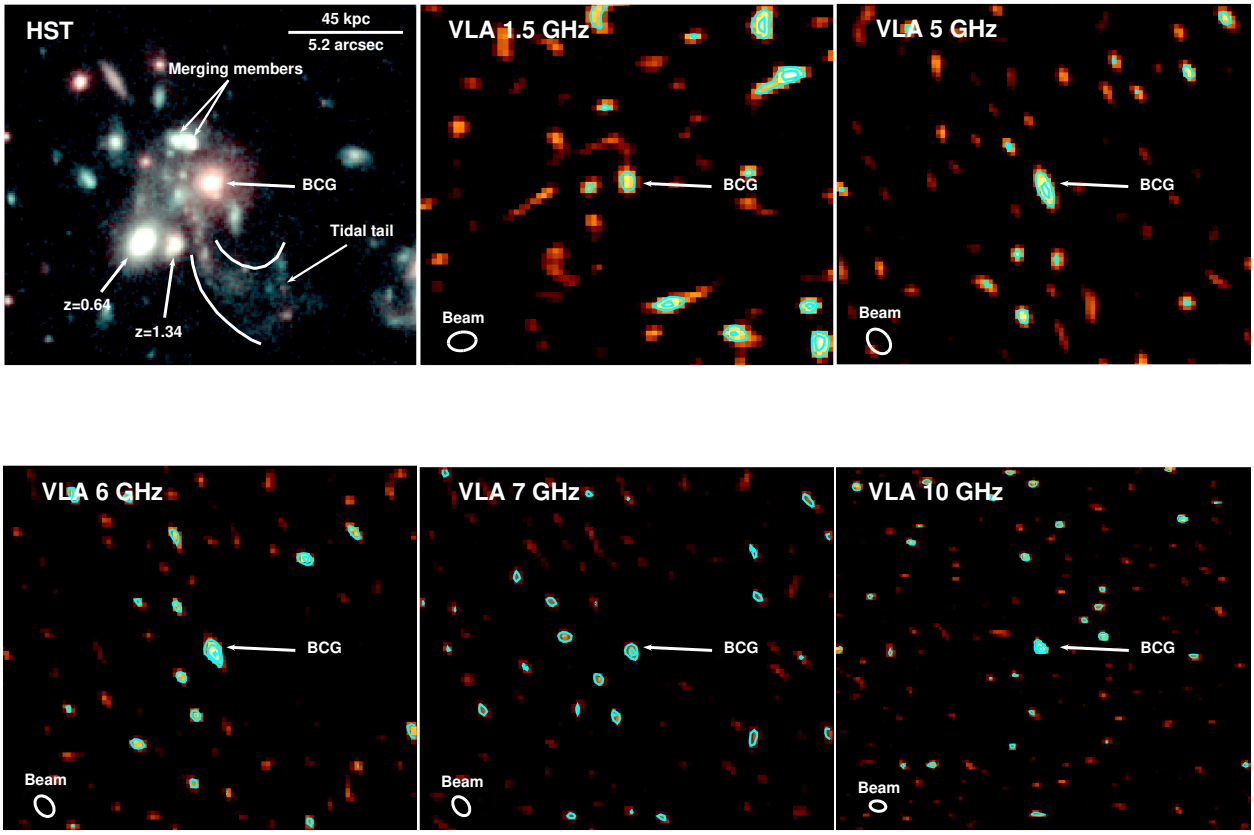

Figure A.1 Deep VLA images of the BCG in SpARCS1049 and its HST counterpart. Top-left: An optical/near infrared view of the BCG of SpARCS1049 and its vicinity. Top-middle: 1.5 GHz VLA image of the same area (RMS of 10.5 μJy beam^{-1}, $3\sigma_{\rm RMS}$ = 31.5 μJy beam^{-1}). Top-right: 5 GHz VLA image (RMS of 4.5 μJy beam^{-1}, $3\sigma_{\rm RMS}$ = 13.5 μJy beam^{-1}). Bottom: 6, 7 and 10 GHz image with RMS of 3.2, 4.7 and 3.7 μJy beam^{-1} respectively. $3\sigma_{\rm RMS}$ levels are 9.6, 14.1 and 11.1 μJy beam^{-1} respectively. No extended emission is detected. The scale is indicated in the top right corner of the HST image. The VLA beams are shown in the lower left corners and the radio contours (3, 4 and 5$\sigma_{\rm RMS}$ levels) are displayed in cyan.

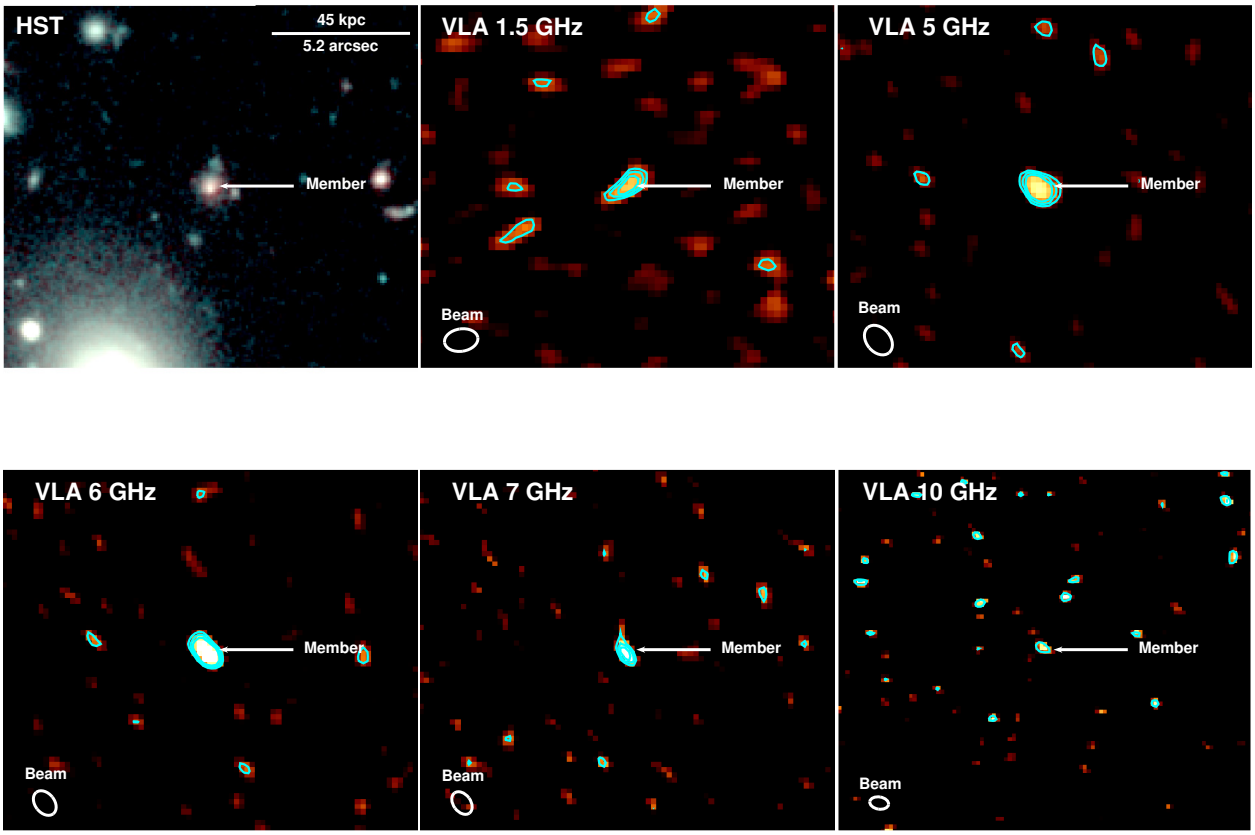

Figure A.2 Same as Figure A.1 but for the second member detected in radio. Radio images are displayed in the same order; RMS and $3\sigma_{\rm RMS}$ levels are similar.

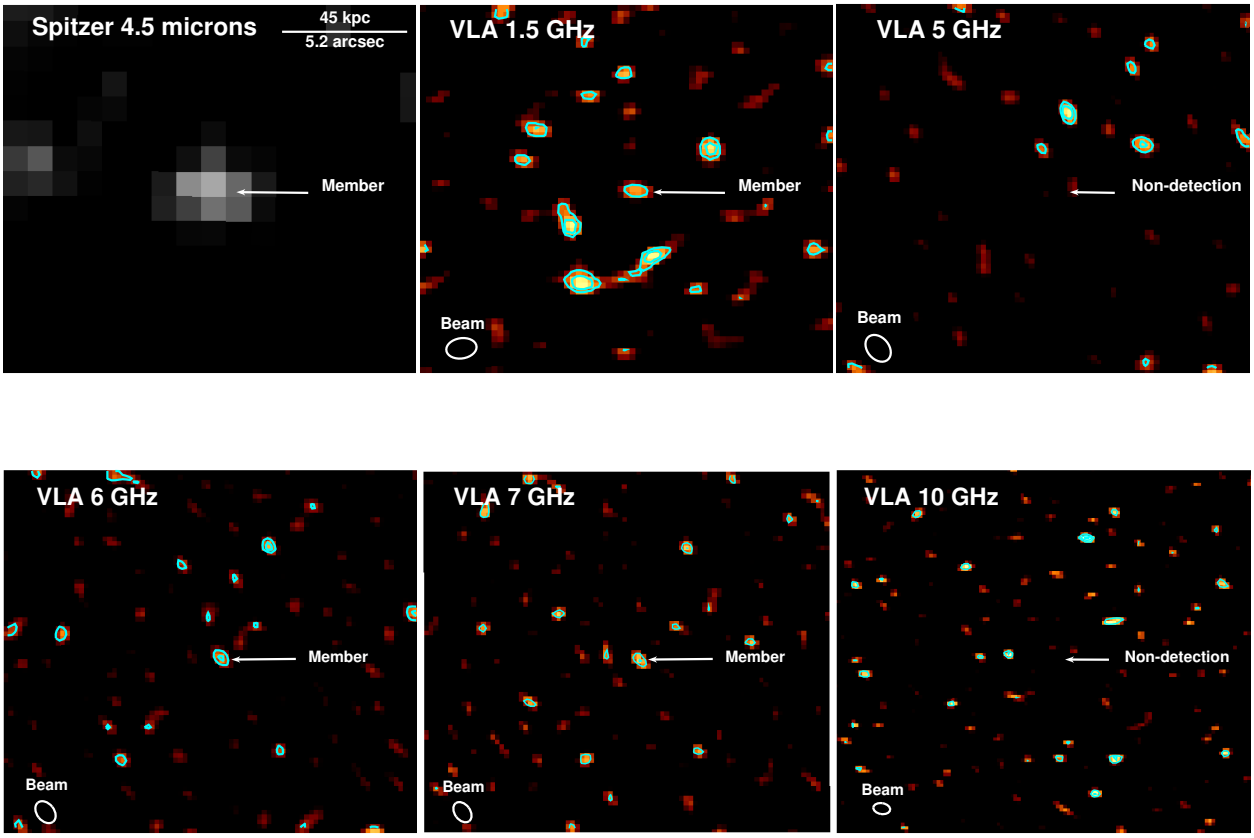

Figure A.3 Same as Figure A.1 but for the third member detected in radio. Radio images are displayed in the same order; RMS and $3\sigma_{\rm RMS}$ levels are similar.

BIBLIOGRAPHY

Cornwell, T. J., K. Golap and S. Bhatnagar. 2008, The non-coplanar baselines effect in radio interferometry: The W-Projection algorithm, *IEEE Journal of Selected Topics in Signal Processing*, vol. 2, n^{o} 5, doi:10.1109/JSTSP.2008.2005290, p. 647–657, ISSN 1932-4553. URL `http://arxiv.org/abs/0807.4161`, arXiv: 0807.4161.

McMullin, J. P., B. Waters, D. Schiebel, W. Young and K. Golap. 2007, CASA Architecture and Applications, p. 127. URL `http://adsabs.harvard.edu/abs/2007ASPC..376..127M`.